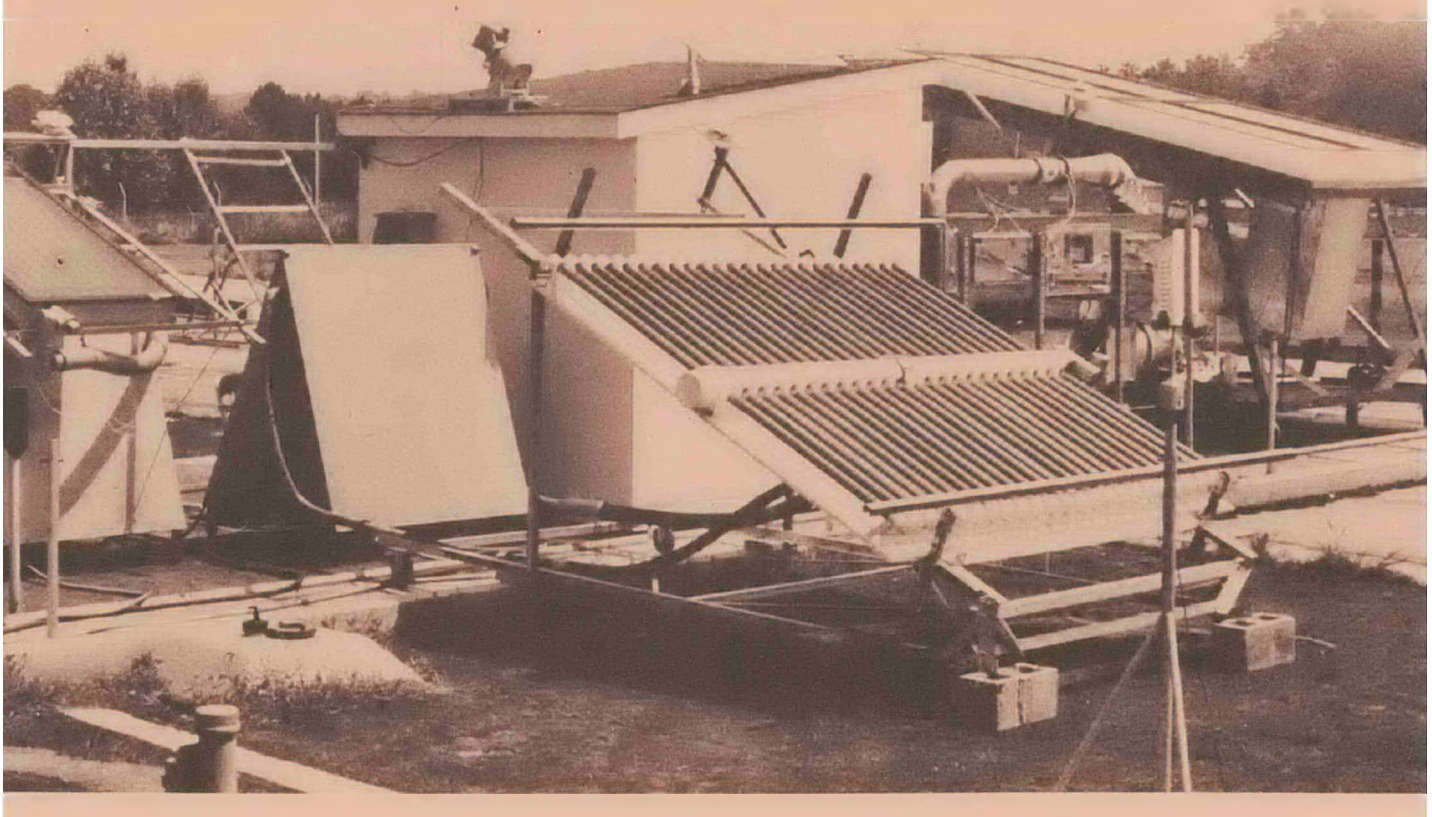

NBS BUILDING SCIENCE SERIES 117

Experimental Verification of a Standard Test Procedure for Solar Collectors

U.S. DEPARTMENT OF COMMERCE • NATIONAL BUREAU OF STANDARDS

NATIONAL BUREAU OF STANDARDS

The National Bureau of Standards[1] was established by an act of Congress March 3, 1901. The Bureau's overall goal is to strengthen and advance the Nation's science and technology and facilitate their effective application for public benefit. To this end, the Bureau conducts research and provides: (1) a basis for the Nation's physical measurement system, (2) scientific and technological services for industry and government, (3) a technical basis for equity in trade, and (4) technical services to promote public safety. The Bureau's technical work is performed by the National Measurement Laboratory, the National Engineering Laboratory, and the Institute for Computer Sciences and Technology.

THE NATIONAL MEASUREMENT LABORATORY provides the national system of physical and chemical and materials measurement; coordinates the system with measurement systems of other nations and furnishes essential services leading to accurate and uniform physical and chemical measurement throughout the Nation's scientific community, industry, and commerce; conducts materials research leading to improved methods of measurement, standards, and data on the properties of materials needed by industry, commerce, educational institutions, and Government; provides advisory and research services to other Government Agencies; develops, produces, and distributes Standard Reference Materials; and provides calibration services. The Laboratory consists of the following centers:

Absolute Physical Quantities[2] — Radiation Research — Thermodynamics and Molecular Science — Analytical Chemistry — Materials Science.

THE NATIONAL ENGINEERING LABORATORY provides technology and technical services to users in the public and private sectors to address national needs and to solve national problems in the public interest; conducts research in engineering and applied science in support of objectives in these efforts; builds and maintains competence in the necessary disciplines required to carry out this research and technical service; develops engineering data and measurement capabilities; provides engineering measurement traceability services; develops test methods and proposes engineering standards and code changes; develops and proposes new engineering practices; and develops and improves mechanisms to transfer results of its research to the utlimate user. The Laboratory consists of the following centers:

Applied Mathematics — Electronics and Electrical Engineering[2] — Mechanical Engineering and Process Technology[2] — Building Technology — Fire Research — Consumer Product Technology — Field Methods.

THE INSTITUTE FOR COMPUTER SCIENCES AND TECHNOLOGY conducts research and provides scientific and technical services to aid Federal Agencies in the selection, acquisition, application, and use of computer technology to improve effectiveness and economy in Government operations in accordance with Public Law 89-306 (40 U.S.C. 759), relevant Executive Orders, and other directives; carries out this mission by managing the Federal Information Processing Standards Program, developing Federal ADP standards guidelines, and managing Federal participation in ADP voluntary standardization activities; provides scientific and technological advisory services and assistance to Federal Agencies; and provides the technical foundation for computer-related policies of the Federal Government. The Institute consists of the following divisions:

Systems and Software — Computer Systems Engineering — Information Technology.

[1]Headquarters and Laboratories at Gaithersburg, Maryland, unless otherwise noted; mailing address Washington,D.C. 20234.
[2]Some divisions within the center are located at Boulder, Colorado, 80303.

The National Bureau of Standards was reorganized, effective April 9, 1978.

NBS BUILDING SCIENCE SERIES 117

Experimental Verification of a Standard Test Procedure for Solar Collectors

James E. Hill
John P. Jenkins and
Dennis E. Jones

Center for Building Technology
National Engineering Laboratory
National Bureau of Standards
Washington, D.C. 20234

Prepared for
The Department of Energy
Research and Development Branch
for Solar Heating and Cooling
Office of the Assistant Secretary for
Conservation and Solar Applications
Washington, D.C. 20545

U.S. DEPARTMENT OF COMMERCE, Juanita M. Kreps, Secretary

Jordan J. Baruch, Assistant Secretary for Science and Technology

NATIONAL BUREAU OF STANDARDS, Ernest Ambler, Director

Issued January 1979

Library of Congress Catalog Card Number: 78-600138

National Bureau of Standards Building Science Series 117
Nat. Bur. Stand. (U.S.), Bldg. Sci. Ser. 117, 127 pages (Jan. 1979)
CODEN: BSSNBV

U.S. GOVERNMENT PRINTING OFFICE
WASHINGTON: 1978

For sale by the Superintendent of Documents, U.S. Government Printing Office, Washington, D.C. 20402
Stock No. 003-003-02008-7 Price $3.00
(Add 25 percent additional for other than U.S. mailing).

CONTENTS

Experimental Verification of a Standard Test Procedure for Solar Collectors

by

James E. Hill, John P. Jenkins and Dennis E. Jones

Abstract

A proposed procedure for testing and rating solar collectors based on thermal performance was published by the National Bureau of Standards (NBS) in 1974. Subsequently, the American Society of Heating, Refrigerating, and Air Conditioning (ASHRAE) developed a modified version of the NBS procedure which was adopted in early 1977 as ASHRAE Standard 93-77. A test facility for water-heating and air-heating collectors has been built at NBS and was used to support the development of Standard 93-77. The purpose of this report is to describe the recently adopted test procedure, the NBS test facility, and the tests that were conducted to support the development of the procedure.

Keywords: Measurement; solar collector; solar energy; solar radiation; standards; standard test; testing.

In discussing this experimental program, certain commercial components were used and are identified in order to provide a descriptive characterization of their features. Inclusion of a given component is this report in no case implies a recommendation or endorsement by the National Bureau of Standards, and the presentation should not be construed as a certification that any component would provide the indicated performance. Similarly, the omission of a component does not imply that its capabilities are less than those of the included components. This report is intended to be informative and instructive and not an evaluation of any commercially available components.

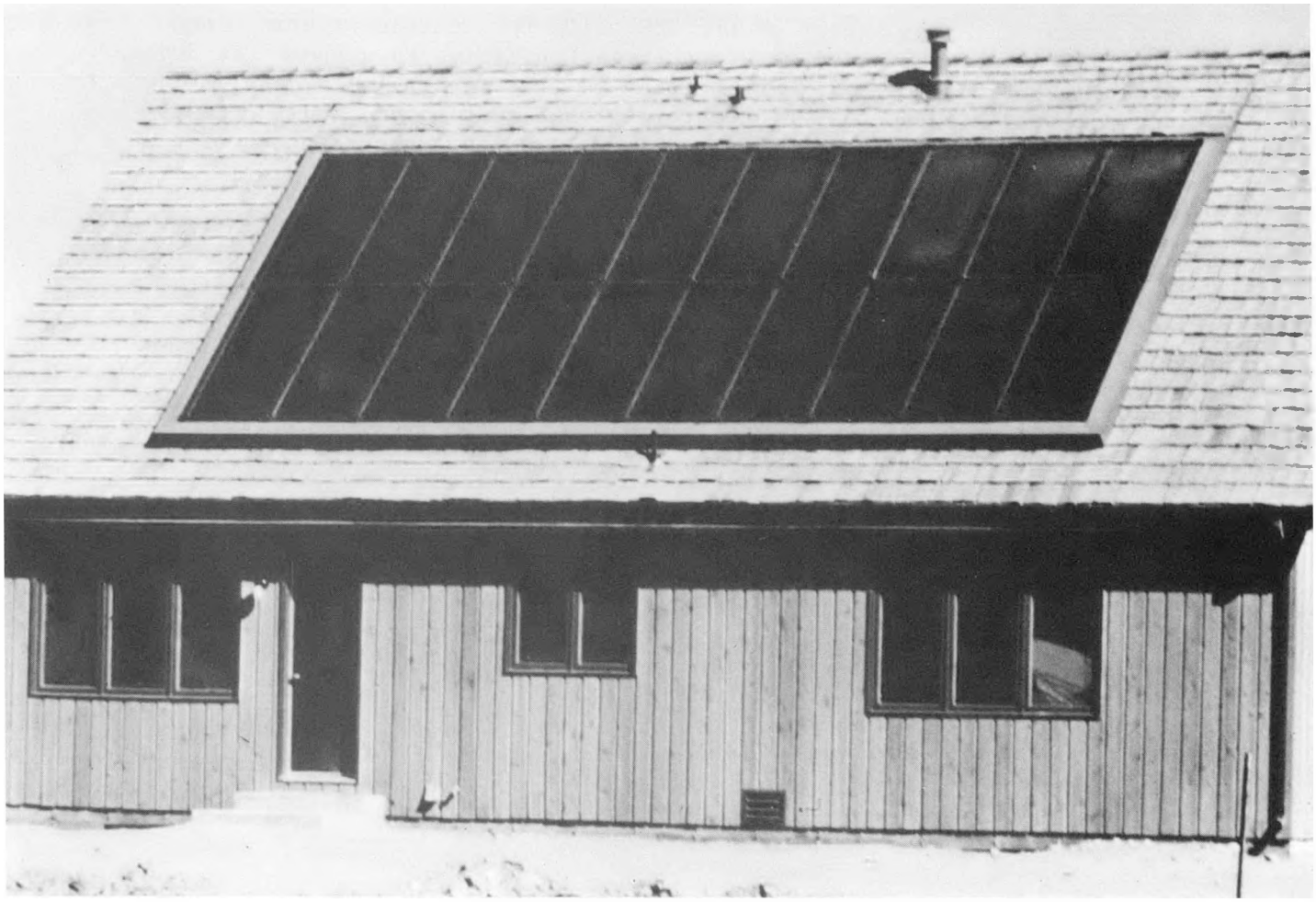

1. INTRODUCTION

A proposal for testing and rating solar collectors based on thermal performance was published by the National Bureau of Standards (NBS) in 1974 [1-3].* The procedure prescribed that a series of outdoor steady-state tests be conducted to determine the near-normal-incidence efficiency of the collector over a range of temperature conditions. The American Society of Heating,Refrigerating, and Air Conditioning Engineers subsequently developed a modified version of the NBS procedure which was adopted in February, 1977, as ASHRAE Standard 93-77 [4]. It is similar to the NBS procedure but calls for additional tests to determine the collector time constant as well as an incident angle correction factor that can be applied to the near-normal-incidence efficiency to determine collector performance both early in the morning and late in the day.

Three test loops have been built at NBS in accordance with ASHRAE Standard 93-77, two for modular water-heating collectors and the other for

*Figures in brackets indicate literature references at end of the report.

air heaters. A major part of the NBS collector testing program since mid-1976 has been devoted to using these facilities to support the development of Standard 93-77. The purpose of this report is to describe the recently adopted test procedure, the NBS test loops, and the tests that were conducted during 1976 and 1977 to support the adoption of the procedure.

A second major part of the NBS collector testing work has been to conduct a round robin program in which two flat-plate liquid-heating collectors were tested by 21 organizations around the United States during 1976 and early 1977. The purpose of the program was to have a a variety of testing laboratories attempt to utilize the NBS test procedure* and then determine the extent to which the results differed or were comparable. The test data and subsequent analysis for this program are available in separate publications [5, 6].

---

*ASHRAE Standard 93-77 was not adopted at the time this program was initiated.

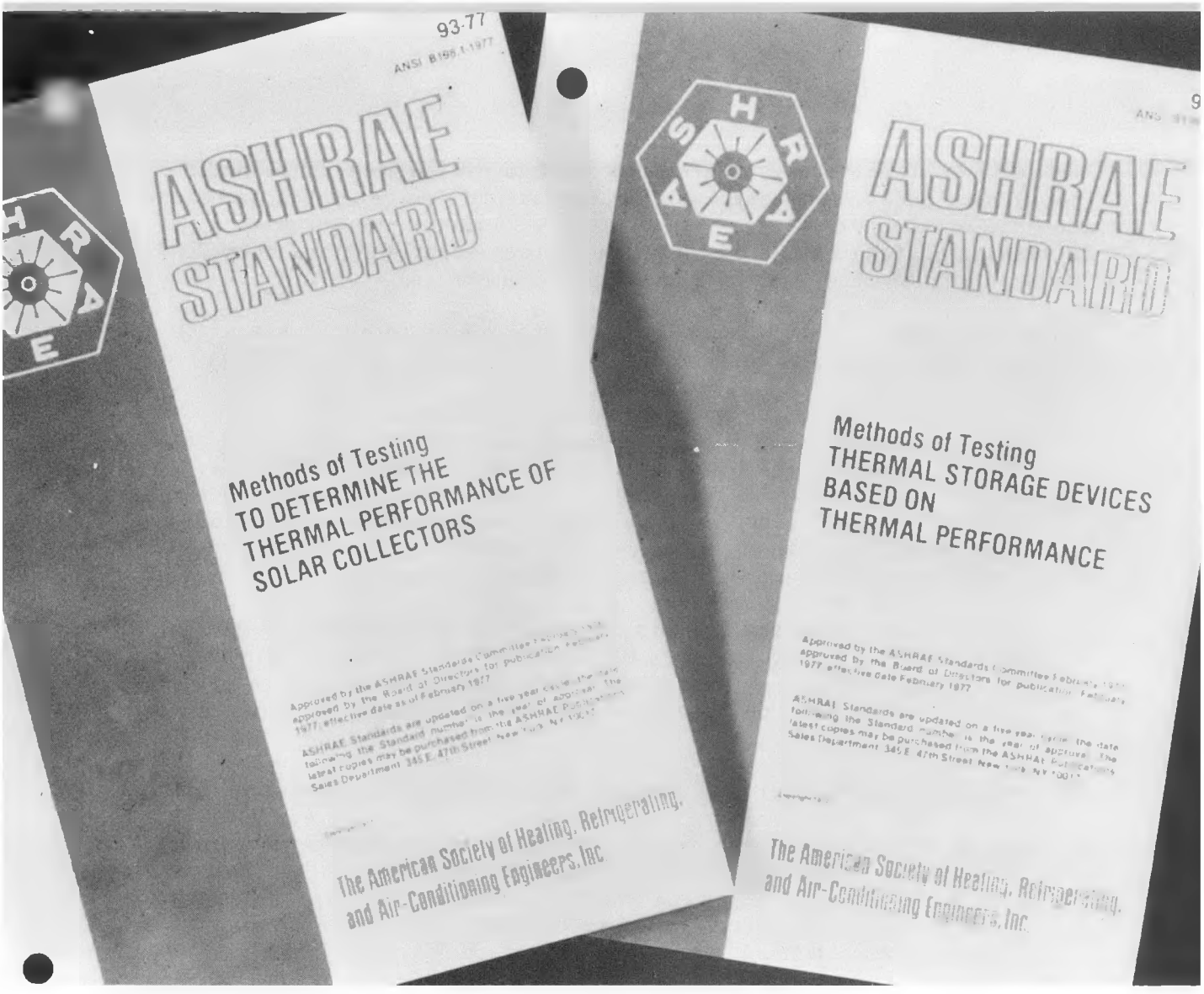

2. ASHRAE STANDARD 93-77

The testing procedure recommended by NBS in reference [1-3] called for the determination of the thermal efficiency of the solar collector by passing the heat transfer fluid through it at a steady rate with the collector mounted outdoors under clear sunny conditions. Measurements were required to be made during the middle of the day and consisted primarily of determining the fluid flow rate, temperature rise in the fluid as it passed through the collector, and the incident solar radiation (also called irradiance). These data could then be used to compute collector efficiency. The tests were to be made so that at least 16 "steady-state" efficiency values could be determined over a range of temperature differences between collector fluid and ambient air in order to draw an efficiency curve for the collector. A significant amount of detail was included on the recommended apparatuses, the instrumentation, and the procedure to follow. The testing procedure specified in ASHRAE Standard 93-77 consists of the

same series of efficiency tests (with some modifications to be noted below) plus additional tests which allow one to determine the transient response of the collector as well as how efficiency changes with increasing incident angle (between the direct solar beam and outward drawn normal to the plane of the collector aperture).

The major changes in the conduct of the efficiency tests as specified in Standard 93-77 compared to that specified in [1, 2] are as follows:

1. The testing apparatus for water-heating collectors has been modified to include a storage tank for damping out thermal transients and a bypass to permit periodic calibration of the flow meter in place. Figure 1 is a schematic drawing of the recommended closed-loop from [4]. In addition, two other alternate open-loop configurations are also given (see Figure 2 and 3) and considered acceptable provided the test requirements and specifications can be met.

2. The testing apparatus for air heaters has been rearranged so that air is "pulled" through the collector instead of being blown through it (slight negative gauge pressure in the collector). Alternately, an open-loop test configuration similar in concept to Figure 3 can be used.

3. More stringent requirements have been included for the measurement of incident solar radiation. Pyranometers are required to meet or exceed the characteristics of a first class pyranometer as classified by the World Meterological Organization [7].

4. In conducting the test, data must be taken when the solar incident angle is less than 30° (compared to 45° in [1, 2]).

5. The time period required for the integration of energy quantities to compute one efficiency value has been decreased from 15 minutes to either 5 minutes or one time constant, whichever is larger.

6. In computing efficiency, the gross frontal area of the collector is used instead of aperture area.

7. The efficiency curve is drawn by plotting efficiency as a function of the difference between inlet fluid temperature and ambient temperature divided by the incident solar radiation. (Average fluid temperature was used in [1, 2].) Inlet fluid temperature was chosen to be used in the plot because the primary characteristics of the collector required for the system design procedures of [8, 9] can be determined directly from the slope and the intercept of the curve.

The major completely new features of Standard 93-77 compared to [1, 2] are:

1. The collector is required to undergo a preconditioning test prior to the start of the thermal tests. The collector must be exposed

for three cumulative days with no fluid passing through it and with the mean incident solar radiation measured in the plane of the collector aperture exceeding 17,000 kJ/(m^2 · day) (1500 Btu/(ft^2 · day)).

2. Prior to conducting the efficiency tests, the time constant is determined (see below).

3. After completing the efficiency tests, a series of tests is conducted to determine the collector's incident angle modifier (see below).

4. The entire group of tests may be made indoors using a solar simulator if desired. The specifications for the simulator are included and follow closely those of references [10-12].

2.1 COLLECTOR TIME CONSTANT

When a solar collector is operating under steady-state conditions, the relationship that governs its thermal performance is:

the rate of useful energy extracted from the collector	=	the rate of energy absorbed in the collector by the absorber	−	the rate of energy loss from the collector by conduction, convection and radiation	=	the rate of energy carried away by the transfer fluid

In equation form:

$$\frac{q_u}{A} = F_R I(\tau\alpha)_e - F_R U_L(t_{f,i}-t_a) = \frac{\dot{m}c_p}{A}(t_{f,e} - t_{f,i}) \qquad (1)$$

where

q_u = rate of useful energy extracted from the collector, W

A = cross-sectional area of the collector, m^2

F_R = collector heat removal factor

I* = total solar energy incident upon the plane of the collector per unit time per unit area, W/m^2

$(\tau\alpha)_e$ = effective transmittance-absorptance product for the collector

U_L = heat transfer loss coefficient for the collector, W/(m^2 · °C)

$t_{f,i}$ = temperature of the transfer fluid entering the collector, °C

*In the technical literature, frequently the symbol E, irradiance or G, global irradiance will be used instead of I [38].

t_a = ambient air temperature, °C

$\dot{m}$ = mass flow rate of the transfer fluid through the collector, kg/(s•m^2)

c_p = specific heat of the transfer fluid, J/(kg•s)

$t_{f,e}$ = temperature of the transfer fluid leaving the collector, °C

Whenever transient conditions exist, the above equations are not valid since part of the energy being absorbed is used for heating-up of the collector and its components. The corresponding relationship for transient conditions is:

the rate of change of energy stored in the collector and its components	=	the rate of energy absorbed in the collector by the absorber	-	the rate of energy loss from the collector by conduction, convection and radiation	-	the rate of energy carried away by the transfer fluid

In equation form [13,14]:

$$\frac{C_A}{A}\frac{dt_f}{d\theta} = F_R I(\tau\alpha)_e - F_R U_L (t_{f,i} - t_a) - \frac{\dot{m}c_p}{A}(t_{f,e} - t_{f,i}) \qquad (2)$$

where

C_A = effective heat capacity of the collector, its components, and the transfer fluid in the collector, J/°C

θ = time, s

Equation (2) can be solved for the exit temperature of the transfer fluid, $t_{f,e}$, as a function of time, θ, after making the following assumptions:

1. The exit temperature, $t_{f,e}$, of the transfer fluid is related to the average fluid temperature, $\bar{t}_f$, by

$$\frac{d\bar{t}_f}{d\theta} = K\frac{dt_{f,e}}{d\theta} \qquad (3)$$

where [13]:

$$K = \frac{\dot{m}c_p}{F'U_L A} \left(\frac{F'}{F_R} - 1\right) \tag{4}$$

and F' = collector efficiency factor

2. I, $(\tau\alpha)_e$, U_L, t_a, $\dot{m}$, c_p, and $t_{f,i}$ are all constant for the period covered by the transient solution.

The solution to equation (2) is then:

$$\frac{F_R I(\tau\alpha)_e - F_R U_L(t_{f,i} - t_a) \quad \frac{\dot{m}c_p}{A} \quad (t_{f,e} - t_{f,i})}{F_R I(\tau\alpha)_e - F_R U_L(t_{f,i} - t_a) - \frac{\dot{m}c_p}{A} \quad (t_{f,e,\,\text{initial}} - t_{f,i})} = e^{-\left[\frac{\dot{m}c_p}{KC_A}\right]\theta} \tag{5}$$

It is conventional practice in the physical sciences that whenever an equation of the form of (5) describes the response of a particular system, the quantity $KC_A/\dot{m}c_p$ is called the system's time constant. The physical interpretation of the time constant is the time required for the quantity on the left side of equation (5) to change from 1.0 to 0.368 where 0.368 = 1/e. It was felt that this concept should be maintained in order to be consistent with the accepted interpretation of time constant. Unfortunately, this has not always been done in the solar collector field. Simon [15] has published the value of "time constant" for nine different water-heating collectors using the 0 to 99% change time. Wijeysundera [16] has computed the "response time" of typical one, two, and three cover air-heaters using the 0 to 90% change time. Fortunately, the conventional time constant can be computed from the published values by multiplying by an appropriate constant in each case.

The time constant for a collector could be calculated theoretically using equation (5). However, there is a large uncertainty in the value of the effective heat capacity, C_A. Duffie and Beckman [14] have shown that the upper limit for this heat capacity is the sum of the products of mass times specific heat for each of the components that make up the collector (absorber, glass, insulation, etc), plus that of the transfer fluid required to fill the collector. However, if this were used for C_A, the time constant would be overestimated. This is due to the fact that the temperature of some materials in the collector only change a fraction of the amount that the fluid temperature changes in such a transient

process. Consequently, the time constant is required to be determined experimentally in ASHRAE Standard 93-77.

The actual test can be carried out in one of two ways. The most straightforward technique is to expose the collector to the solar radiation and after the entering and exiting fluid temperatures have stablized, suddenly shield the collector from the sun and record the exit fluid temperature on a strip chart recorder. The incident radiation must be above 790 W/m^2 (250 $Btu/(h \cdot ft^2)$). The entering fluid should be within $\pm 1°C$ ($\pm 2°F$) of the ambient temperature for the duration of the test. This latter requirement simplifies the data reduction process using the left side of equation (5).

A second technique that can be used is to shield the collector from the sun altogether (conduct the test inside for example). The inlet fluid temperature is adjusted to 30°C (54°F) above the ambient and after the exit temperature has stabilized, the inlet temperaure is suddenly decreased to within $\pm 1°C$ ($\pm 2°F$) of the ambient, and the exit fluid temperature is again recorded as a function of time. It should be noted that the time constant determined experimentally according to either of the above procedures is valid only for the range of ambient temperatures used in the test. Its value is temperature dependent as can be seen from equation (5) (U_L is temperature dependent) and from Figure 5 of reference [16]. However, since the main value of such a test is to allow a relative comparison of collectors, it was felt that the one test would be adequate.

2.2 COLLECTOR INCIDENT ANGLE MODIFIER

Simon and Buyco [17] have shown that the effective transmittance-absorptance product, $(\tau\alpha)_e$, of a solar collector can be satisfactorily described by:

$$(\tau\alpha)_e = K_{\alpha\tau}(\tau\alpha)_{e,n} \qquad (6)$$

where $K_{\alpha\tau}$ = incident angle modifier

$(\tau\alpha)_{e,n}$ = effective transmittance-absorptance product for the collector at normal incidence

The incident angle modifier, $K_{\alpha\tau}$, is nothing more than a correction factor which is a function of the incident angle, the angle between the direct solar beam and the outward drawn normal to the plane of the collector aperture. It describes how the optical efficiency of the collector changes as the incident angle changes. It is an essential factor for predicting all-day efficiency for a stationary solar collector.

Figure 4 shows how the effective transmittance-absorptance product, $(\tau\alpha)_e$ varies as a function of incident angle for two types of flat-plate collectors exposed to 100% direct radiation [18]. Using the relationship for the incident angle modifier as given in equation (6), the variation

of incident angle modifier with incident angle for these same collectors is shown in Figure 5. Based on the optical characteristics of flat-plate collectors, data from Figure 5 can be replotted as in Figure 6 and will result in linear plots as shown. This same linear relationship may or may not exist for non flat-plate collectors depending on their optical characteristics.

As with the time constant test, there are two ways in which the incident angle modifier can be determined. The first technique is applicable when the incident angle can be arbitrarily adjusted such as with a solar simulator or with an outdoor movable test rack. In this case, a thermal efficiency test is conducted in accordance with all the requirements of the procedure used to get the near-normal-incidence efficiency curve except that:

1. The inlet fluid temperaure is held within $\pm 1°C$ ($\pm 2°F$) of the ambient temperature.

2. The test is made at incident angles of 0, 30, 45, and 60°.

By comparing the above test results with those obtained in establishing the efficiency curve at incident angles of less than 30°, values of $K_{\alpha\tau}$ can be computed as a function of incident angle.

The second technique is applicable for outdoor testing with a permanent test rack where the collector orientation cannot be arbitrarily adjusted with respect to the direction of the incident solar radiation (except for perhaps adjustments in tilt). The collector is tested for a complete day with the inlet fluid temperature held constant as above. The efficiency values are computed continuously and "pairs" of values are selected, one from the morning and one from the afternoon, which correspond to values of 30, 45, and 60° in incident angle. The two efficiency values in each pair are averaged to compensate for transient effects and then used as above to compute the incident angle modifier.

3. DESCRIPTION OF NBS TEST FACILITY

The collector testing loops designed, built, and used in the experiments described in this report are housed at an abandoned NIKI Missile Site adjacent to the NBS Laboratories in Gaithersburg, Maryland. One of the underground bunkers built originally for storage of missiles was used for fabrication of the test loops and they were mounted on the elevator used originally for transporting the missiles up to ground level. This unique facility allows NBS personnel to expose the test equipment to the outdoor environment only on days when tests are run. In addition, the same test equipment can then be used for conducting indoor tests of collector heat loss characteristics.

Figure 7 shows the elevator door closed over the underground bunker occupied by the NBS collector testing group*. Figure 8 shows the equipment

*Two additional underground bunkers are currently occupied and being used by the NBS Fire Research Center.

mounted on the elevator just after the doors have opened. Figures 9 and 10 show the equipment being raised and stopped in a convenient position to clean the collector cover plate assembly on an air collector array prior to the start of a test day. Figure 11 shows the equipment in the testing configuration with the two water loops in the foreground, the room holding the data acquisition system and associated instrumentation in the center, and the air loop on the far side. Some collector arrays that have been tested were too large to mount on the test loop structure and had to be kept permanently above ground and connected to the test loops through flexible hoses. An example is the evacuated tubular collector array in the foreground.

3.1 TEST LOOPS FOR WATER-HEATING COLLECTORS

Two separate test loops were built for the water-heating collectors in contrast to a larger single loop which could accommodate 2-4 collectors. This was done to be able to test more than one collector at a time and still have the flexibility to make adjustments to individual collectors during testing and yet not affect the other collectors being tested. Both test loops are essentially identical and consist of an integral test unit capable of supporting a typical flat-plate collector at a chosen orientation while containing the flow loop within the enclosed base. The tested collector can be adjusted over a wide range of tilt angles (0-70°) and orientations (0-360°) and easily added to or removed from the structure. As already indicated, a separate adjustable collector support frame is used in cases where an exceptionally large collector is being tested.

Figure 12 shows a close-up of one of the test loops with a flat-plate collector (collector No. 2) mounted to the top of the frame. Figure 13 is a schematic drawing of the test loop. As can be seen, it is a closed loop similar in principle to that of Figure 1 and was designed to be able to control and stabilize the collector fluid inlet temperature to within ±0.5°C (±1.0°F) and the fluid flow rate to within ±1%. Pure water has been used as the working fluid in all collectors whose characteristics are reported herein. This has eliminated uncertainties and possible errors associated with knowing the working fluid properties. Figure 14 shows the loops from the north and, as can be seen, all equipment is sufficiently protected from the environment by having it enclosed within the housing and also insulated to minimize heat loss. Plumbing and hardware within the test stand base are encased with 1.3 cm (0.5 in.) foamed rubber insulation and all exposed extension plumbing is wrapped with 3.8 cm (1.5 in.) foamed rubber insulation. The following paragraphs describe the details of the equipment used in the flow loops starting with the collector and moving clockwise in Figure 13. The specifications for the equipment and sensors are included in Table 1.

The temperature measurement sections are located immediately upstream and downstream of the collector allowing temperature sensors to be inserted for measurement purposes. Figure 15 is a schematic drawing of the temperature measurment section at the outlet of the collector

and Figure 16 is a photograph taken prior to insulating the pipe. These sections are located as close as possible to the connection of the collector and are insulated with 3.8 cm (1.5 in.) foamed rubber insulation in order to minimize thermal heat losses and to insure a temperature change of less than 0.05°C (0.1°F) between the sections and the collector. Proper fluid mixing is provided by allowing the fluid to pass through at least one right angle bend immediately before entering the measurement section. The sections are constructed so that two temperature sensors can be inserted simultaneously. One temperature sensor can be a sheathed thermocouple or resistance thermometer inserted through a compression fitting while at the opposite end a set of thermopile junctions can be inserted into a thin-wall copper oil-filled well. To provide proper bleeding of trapped air from the entire system, air bleed valves are located immediately adjacent to the wells. An alternate technique for insuring a well-mixed fluid stream at the temperature measuring station is shown in Figure 17. This technique should work well but was not used in either of the two loops described here.

Three types of temperature sensors have been used to monitor the absolute temperature and the temperature difference between the inlet and outlet of the collector. Only two types of temperature sensors are used simultaneously. Calibrated platinum resistance thermometers (PRT) or sheathed type-T thermocouples are inserted in one end of the well for measuring absolute temperatures while a six junction thermopile or PRT is used at the other end to sense the temperature difference across the collector.

The choice between platinum resistance thermometers or thermocouples for measuring absolute temperatures is primarily a matter of cost. Typically, commercially available platinum resistance thermometers are accurate to within ±0.1°C (±0.2°F). NBS calibrated 0.47 cm (3/16 in.), sheathed platinum precision resistance thermometers with related electronic bridges used in this study are accurate to within ±0.05°C (±0.1°F). In comparison, calibrated 0.64 cm (1/4 in.) sheathed type-T thermocouples that were also used in this study are accurate to within ±0.1°C (±0.2°F). Therefore, both types of sensors meet the required accuracy for absolute temperature measurements of within ±0.5°C (±1.0°F) as given in [4]. In either case, caution should be taken to insure that the temperature sensor immersion length into the temperature well agrees with the immersion depth at calibration.

A type-T six-junction thermopile is used to measure the temperature difference across the solar collector. At least six junctions were determined to be necessary in order to determine small temperature differences to an accuracy of within ±0.1°C (±0.2°F) (assuming the thermopile readout instrumentation accuracy is within ±0.01 mv). Currently the test procedure in [4] allows either resistance thermometers or a thermopile to be used for determining the temperature differences across the collectors. For reasons of accuracy and reliability, the thermopile proved to be superior. Because of the large number of junctions at either end of the thermopile, the wire gauge should be as small as practically possible in order to minimize thermal conduction

losses along the thermopile leads away from the temperature measuring junctions. For this installation, 30 or 36 gauge thermocouple wire was found to be adequate. To further eliminate error due to thermal conduction losses, the thermopile leads were doubled back along side of the oil-filled temperature well as shown in Figure 15. The thermopile is inserted into the well to at least a depth of 10 cm (4 in.). The entire thermopile was constructed from the same spool of calibrated wire.

A water-to-air heat exchanger is used in each flow loop and an additional water-to-water heat exchanger is used in one of the loops in order to allow for a wider range of heat dump for some of the higher performance collectors being tested. The water-to-air heat exchanger is a 36 cm (14 in.) square by 2.5 cm (1.0 in.) deep fluid radiator (see Figure 18) while the other is a counter-flow single-pass water-to-water exchanger. For adjustment purposes, the water-to-air heat exchanger uses ganged ball valves to serve as a bypass and modulate the heat dump. The ganged bypass valves produce a constant back pressure and consequently a steady flow rate over the full range of adjustment. The heat dump of the water-to-water heat exchanger is adjusted by controlling the secondary side fluid flow rate supplied from a local water main.

Although not shown in the schematic drawing of Figure 13, the flow loop can be opened in order to provide a means of periodically calibrating the flow meters in place against a weigh tank and stopwatch. In addition, the flow meters can also be easily removed for cleaning, checking, and additional calibration.

Further downstream are the storage and recovery tanks including a pressure relief valve. The 38 liter (10 gal.) hot water storage tank can be seen in Figure 10 and is incorporated within the flow loop to act as a buffer and eliminate thermal cycling which tends to occur within a closed system. In addition, the storage tank contains a 1.5 kW immersion heater which is periodically used to increase the overall flow loop temperature. In order to further eliminate any air within the closed system, a fluid recovery tank was substituted for the recommended expansion tank. Whenever the flow loop pressure exceeds the 210 kPa (30 psi) relief valve setting, the fluid is dumped into a 3 liter (0.8 gal.) recovery tank and later recovered as the pressure in the loop drops.

Mercury-in-glass thermometers calibrated from 0-100°C (32-212°F) and accurate to within ±1°C (±2°F) are inserted into oil filled 0.93 cm (3/8 in.) copper wells in line with the inlet and outlet to the storage tank in order to monitor the respective temperatures. The inlet and outlet temperatures are required for adjusting the heat exchanger bypass in order to properly maintain steady conditions in the flow loop. To obtain a steady-state condition, the heat exchanger bypass is adjusted so that the storage tank inlet and outlet temperatures are equal to within 2°C (4°F).

A provision for make-up fluid in the flow loop serves several purposes. It can be used for filling or draining the loop or for pressurizing the entire system. Make-up water is provided from a local water main.

A 0-0.4 ℓ/s (0-6 gal./min.) 5-micron particulate fluid filter is incorporated within the loop in order to protect the system from foreign particles. The filter is located upstream of the pump and flow meter since they are both very susceptible to damage by particulate matter.

The controlled 500-watt heater downstream of the filter serves to stabilize the inlet fluid tempeature to the collector. The input power to the heater is adjusted so that the fluid temperature downstream of the pump is held constant to within ±0.1°C (±0.2°F). The heater power is controlled by a proportional temperature controller which senses the temperature downstream of the heater immediately after the pump with a type-T thermocouple and then proportionally controls the heater power in response to the sensors' deviation from a set point temperature. The proportionality of power output to set point deviation is adjustable in order to minimize temperature cycling within the flow loop.

The flow rates encountered with the flow loop are very low (0-0.63 ℓ/s (0-1 gal./min.)) requiring a stability of ±1% while periodically operating against high back pressures. For such circumstances, a low-flow 0-0.32 ℓ/s (0-5 gal./min.) positive-displacement eccentric-disc pump capable of pressures up to 340 kPa (50 psi) was selected over several centrifugal pumps. Most typical centrifugal pumps are limited to higher flow rates and lower working pressures. This pump is further capable of coarsely adjusting the flow rate to within ±0.0013 ℓ/s (±0.02 gal./min.) while a 1.3 cm (0.5 in.) needle valve downstream of the pump allows for fine adjustment.

Different types of flow meters are used in the two different flow loops. The first is a turbine type flow meter with a passive magnetic transducer and the second, a positive-displacement oval-gear flow meter with an active transducer. Each flow meter produces a digital signal output proportional to the monitored flow rate. The low-flow omnidirectional turbine meter and electronic display were initially calibrated over a flow and temperature range of 0-0.063 ℓ/s (0-1 gal./min.) and 20 - 100°C (68-212°F) respectively with stated accuracy and linearly of within ±0.9%. Likewise, the low-flow oval-gear positive-displacement meter was calibrated over a flow range of 0.01-0.07 ℓ/s (0.17-1.1 gal./min.) and temperature from 20-100°C (68-212°F) with a similar accuracy. When calibrated on a monthly basis, each flow meter can retain the specified accuracy of within ±1%.

During this test program, each flow meter was always calibrated in-situ with a typical open-loop weight tank arrangement and in conjunction with any related electronic displays or readouts. Over a period of a year, the accuracy of the turbine flow meter would have changed by + 2.5% if it were not for frequent calibration. It is believed that the 2.5%

drift was primarily due to wear and scale building up within the turbine ball bearings. In comparison, the oval gear flow meter was not subject to any similar drift in calibration over the same time interval. However, the oval gear meter did experience a gradual increasing internal flow resistance due to bearing wear. Consequently with time, the pressure drop across the flow meter became unstable resulting in a pulsating flow and the use of the meter was discontinued.

A visual flow meter is located immediately downstream of the electronic flow meter in each loop. Functioning as a course flow indicator, the visual flow meter also serves as a sight glass for determining whether air is trapped within the system. Because the flow meter is used for adjusting the coarse flow rate, the accuracy and resolution could be quite low. The flow meter used, a rotometer, is capable of measuring flows of 0-0.07 ℓ/s (0-1.1 gal./min.) with an accuracy of within ±2% of full scale.

For safety purposes, a 0-210 kPa (0-30 psi) static pressure gauge is connected at the solar collector inlet. The purpose is to visually indicate the system pressure and guard against collector and system overpressurization.

3.2 TEST LOOP FOR AIR-HEATING COLLECTORS

The test loop for air-heating collectors is shown in Figure 20 and schematically in Figure 21. It is divided into two major parts, the air handling module and the collector stand. The air handling module is mounted on a portable cart for ease of movement. The blower delivers air to the air reconditioning apparatus where it is conditioned to the desired temperature before entering the secondary flow measuring device. The air then flows through flexible ducting to the collector inlet measuring section which is attached directly to the collector array. Leaving the collector array, the air passes through the collector outlet measuring section and into another section of flexible ducting which is connected to the primary flow measuring device. The air then passes to the blower, thus completing the loop.

The primary details to note in the layout of the loop are the placement of flow measuring devices on both the collector array inlet and outlet with the primary flow measurement being on the collector outlet. Collector temperature and pressure measurements are made as close to the collector array as possible in duct sections which approximate actual installed duct sections. The blower is located on the downstream side of the collector array with creates a negative gauge pressure in the collector. This is generally the way most solar air-heating systems are configured. The details of the equipment in the flow loop will be described in the following paragraphs starting with the collector and moving clockwise in Figure 21. The specifications for the equipment and sensors are included in Table 2.

The collector stand is shown in Figure 22 from the side and is designed to accommodate a 2.5 m (8 ft) by 4.5 m (15 ft) collector array. The collector array can be tilted from 0 to 65 degrees from the horizontal. Casters on the base provide for rotation and mobility as shown in Figure 23. The stand is constructed of 7.6 x 7.6 cm x 0.64 cm (3 in. x 3 in. x 1/4 in.) angle iron except for the pivot beams which are 10 cm x 10 cm x 0.95 cm (4 in. x 4 in. x 3/8 in.) angle iron. The base is a solid welded unit mounted on locking casters. Two hand winches provide a means for setting the collector tilt.

A 2.5 m (8 ft) by 4.5 m (15 ft) stud and plywood platform insulated with glass fiber batts is mounted on top of the stand. The collectors are mounted on this platform as normally installed on a roof. The outside edges of the collector array are also insulated to simulate the effect of adjacent collectors. The collector measurement sections are attached directly to the collector manifold and are suspended from the bottom of the platform as can be seen in Figure 22. The collector measuring sections were constructed in accordance with reference [4] and are located at both the collector inlet and exit. Collector inlet and exit temperature difference, and pressure drop are measured at these locations. Reference [4] requires a length of $2.5\sqrt{a \times b}$ at the inlet and $6.5\sqrt{a \times b}$ at the exit between the temperature measuring station and the collector manifolds where a and b are the cross-section dimensions of the duct. A second requirement is that the air inlet and air outlet ducts shall be insulated in such a manner that the heat loss to the ambient air would not cause a temperature change for any test of more than 0.3°C (0.5°F) between the temperature measuring locations and the collector. In order to satisfy both of the above requirements, highly insulated measuring sections were required.

The collector stand is designed to test collector arrays of up to 10 m^2 (100 ft^2) in area. Assuming that the maximum flow rate used with a 10 m^2 (100 ft^2) collector would be 0.20 $m^3/(s.m^2)$ (4 $ft^3/min.ft^2$) for a total of 2 m^3/s(400 $ft^3/min.$), a 20 cm (8 in.) diameter circular duct was selected. This size provides duct velocities of approximately 5.9 m/s (1150 ft/min.) for the maximum size collector array. The amount of insulation required was then calculated assuming a minimum flow rate of 0.03 m^3/s (64 $ft^3/min.$)* and a maximum temperature difference between the air stream and ambient of 70°C (126°F). Based on the properties of glass fiber insulation and a length of 1.5 m (5 ft) between the collector exit and the measuring section, it was found that 7 ft (2.1 m) of insulation was needed to meet the requirements of [4]. A more reasonable thickness of 20 cm (8 in.) was chosen and based on actual test conditions for the collector tested in this study, it was calculated that the maximum error possible in collector efficiency due to duct heat loss between the collector and measuring sections was less than 1%.

---

*This would correspond to a flow rate of approximately 0.01 $m^3/(s \cdot m^2)$ (2 $ft^3/(min.ft^2)$) for a two module array and is the minimum measurable flow rate through the minimum size nozzle in the present test loop.

The duct sections were constructed with 20 cm (8 in.) inner diameter thin-walled aluminum tubing. The "L" shape seen in Figures 22 and 23 was necessary due to physical dimension limitations imposed by the collector stand. The flow duct and surrounding insulation are all contained in the 61 cm (24 in.) square sheet metal box.

The pressure measuring stations consist of four 0.48 cm (3/16 in.) nipples soldered to the duct and centered over 1 mm (0.04 in.) diameter holes. The four static pressure taps located symmetrically around the duct at each station are manifolded to a single tygon tubing pressure line. The pressure taps inside the duct were smoothed using emery cloth to remove any possible burrs. The pressure drop across the collector is measured by using a 0-0.25 kPa (0-1.0 in. H_2O) inclined manometer.

The temperature measuring stations consist of thermocouples mounted in probes which are inserted into the air stream through compression fittings. The probes were made using 0.3 cm (1/8 in.) o.d. brass tubing inserted into 0.32 cm (1/8 in.) compression fittings which were threaded into the duct wall. The thermocouples were made from 24 gauge type-T thermocouple wire. Thermocouples are permanently positioned at three different points in the duct in order to indicate any variation in temperature across the duct. In addition, a thermocouple is mounted on a probe which can be moved across the duct when desired to determine the temperature distribution. Temperature difference between the inlet and outlet of the collector is determined using a six-junction type-T thermopile constructed from a single spool of 24 gauge thermocouple wire. The thermopile junctions are located at the centers of equal cross-sectional areas as shown in Figure 24.

Flow mixers were not installed in the duct. Flow conditions at the temperature measuring sections were found to be uniform (temperature traverses were made). Flow mixers should only be used when really necessary. They will cause a larger pressure difference between the collector and ambient than normally experienced in an actual system installation, resulting in increased collector air leakage and thus different performance.

The primary air flow measuring apparatus consists basically of a receiving chamber, a discharge chamber, and an air-flow measuring nozzle as shown in Figure 7 of reference [4]. The two chambers were formed separately using 24-gauge sheet metal to construct two boxes, one 100 x 40 x 40 cm (39 x 16 x 16 in.) and the other 70 x 40 x 40 cm (27 x 16 x 16 in.). The nozzle mounting plate is a 0.5 cm (3/16 in.) steel plate with outside dimensions of 50 cm (20 in.) square framing a center hole of 32 cm (12.5 in.) square. The plate surface was ground flat and smooth where the nozzle is mounted. Diffusion baffles which are decorative grills having approximately 40% free area were purchased from a local hardware store and installed in the two chambers at the locations specified in [4]. The two chambers and the nozzle mounting plate are joined with gaskets and bolted together. An air-tight window was formed in the duct to allow access to the nozzle. Holes were cut in the back walls of the two chambers to allow connections through duct work with the rest of the loop.

Nozzles were constructed in accordance with reference [4] and are fixed to 36 cm (14 in.) squares with magnetic mounting strips. The magnetic mounting strips and pressure of the air hold the nozzle in place and form a tight seal. Five interchangeable nozzles were purchased, in sizes of; 5, 6.5, 7.5, 10, and 12.5 cm (2, 2.5, 3, 4, and 5 in.) throat diameters, which provide a range of flow rates from 0.03 to 0.41 m^3/sec (70 to 950 ft^3/min.). Pressure taps are incorporated into the duct walls as specified in [4] by centering and soldering 0.5 cm (3/16 in.) nipples over 0.013 cm (0.04 in.) holes located on the four duct walls. The two sides of the pressure sensing devices for the nozzle pressure difference and the nozzle discharge gauge pressure each are connected to four externally manifolded pressure taps. In addition, a pitot tube is used to sense velocity pressure at the nozzle throat. The pressure difference across the nozzle is determined using a 0-1.2 kPa (0-5 in. H_2O) inclined manometer in parallel with an electronic pressure transducer. The pressure transducer is an elastic diaphragm type and produces a 0 to 5 volt signal over the 0-1.2 kPa (0-5 in. H_2O) pressure range. The output signal is reduced to a 0 to 500 mv range using a voltage divider network. The nozzle discharge gauge pressure is determined using a 0-2.5 kPa (0-10 in. H_2O) vertical manometer. The pitot tube is connected to a 0-1.2 kPa (0-5 in. H_2O) inclined manometer. The procedure for calculating air flow rate using these measurements is given in Appendix A.

The blower is a centrifugal industrial model with a 3 phase 220 volt 3 horsepower motor capable of 0.47 m^3/s (1000 ft^3/min.) at standard conditions and a static head of 2.5 kPa (10 in. H_2O). This is a great deal more capacity than is needed for most test size collector arrays. However, the air handling module was designed to also be used for testing full-sized thermal storage units. The blower must be sized to provide the required flow rate over the pressure losses in the test loop. For the present system, the major pressure loss occurs at the flow measuring nozzle and is 0.25 to 0.75 kPa (1 to 3 in. H_2O). The amount of air delivered by the blower is controlled by the bayonet-type damper on the blower outlet (coarse control) and stovepipe-type damper on the inlet (fine control). The blower assembly is mounted on rubber vibration isolators and duct connections to the blower are made using flexible rubber connections which results in nearly complete vibration isolation of the blower.

The air reconditioning apparatus was designed to deliver air at a set temperature at its exit. Through the use of two hand-set dampers, part of the hot air from the blower is allowed to pass on to the collector while the rest of the hot air is exhausted to the atmosphere. Further downstream, a third handset damper is used to bring in ambient make-up air. Through proper positioning of the three dampers, the resulting air stream temperature can be adjusted to a value slightly below the desired temperature. The final temperature is attained and finely controlled using 6 kW electric resistance heaters coupled to a proportional power controller. The heater provides the correct amount of

energy needed to bring the air-stream up to the desired temperature. It is important that the temperature sensor be placed far enough away from the heaters to sense the true temperature of the air stream. In addition to the proportionally controlled heaters, two 18 kW industrial duct heaters are also built into the loop. These duct heaters are controlled in 3 kW increments by hand set switches and are used primarily to provide high temperature step inputs for thermal storage device testing.

Based on analysis and experience gained during this test program, it is felt that steady-state conditions are easier to maintain if the temperature difference between inlet fluid and ambient air is held constant rather than holding the inlet fluid temperature constant alone. Thus, electric duct heaters with no controls (other than manual) can be used when operating the test equipment in an open-loop configuration. Since ambient temperature is fairly constant over typical test periods, the test requirements in the current Standard 93-77 can still be met.

The dry bulb and wet bulb temperatures of the air stream are measured just downstream of the air reconditioning apparatus in order to be able to determine the specific volume and humidity ratio of the air. Both are measured using thermocouples, the latter with a saturated thermocouple exposed to the air stream. The humidity ratio is used in the calculation of air flow rate as explained in Appendix A and needs to be measured at only one point in the loop.

The secondary flow-measuring apparatus is a commercial unit consisting of air flow straighteners upstream of an averaging pitot tube arrangement. An aluminum honeycomb flow straightener precedes a pitot tube station. The pitot tube station consists of several total and static pressure taps carefully spaced to produce an average duct velocity reading. The static and total pressure taps are connected to common static and total pressure manifolds. The pressure difference between the two manifolds is read by a 0-0.25 kPa (0-1 in. H_2O) slant gauge manometer and a "cfm meter". The "cfm meter" is a bourdon-tube pressure gauge with a cfm scale calibrated to match the specific design of the unit. This dial reading was only used to adjust the blower and its dampers to the approximate flow rate desired for a particular test. This secondary flow-measuring apparatus was found to yield flow rates approximately 15% high when calibrated against the nozzle apparatus.

3.3 METEORLOGICAL MEASUREMENTS

The specifications for the instrumentation is given in Table 3. Two types of ambient air sensors are being used in conjunction with a standard calibrated total immersion, ASTM liquid-filled thermometer. One is a type-T calibrated thermocouple and the other a precision platinum resistance thermometer. The liquid-filled and resistance thermometers are accurate to within ±0.1°C (±0.2°F) while the calibrated thermocouple uncertainity is ±0.1°C (±0.2°F). All are housed within a well ventilated small instrument shelter located 1.25 m (4.1 ft) above the ground with its door facing north.

The wind speed is measured by a 3-cup wind anemometer delivering a dc voltage proportional to the wind velocity. Being mounted upon a portable adjustable base, the wind anemometer can be located close to any tested collector and adjusted in height. As the result of a wind tunnel calibration, the resulting uncertainty in wind velocity measurement is $\pm$0.35 m/sec ($\pm$ 0.8 mi/h).

The wind direction was recorded by visual observation of a directional wind vane during each test interval for the first part of the test program. Later in the testing program, a weather vane producing an analog output proportional to wind direction was installed to continuously monitor wind direction.

For measuring total solar radiation incident on a solar collector two types of pyranometers were used. Initially, a "black-and-white" model 8-48* pyranometer was used and was later replaced with an "all-black" model PSP*. Both pyranometers have a thermopile sensing element and similar protective dome glazings but differ in the receiver optical coatings and patterns. An intercomparison was made between two of the model 8-48 instruments and a model PSP when all were tilted at several angles from the horizontal up to 56°, typical of collector tilt angles to be used in testing. The results are shown in Table 4. There was as much as a 7.4% difference even though the instruments agreed within 1.5% in the horizontal position. Similar experiences by other researchers in the field lead to the adoption of the requirement for using a first class pyranometer as classified by WMO [5]. The model PSP pyranometer is capable of an uncertainity of $\pm$ 3.0% and has been shown to have typical tilt errors of less than 0.9% for angles ranging from 0° to 50°. These data were obtained during an intercomparison against an Angstrom pyreheliometer.**

The pyranometer is mounted on an adjacent surface parallel to the collector in such a manner that it does not cast any shadow onto the collector. Care is taken to insure that the pyranometer is at the same tilt as the solar collector and to minimize reflected and reradiated energy from the solar collector onto the pyranometer. The typical mounting scheme is shown in Figure 25.

The diffuse component of the incident solar radiation is determined for each efficiency test point by shading the pyranometer following the recommended technique of reference [4] (see Figure 26).

---

*Eppley Laboratories, Newport, Rhode Island.

**Personal communications with the Solar Energy Research and Educational Foundation, Washington, D.C.

In addition to monitoring the total solar radiation, the direct normal radiation is measured using a pyrheliometer. The pyrheliometer tracks the sun and thereby measures the direct normal incident solar radiation throughout the day.

The sky temperature is being determined for some tests by the use of either of two instruments. One is a commercially-available pyrgeometer and the other is a net radiometer designed and built by the French Building Research Center for NBS and described in Appendix B. Both the pyrgeometer and net radiometer are located within the collector plane. Based upon a calibration against a blackbody source, the pyrgeometer is capable of determining the absolute incoming long wave radiation to an uncertainity of $\pm$ 3% over the spectrum of 0.35 to 50μm. The net radiometer has a greater degree of uncertainty (typically $\pm$ 8% in net radiation) when compared against the pyrgeometer. The principal cause of the large uncertainty is suspected to be the variable effective optical properties of the net radiometer in response to exposure and solar spectral distribution.

Barometric pressure is determined periodically throughout the test period using a precision barometer.

A special incident angle meter was designed and built for determining the angle between the sun's direct beam and the outward drawn normal to plane of the collector aperture. A schematic drawing of the meter is shown in Figure 27. The principle of operation is very similar to that of a sun dial. It consists of two flat 0.64 cm (1/4 in.) thick clear plastic 10 cm x 10 cm (4 in. x 4 in.) sections joined and braced orthogonally. The vertical clear plastic member contains a quarter-circular graduated scale in angular degrees identical to a protractor, and a shadow pointer located at the center of curvature of the angular scale. In operation, the meter base is placed on the surface of the collector and rotated until the shadow cast by the pointer is located within the plane of the vertical member. The incident angle is then determined by the intersection of the shadow and the graduated scale. The incident angle meter has consistently agreed to within 1° to 2° when compared against the analytically-predicted incident angle upon a tilted surface for typical test conditions.

3.4 DATA ACQUISITION

A variety of data are monitored and recorded by the data acquisition system and other recorders. Data such as flow rates, temperatures, and pressures in the air and liquid collectors test loops as well as meteorological data are read into one central instrumentation room. The room is environmentally controlled and is located between the air and liquid collector test loops as shown in Figure 11.

The input signals from the various test loop transducers consist of analog voltage, digital voltage, or variable resistance. Analog signals are produced by thermopiles, pyranometers, anemometers, or pressure

transducers; digital signals by liquid flow meters; and variable resistance from resistance thermometers. The digital and variable resistance signals are converted into analog signals before input to the data acquisition system. A flow rate monitor interprets and converts the flow transducer digital signals into analog form while separate individually matched and calibrated bridge amplifiers interpret and convert the resistance thermometer signals. Type-T thermocouples are provided with an automatic electronic reference junction or an ice bath.

After conditioning the input data into either analog or digital signals, the information is fed into the equipment shown in Figure 28. The equipment is comprised of a combination of strip chart recorders and electronic integrators connected in parallel with a data logger. The purpose of the strip chart recorders is to monitor pertinent specific information on a continuous basis while the data logger scans and records all the input data on a periodic basis. Information such as insolation, flow rates, and inlet-outlet temperature differences, are continuously recorded on strip chart recorders in order to readily observe any transients. Electronic integrators are periodically used to integrate quantities such as incident solar radiation or fluid temperature rise across a solar collector. The data logger scan interval should be as small as possible and has most often been one minute. Of course, the rate of data scanning should depend on the type and intensity of transients being monitored. The data logger is capable of calculating and recording the arithmetric average of up to 16 inputs over a specific time interval; thus the scan rate can be once per minute, whereas the average of the inputs can be automatically calculated and printed every five minutes. Both the scan rate and the averager time interval are independent and adjustable. Typically input quantities such as wind speed, air temperature, and collector fluid flow rate are averaged using the built-in averager and printed on paper tape for later analysis. Approximately half-way through the experimental study described in this report, a magnetic tape drive recording system was interfaced with the data logger system to expedite the data reduction on the NBS central computer facility.

Table 5 includes the specifications for the strip chart recorders, integrators, and data logger used.

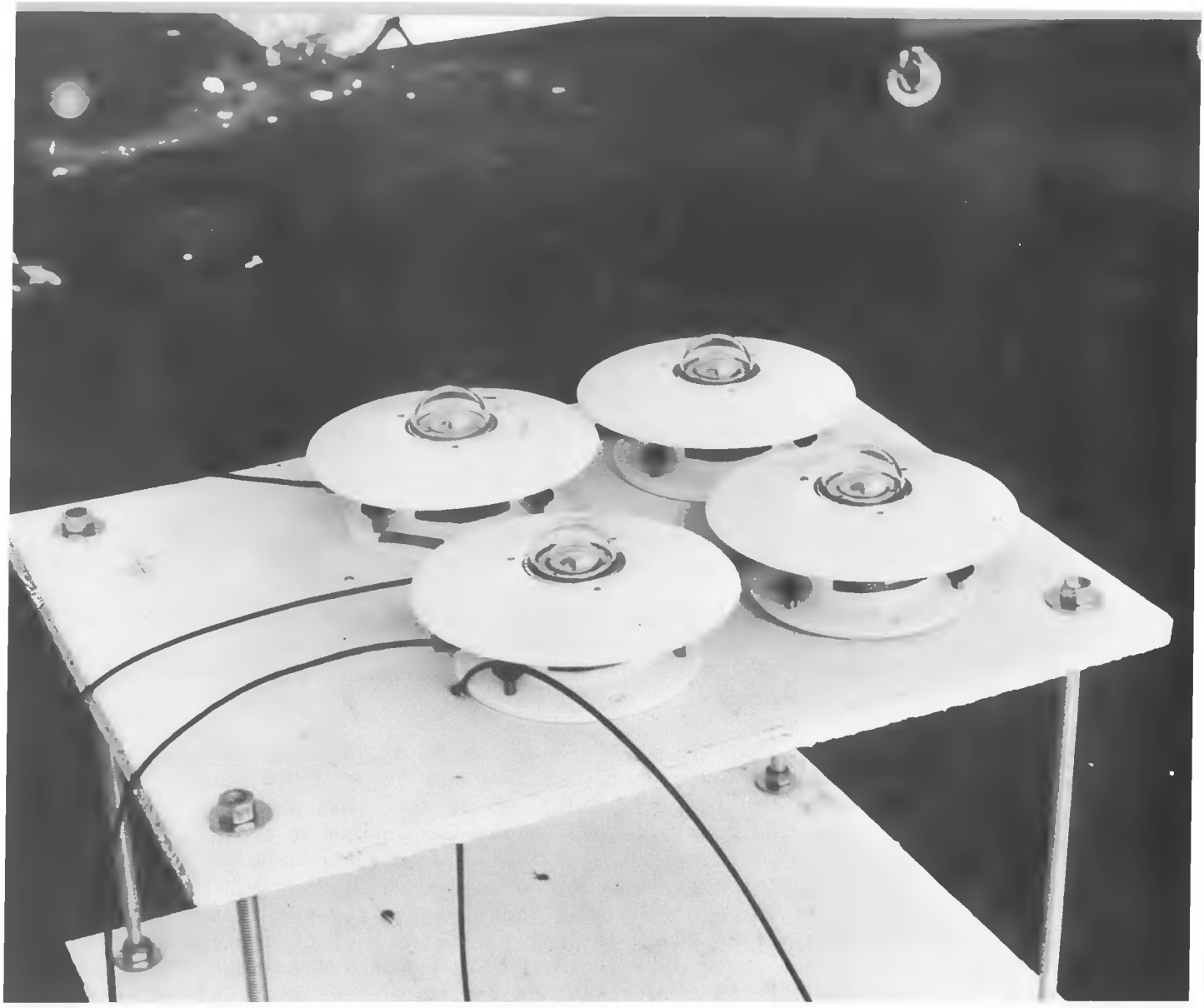

4. TEST RESULTS

During the period covered by this report (1976 and 1977), six different collectors were tested. They are described in Table 6. Five were liquid-heating collectors, the other an air heater. The following sections describe the tests conducted and results obtained.

4.1 LIQUID-HEATING COLLECTORS

Time Constant: The collector time constants were determined following the procedures described in Section 2.1 of this report and reference [4]. To provide a radiation step-change, the collectors were either suddenly shaded or unshaded with a white opaque cover suspended above the collector. The opaque cover is shown in place above collector no. 4 in Figure 29. In the case of the linear Fresnel lens tracking collector (collector no. 5), the step-change was accomplished by rotating the collector off the track of the beam radiation toward the diffuse sky.

A graph of inlet and outlet temperature for collector no. 1 during a time-constant test when the collector was suddenly shaded is shown in Figure 30. The time constant of each of the five liquid-heating collectors is given in Table 7. The tabulated time constant was calculated by averaging the results from numerous tests where the collector was both shaded and unshaded. On the average, the difference in the measured time constant between shading and unshading was less than 6%. In order of decreasing magnitude, the time constant was largest for collector no. 4 then collectors no. 3, 2, 1, and shortest for collector no. 5. Collectors no. 3, 2, and 1, being of the flat-plate design, exhibited very similar time constants (on the order of 100 s). The short time constant (55 s) for collector no. 5 was due to a smaller absorber mass and high flow rate compared to the flat-plate collectors. The very large time constant (20 min.) for collector no. 4 was primarily the result of a large collector fluid capacity (34 liter (9 gal.)) and a very low flow rate (0.018 liter/s(0.3 gal./min.)).

The alternate technique of conducting the test indoors and suddenly changing the inlet fluid temperature was used for one collector and found to give comparable results. However, this technique is much more difficult to use experimentally.

During the deliberations that led to the adoption of ASHRAE Standard 93-77, there was controversy over what time constant is actually being determined by this test. In reality, there can be more than one time constant for a given collector since the various components of the collector respond over a different time period to a sudden change in the solar insolation conditions. Although not shown in Figure 30, several strip chart recordings of the exit temperature from the flat-plate collectors during a time constant test indicated another noticeable but more gradual response after 6 or 7 min. which was an indication that some parts of the collector were just beginning to respond. The time constants indicated in Table 7 and determined in accordance with Standard 93-77, are primarily a function of the fluid dwell time and the absorber plate response.

Near-Normal-Incidence Efficiency: Collector no. 1 was the first collector tested. It was encased within a wooden frame on the edge in order to simulate the effect of adjacent collectors that would exist in an actual field installation. This was felt to be particularly important for this collector due to a design that put the absorber plate in intimate contact with the edge of the collector case. Throughout the testing of this collector, the "black-and-white" model 8-48 pyranometer was used for measuring the incident solar radiation in the plane of the collector aperture. As already mentioned in Section 3.3 of this report, possible errors exist in the efficiency values due to the collector being tested at tilt angles (from the horizontal) of 20-40°. Correction factors were not introduced to account for the pyranometer error in analyzing the data for this collector since no reproducible correction factors have yet been determined for this

pyranometer. For example, the data from Table 4 indicates the correction factor could be anywhere from 3.9% to 7.4% for the 45° tilt position depending on the insolation level and the particular instrument used.*

A more comprehensive laboratory study has recently been completed [19] in which the error is indicated to be only between 1.5 and 2.0%. This pyranometer was not used for any further tests following the tests on collector no. 1.

The results of the efficiency tests are shown in Figures 31 and 32. The efficiency values are based on the aperture area of the collector, 1.61 m^2 (17.3 ft^2). In Figure 31, all data were taken at solar noon on a number of different test days whereas in Figure 32, the data were taken ± 3/4 h symmetrical with solar noon. A linear regression** curve fit of the data in both figures resulted in identical curves. Therefore, for this type of collector, the data scattering caused by collector thermal capacitance can be averaged out if care is taken to make the measurements symmetrical with solar noon as required by [4].

A solar screen was placed over the collector as shown in Figure 33 to reduce the solar radiation incident upon the collector. The screen was a flat-weave opaque glass fiber type and allowed efficiency data to be taken at larger values of $\Delta t/I$. Normally, test data are obtained over the entire range of $\Delta t/I$ values primarily by changing the operating temperature of the collector, $t_{f,i}$. This is because the ambient temperature and incident solar radiation are generally fixed (within limits) for the location and time of year in which the test is being conducted. However, Figure 32 shows that is was possible to establish part of the efficiency curve by using the screen. This technique is not generally recommended since in reality using lower insolation levels is not equivalent to operating the collector at elevated temperatures. However, the error is small for flat-plate collectors which operate at relatively low temperatures (<80°C (175°F)).

Figures 34 and 35 show the results of the efficiency tests for collectors no. 2 and no. 3 (again based on aperture area). The edges of these collectors were not encased in a wooden frame nor insulated on the edge due to a good thermal design of the modules themselves.

Collector no. 4 was a single-glazed evacuated tubular collector with a back diffuse reflector. The results of the efficiency tests are shown

---

*This is assuming the calibration factor for the "all-black" model PSP does not change with the tilt angle.

**It is felt that a linear plot is adequate for most collectors. Even though collectors don't have a constant heat loss coefficient as is indicated by a linear plot, data scatter caused by variable ambient conditions and experimental uncertainties prevent the determination of the "true" 2nd-order response of the collector.

in Figure 36 and a photograph of the collector under test is shown in in Figure 25. The collector array consisted of two modules connected in parallel. The large thermal time constant resulting from the large collector fluid capacity and low operating flow rate coupled with a large temperature rise across the collector contributed to problems of stabilization during testing. Extreme care had to be taken to eliminate any perturbations within the collector to insure steady-state conditions. At least one hour was allowed for temperature stabilization after reaching operating conditions. The time interval over which the experimental data are collected and integrated should be at least one time constant, according to [4], amounting to a period of 20 min. for this collector. Initially, a period of one hour was used for integration and it was found the 20 min. period resulted in efficiency values only 1.2% different for data collected across solar noon.

The aperture area was used in computing the efficiency values in Figure 36 and was interpreted as the area of the collector tubes and the interstitial spacing between the tubes excluding the end brackets and center manifold.

Collector no. 5 was a tracking, concentrating collector utilizing a linear Fresnel lens and a selective-black-chrome-coated absorber. The efficiency curve is shown in Figure 37. The tested collector consisted of two modules connected in parallel, whose tilt angle could be periodically adjusted and which automatically tracked the diurnal movements of the sun. The tested modules are shown in Figure 38. In Figure 37 two curves are shown, one representing a 0° incident angle efficiency and the other a 23° incident angle efficiency. The efficiency values in Figure 37 were calculated, only using the direct component of the solar radiation and based on the aperture area of 1.8 m^2 (19.4 ft^2). During three of the five days of testing, the collector tilt angle was such that the incident angle across solar noon was 23°. On two other days, the collector had an incident angle of 0 and 10° across solar noon. Based on results obtained by Pendleton [20], the incident angle has little or no effect for angles up to 10 degrees. Therefore, a single curve was used for data collected at 0 and 10 degrees. Note that the efficiency decreases by 8% for an incident angle of 23° at solar noon. This is equivalent to the yearly declination variation for a collector tilt angle equal to the latitude.

Figure 39 shows the results of the near-normal-incidence efficiency tests for all five of the water-heating collectors. The efficiency values are based on the aperture area as given in Table 7. The data are replotted in Figure 40 with the efficiency values based on gross collector area as required by ASHRAE Standard 93-77. The change in efficiency between these two figures is small for collectors 1 through 4 since there is only a relatively small difference in aperture and gross area for these collectors (<15%). For collector no. 4, the gross area was assumed to to include the end brackets and center manifold. There is a large change in the efficiency of the concentrating collector (collector no. 5) because of the authors' interpretation of gross area for this collector. The aperture area of collector no. 5 was assumed to be the frontal area

of the linear Fresnel lens; the gross area was calculated based on the center to center spacing between individual collectors.

During all tests, the pressure drop across the collector was measured and recorded. Figures 41 and 42 show how the pressure drop varied as a function of flow rate for one of the flat-plate collectors (Figure 41) and the evacuated tubular collector (Figure 42).

Incident Angle Modifier: Two different techniques were used to determine the incident angle modifiers of the water-heating collectors. The first technique involved keeping the collector test stand stationary with the collector facing south, as was done when determining the near-normal-incidence efficiency, and allowing the incident angle to change with respect to the diurnal movement of the sun. In this procedure, the instantaneous collector efficiency was determined throughout the day as a function of incident angle, and morning and afternoon values (for the same incident angle) were averaged to eliminate the thermal lag effect. In this way, the incident angle modifier was determined for a wide range of incident angles in one day. The second technique involved orienting the test stand so that the collector faced north but tilted to a near-horizontal position with the tilt angle adjusted in order to obtain a specific incident angle across solar noon. With this procedure, it was only possible to obtain one value of incident angle modifier per test day.

The results for collectors no. 1, 2, and 3 are shown in Figures 43, 44, and 45, respectively. The second technique described above was used to obtain the curves shown in Figures 43 and 45. Both techniques were used for collector no. 2 and, as can be seen in Figure 44, gave comparable results. The second technique or orienting the test stand to the north was used to determine the solid line in the figure. The first technique was completed in one day, the data points indicated by circles taken in the morning and those by triangles in the afternoon. The dashed line is a curve fit through the average of these points. As can be seen by the fact that the circles and triangles are relatively close together, there was only a small thermal lag with this collector. This is consistent with its small time constant of 1.6 minutes. As can also be seen in Figure 10, there was essentially a linear relationship between $K_{\alpha\tau}$ and the term $(1/\cos\theta) - 1$, which is consistent with the theoretical model for optical efficiency of a flat-plate collector [17].

Figure 46 shows test results for collector no. 4, the evacuated-tubular collector. Note that the thermal lag effect is more pronounced in Figure 46 than in Figure 44 which is consistent with the fact that collector no. 4 has a time constant of 20.3 minutes. In addition, the incident angle modifier increases with increasing incident angle, the opposite from that of the flat-plate collector in Figures 43-45. Since the tubes were not used with a concentrating reflector, this tubular collector has its minimum efficiency at solar noon and larger values at other times of the day. This is explained by the fact that the tubes intercept a larger fraction of of the incoming solar radiation at the large incident angles and also that the transmittance of solar

radiation through each glass cover tube does not change with time of day since the sun is practically always normal to the glass surface.

With simple glazed flat-plate collectors, the incident angle modifier varies in a smooth manner with incident angle and is basically independent of orientation (except for perhaps secondary effects due to changes in tilt and hence convection heat loss or different shading of the absorber by the collector frame at different orientations). The testing procedure in Standard 93-77 for determining the incident angle modifier was based on these characteristics and as a result is only really valid for simple flat-plate collectors. The way in which the test should be conducted for other types of collectors depends in general on the specific collector being tested. For example, the tubular collector tested and described in this report is sensitive to changes in incident angle due to changes in both the sun's altitude angle and hour angle. Therefore, determination of two incident angle modifiers would be appropriate; one describing how the collector's efficiency changes as the angle between the outward drawn normal and direct beam increases in a direction parallel to the axis of the tubes and a second modifier for the direction perpendicular to the tube's axis. The data in Figure 46 were determined by keeping the collector facing south in a fixed position with the tilt adjusted so that the incident angle was zero at solar noon. Therefore, the data is representative of changes due primarily to a change in the diurnal hour angle.

A testing procedure to get the two incident angle modifier curves for a non-movable trough-type concentrating collector with an east-west axis using a south-facing outdoor test stand has recently been described by Thomas [21]. In a similar fashion, Johnson [22] has demonstrated the difficulty of this type of testing for a single-glazed flat-plate collector. The collector had a non-selective coating on a copper roll-bond absorber. Mylar strips running the width of the collector were installed between the absorber and glazing to decrease convection and reradiation losses. The strips were approximately 10 cm (4 in.) deep and 0.95 cm (0.37 in.) apart. The optical characteristics of this collector were similar to that of a trough-type concentrator with the trough axis running east-west.

Figure 47 shows the results of tests conducted by Johnson using an indoor simulator at the NASA Lewis Research Center. With the collector tilted at 57° and oriented normal to the simulator source, the collector was then rotated about a vertical axis and data taken to establish the upper dashed curve. Then the tests were repeated for other tilt angles as indicated. Unfortunately, by rotating the collector about a vertical axis, the angle between the "sun's" beam and both principal axes in the plane of the collector aperture were changing simultaneously. As a result, the effect of incident angle changes perpendicular to each principal axis could not be isolated. Notice in the figure that with each of the lower three dashed curves, one of the data points lies far from the indicated curve.

If the tests were to be repeated, the collector orientation could be changed in such a way as to establish two incident angle modifiers for the collector. To show both effects, a family of curves should be plotted for $K_{\alpha\tau}$ as a function of the incident angle projected into an east-west plane with β_1 of Figure 48 as a parameter. The test itself would be relatively easy to conduct using a simulator.

The experimental incident-angle-modifier curves for collectors no. 1-4 are shown collectively in Figure 49 and in Figure 50 in comparison with the theoretically-predicted curves for single and double-glazed flat-plate collectors with non-selective coated absorbers exposed to direct beam radiation. The experimental results are in approximate agreement with the theoretical curves. The differences are due to several reasons. Collector no. 2 was a double-glazed collector but its incident angle modifier was not as dependent on incident angle as was expected from the theoretical curve. The experiment was conducted under 18-40% diffuse radiation which should cause the collector's efficiency to decrease less with incident angle than if it were exposed to 100% direct beam radiation. In contrast, the efficiency of collector no. 3 decreased more rapidly than would have been though since it was a single-glazed collector and tested under 11-24% diffuse radiation. However, the absorptance of the selective surface on the absorber could have been a function of incident angle and hence caused the indicated response. The angular response for collector no. 1 may be in error due to (1) the use of the "black-and-white" pyranometer during the tests or (2) as a result of 15-25% diffuse radiation during the test.

An incident angle modifier was not determined for collector no. 5, the tracking, concentrating collector. As with collector no. 4, two incident angle modifiers would be in order. The value of one of them, that which describes the change in efficiency as the angle between the direct beam and the outward drawn normal increases in a direction perpendicular to the axis of the concentrator, is identically 1 since this collector tracks the sun in the east-west direction to a tolerance of 0.2°. However, the collector tilt angle is not normally changed during the year to reflect changes in the sun's declination. Therefore, an incident angle modifier should be used to account for the resulting change in performance. As already indicated in Figure 37, efficiency data were taken on this collector for constant incident angles of both 0° and 23°. The incident angle modifier was computed, based on these data, and is shown in Figure 51. Additional tests could be conducted at other angles to establish a complete incident-angle-modifier curve for this collector.

4.2 AIR-HEATING COLLECTORS

Time Constant: Figure 52 shows results of the time constant test on collector no. 6, the air heater. The test was conducted outside under a clear, sunny sky by shading the collector after steady-state conditions had been reached. Initially the fluid entered the collector at 28.5°C (83.3°F) and exited at approximately 63°C (145°F) with a flow rate of

0.01 $m^3/(s.m^2)$ (2 $ft^3/(min.\ ft^2)$. As can be seen, the time constant was found to be approximately 12.7 minutes. This is much longer than for flat-plate collectors which use water as the transfer fluid, but less than that for the water-heating evacuated-tubular collector (collector no. 4).

Near-Normal-Incidence Efficiency: Figure 53 shows the results of the near-normal-incidence efficiency tests for the air heater. As can be seen, curves are shown for two different flow rates. A recommendation is given in Standard 93-77 that two different curves be established because, unlike water-heating collectors, the efficiency of air heaters is significantly affected by flow rate. The curves in Figure 53 are based on the gross area of 7.25 m^2 (78.0 ft^2) as recommended in the Standard. Figure 54 shows how the curve for the test with the lower flow rate changes if the aperture area were used to compute efficiency.

The efficiency values in Figure 53 are lower than expected, based on theoretical predictions for this collector. It was found during the test that air was leaking into the four-module array. Air leakage in air heaters is a troublesome problem that can affect test results, as well as the actual performance of an installed system. During testing, the test loop can be sealed sufficiently well with duct tape, caulking, etc. Leakage in and around the collector may occur as a result of the collector design and recommended installation practice. This type of leakage of course should not be eliminated. However, measurements should be made in such a way as to determine the true output of the collector array. In addition, the array should be tested in a manner such that the air leakage occuring during the tests will be indicative of the leakage that will occur in an actual installation.

Close and Yasoff [23] have recently published the results of an analysis of air leakage in air-heating collectors. They assumed a constant leakage rate along the length of the collector and determined its effect on the efficiency measurements for all combinations of:

a. operating the collector under negative pressure (air leaking in) and positive pressure (air leaking out), and

b. measuring the air flow rate before (upstream) the collector or after (downstream) the collector.

The results are shown in Figure 55. The abscissa of the plots is the leakage rate divided by the measured flow rate and the ordinate is the ratio of the actual collector efficiency to the measured efficiency. As can be seen, for three of the testing configurations, the discrepancy between measured and actual efficiency is a direct function of the leakage rate. In addition, for the case where the collector is operating under negative pressure and air is leaking in, the difference in efficiency depends on the difference in temperature between the ambient air and the entering air stream to the collector. Therefore, the error in efficiency for this case is larger for the data points at the higher

inlet fluid temperatures relative to ambient. Also note that when the air leaks in, the actual efficiency is larger than indicated by the measurements whereas just the opposite is true when air leaks out. This is consistent with what one would intuitively expect. When air leaks into the collector at a cooler temperature than is measured at the collector inlet, the collector is heating up the air over a larger temperature difference than is indicated by the measurements. In addition, if the air flow measurement is upstream of the collector, the collector is heating a larger quantity of air than is indicated by the measurements. When air leaks out of the collector, and the flow rate is measured upstream, the quantity of useful heated air is less than indicated by the measurements. However, if air leaks out and the air flow measurement is made downstream of the collector, the quantity of useful heated air is precisely what is measured and as a result, there is no difference between actual and measured collector efficiency. Data for this case are not shown in Figure 55 since they would produce a horizontal straight line with an ordinate value of 1.

The results of the above analysis have a direct implication for the testing of air-heating collectors:

1. If the collector is normally operated under positive pressure, it should be tested while operating under positive pressure and the air flow rate measured downstream of the collector.

2. If the collector is normally operated under negative pressure, it should be tested while operating under negative pressure and the air flow rate measured both upstream and downstream of the collector in order to quantify the leakage rate. In this manner, an estimate of the actual collector efficiency could be made by the user of the collector with the data of Figure 55 even though the "correction" might not be made and published as part of the test results.

The data of Figure 53 were obtained with collector no. 6 operating under negative pressure (normal installation practice for this collector) and the flow rate measured downstream of the collector. Use of "smoke-bombs" around the collector indicated air leakage into the collector. Therefore, the actual collector efficiency was higher than that indicated in Figures 53 and 54.

As indicated by equation (1), the useful heat output of the collector is directly proportional to the collector heat removal factor, F_R. If the collector test results are to be used without correction to predict the performance of the collector in an actual field installation, then the value of F_R which occurs during the test should be approximately the same as that which will occur in the field. The expression for F_R is [14]:

$$F_R = \frac{\dot{m}c_p}{AU_L} \left\{ 1 - \exp - \left[\frac{AU_L F'}{\dot{m}c_p} \right] \right\} \qquad (7)$$

Therefore, the conditions during testing and in actual field operation should be such that $\dot{m}/A$, c_p, U_L, and F' are approximately the same in both cases. For liquid-heating collectors, this is easy to accomplish. The flow rate per unit collector area, $\dot{m}/A$, the type of fluid and hence specific heat, c_p, and the collector tilt angle, temperature, incident solar radiation, and ambient conditions are such that the heat loss coefficient, U_L, is approximately the same. In addition, the collector efficiency factor, F', is primarily a function of the geometry of the absorber (material, thickness, distance between tubes, etc.) and of course is the same for the tested and installed collectors at any flow rate.

The situation is slightly different for air heaters. Although $\dot{m}/A$, c_p, and U_L can be made the same in a similar fashion as with the liquid-heating collectors, assuring the same value of F' is more difficult. For air heaters, F' is primarily a function of the convection heat transfer coefficient between the absorber and the air stream. Since the air flow is nearly always in the turbulent flow range (to maximize the heat transfer), the heat transfer coefficient is determined primarily by the value of the Reynolds number in the collector. For a collector designed with a simple rectangular channel under the absorber such as in collector no. 6, the Reynolds number is given by:

$$Re = \frac{VD_H}{\upsilon} \tag{8}$$

where V = velocity of the air in the collector, m/s

D_H = hydraulic diameter of the channel through which the air flows, m

υ = kinematic viscosity of the air, m^2/s

Since the hydraulic diameter of the channel is equal to twice its width, equation (8) can be rearranged to give:

$$Re = \frac{2}{\mu}\frac{\dot{m}}{A}L \tag{9}$$

where

μ = dynamic viscosity, Pa•s

L = flow path length of the collector array, m

Consequently, since the mass flow rate per unit area is being maintained the same between the tested collector and the value to be used in the field installation, the length of the collector or flow path length should be maintained to insure the same Reynolds number, convection coefficient, and hence F'.

The particular collector tested in this program is designed to be installed in the field with two modules in series and a flow path

length of approximately 4 m (13 ft). Therefore, four modules (two in series and in parallel with two others) were used in obtaining the data of Figure 53.

It would be useful to be able to test only one collector module and then apply a correction technique to the data in order to predict the performance of an array consisting of two or more collectors in series. This would simplify the testing of air heaters. Two techniques are suggested here for doing this. In both techniques, the single module must be tested at a flow rate that will result in the same flow velocity which will occur in the array of collector modules in series. This will insure the same Reynolds number, same convective heat transfer coefficient, and hence same F'. As an example, if one collector module were being tested and two are normally installed in series, by equation (9), the flow rate per unit collector area to be used in the test would be twice the value to be used in the actual installation in order to have the same Reynolds number and the same flow velocity.

Technique No. 1*:

After the test on the single module is completed, the y intercept of the efficiency curve is determined and set equal to $F_R(\tau\alpha)_e$. By separate measurement or calculation, $(\tau\alpha)_e$ is determined for the cover plate assembly. F_R is then calculated. In a similar fashion, the slope of the efficiency curve is set equal to $F_R U_L$ and then U_L is calculated from knowing F_R. From the above information and knowing $\dot{m}c_p$ for the test, equation (7) is used to compute F'. Assuming F' and U_L to be the same for the collector modules in series, the new value of mass flow rate per unit collector area is used to calculate the value of F_R applicable for the modules in series from equation (7). The new efficiency curve is then constructed from the value of F_R, $(\tau\alpha)_e$, and U_L.

Technique No. 2:

A correction factor is applied to the test data on the single module. The correction factor is derived as follows. Equation (1) governs the performance of the single collector. For two collectors in series:

$$q_u = \frac{A}{2}\left[F_R I(\tau\alpha)_e - F_R U_L (t_{f,i} - t_a)\right] + \frac{A}{2}\left[F_R I(\tau\alpha)_e - F_R U_L (t_{f,e,1} - t_a)\right] \qquad (10)$$

*Suggested by Bruce Cole-Appel, Solaron Corporation, Denver, Colorado.

where

$t_{f,e,1}$ = the exit fluid temperature of the first collector equal to the inlet fluid temperature of the second, °C

Solving equation (1) for the exit fluid temperature of the first collector,

$$t_{f,e,1} = t_{f,i} + \frac{A}{\dot{m}c_p} [F_R I(\tau\alpha)_e - F_R U_L (t_{f,i} - t_a)] \qquad (11)$$

Substituting equation (11) into equation (10) and rearranging,

$$q_u = A[F_R I(\tau\alpha)_e - F_R U_L (t_{f,i} - t_a)] \left[1 - \frac{1}{2} \frac{AF_R U_L}{\dot{m}c_p}\right] \qquad (12)$$

The single module is tested and its efficiency curve determined. Then a new efficiency curve is established by correcting the collector output for the single module by the multiplying factor

$$\left[1 - \frac{1}{2} \frac{AF_R U_L}{\dot{m}c_p}\right]$$

In a similar fashion, the correction factor for applying the single module test results to three modules in series can be shown to be,

$$\left[1 - \frac{AF_R U_L}{\dot{m}c_p} + \frac{1}{3} \left(\frac{AF_R U_L}{\dot{m}c_p}\right)^2\right]$$

and to four modules,

$$\left[1 - \frac{3}{2} \frac{AF_R U_L}{\dot{m}c_p} + \left(\frac{AF_R U_L}{\dot{m}c_p}\right)^2 - \frac{1}{4} \left(\frac{AF_R U_L}{\dot{m}c_p}\right)^3\right]$$

The second technique above was verified by conducting an experiment on one-half of the four module array of collector no. 6. Two of the modules were connected in parallel and efficiency data were gathered for a flow rate per unit collector area of 0.02 $m^3/s.m^2$ (4 $ft^3/min.\ ft^2$). Therefore, the flow path length was only one-half of that used when gathering the data shown in Figure 53 but the flow rate per unit area was twice the value of 0.01 $m^3/s.m^2$ (2 $ft^3/min.\ ft^2$) used for those

tests. The results of these second tests and comparisons were as follows:

	Two Module Test	Corrected to Four Module Performance	Four Module Test, Figure 53
$F_R(\tau\alpha)_e$	0.52	0.46	0.46
$F_R U_L$ ($W/m^2 \cdot °C$)	5.61	4.95	4.69

The data from the two tests are shown together in Figure 56 along with additional data for the two collector modules in parallel tested at a flow rate of only 0.01 $m^3/s \cdot m^2$ (2 $ft^3/min \cdot ft^2$), indicated by the data in triangles and the long-short dash curve.

The discrepancy noted above between the heat loss factor, $F_R U_L$, for the four module array and the corrected heat loss factor from the test on the two modules in parallel at twice the flow rate per unit area could have been due to the different leakage rates which occured during the two different tests.

Incident Angle Modifier: Figure 57 shows the results of the incident angle modifier test being run on the air heater using both of the techniques that were used with the liquid-heating collectors. As can be seen, there was a large difference in the results using the two different procedures. The most reasonable result was obtained by keeping the collector stationary, facing south and using the efficiency data all through one test day to obtain the incident angle modifier values indicated by the triangular data points in Figure 57. Notice the large difference between the morning and afternoon values. This is consistent with the large time constant of the collector and is the same characteristic that was observed for collector no. 4 and shown in Figure 46. The second technique of orienting the test stand to the north and tilting the collector so that a specific incident angle occurs across solar noon gave completely erroneous results as indicated by the circular data points in Figure 57. This is not considered an acceptable procedure for collectors with large time constants.

4.3 ALL-DAY SOLAR COLLECTOR EFFICIENCY

Based on the tests run according to ASHRAE Standard 93-77, it is possible to predict the all-day performance of the solar collector. In addition to having the two curves of near-normal-incidence efficiency and incident angle modifier, the following must be known as a function of time throughout the day:

1. inlet fluid temperature to the collector, $t_{f,i}$

2. ambient temperature, t_a, and

3. incident solar radiation in the plane of the collector, I

The step by step procedure in Table 8 can then be carried out. A similar procedure has been used and reported by Zerlaut, Dokos, and Heiskell [25].

Three separate all-day tests were conducted on collectors no. 2 and no. 3 in which the all-day efficiency was measured. The test days were completely clear with steady insolation. The above procedure was used to compute the all-day efficiency using the same test conditions ($t_{f,i}$ and I) and the incident angle modifier and near-normal-incidence efficiency curves previously determined. The results are given in Table 9 and a comparison of instantaneous efficiency throughout one of the test days for collector no. 3 is shown in Figure 58. As can be seen, the agreement is very good.

The all-day collector performance can of course be determined by experiment as was done above. Many researchers over the past several years have proposed that this would be a preferable way to collect data and report performance instead of performing separate tests to determine the near-normal-incidence efficiency and the incident angle modifier. Indeed, if a large amount of daily efficiency data were collected for all types of weather conditions and incident angle variations over perhaps a complete year, then a plot of daily efficiency versus daily $\Delta t/I$ would give a good estimate of the expected long-term performance of the collector in actual operation. This concept has been proposed by Tleimat, Howe, and Buckland [26] and has been successfully used by them to characterize the performance of solar stills. However, in solar collector testing, data are usually collected over as short a period as possible and only a few daily data points could lead to erroneous performance predictions.

It should be recognized that on a plot of daily efficiency versus daily $\Delta t/I$, the y intercept of the plot is:

$$F_R(\tau\alpha)_{e,n}\ \overline{K_{\alpha\tau}}$$

and not just

$$F_R(\tau\alpha)_{e,n}$$

where

$$\overline{K_{\alpha\tau}} = \frac{\int_{day} K_{\alpha\tau}\, I_{d\tau}}{\int_{day} I_{d\tau}} \qquad (13)$$

Consequently, the resulting curve is only valid for days in which the incident angle variation, percent diffuse radiation, and hence $\overline{K_{\alpha\tau}}$ are approximately the same as on the test days. Simon and Miller [27, 28]

have used a technique for adjusting all-day collector efficiency obtained outdoors to an effective efficiency value at normal incidence, in order to compare the test data with data obtained on the same collector indoors using a solar simulator. In essence, the all-day efficiency values and the daily average values of $\Delta t/I$ were both divided by a calculated value of $\overline{K_{\alpha\tau}}$ before plotting. $\overline{K_{\alpha\tau}}$ was calculated by knowing the incident angle variations throughout the test days as well as the curve of $K_{\alpha\tau}$ versus θ from previous tests*. The resulting comparison with the indoor near-normal-incidence data was excellent.

Figure 59 shows data taken over several days for collector no. 6, the air heater, and shows the kind of scatter that can exist when data other than those collected on clear sunny days is used. The maximum integration period used on any of the data in Figure 59 was four hours. Since this was a flat-plate collector tilted so that the incident angle was approximately 0 at solar noon and the data were all taken symmetrically with solar noon, the maximum incident angle for any of the data was approximately 30° and hence $\overline{K_{\alpha\tau}} \tilde{} 1$. Even though the scatter is relatively large, a mean curve through a large amount of such data should result in a reasonable performance curve for the collector in actual operation.

---

*The actual technique was slightly more complicated since Simon and Miller also accounted for the fact that the curve of $K_{\alpha\tau}$ was determined indoors using the simulator and hence under 100% direct radiation and the outdoor data was taken under condition of up to 50% diffuse radiation.

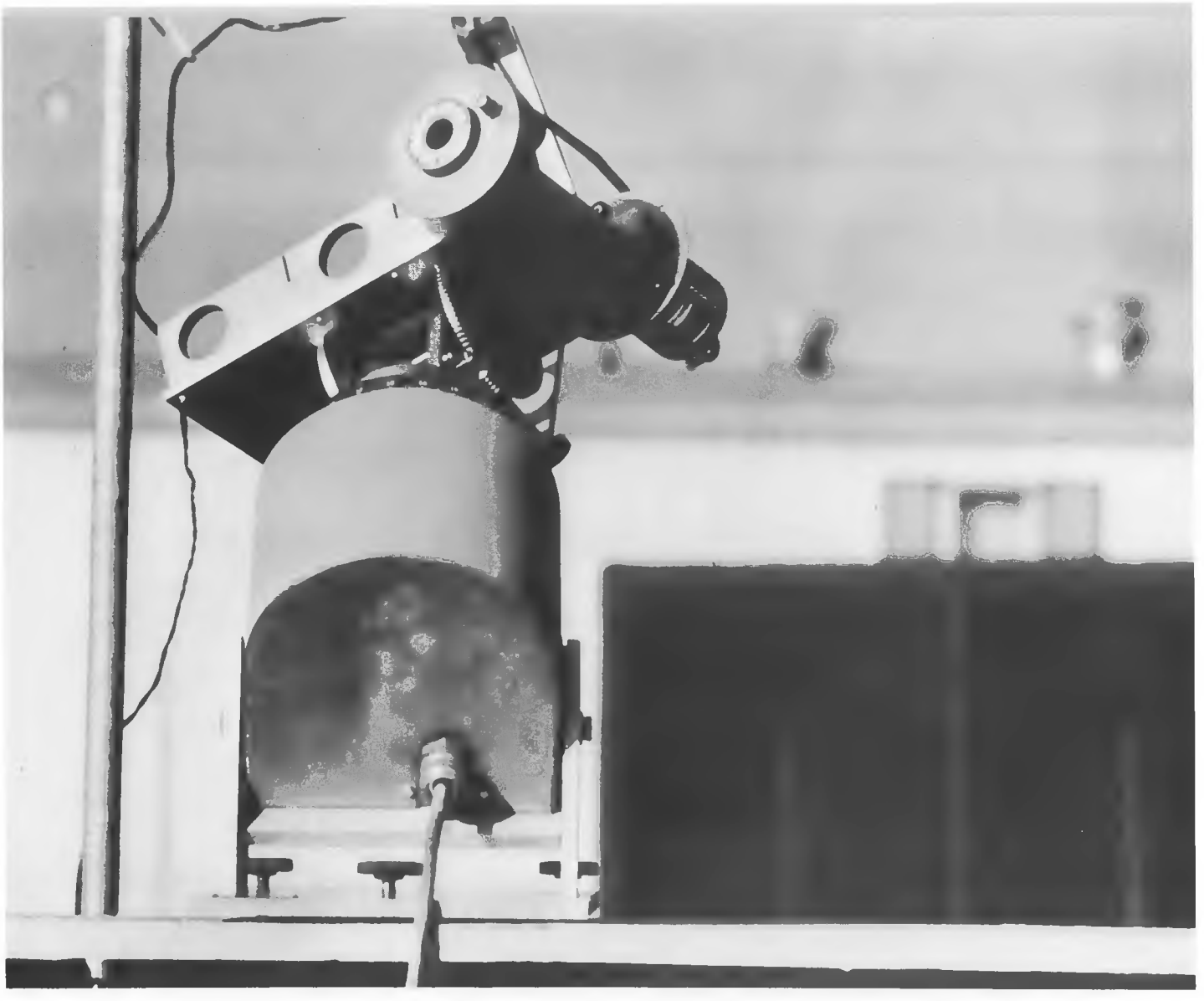

5. SUMMARY AND CONCLUSIONS

This report has briefly summarized the test procedure adopted in February 1977 by the American Society of Heating, Refrigerating, and Air Conditioning Engineers and known as ASHRAE Standard 93-77, "Method of Testing to Determine the Thermal Performance of Solar Collectors." A testing facility has been constructed at the National Bureau of Standards in Gaithersburg, Maryland, in accordance with this Standard. It consists of two test loops for the liquid-heating collectors and one for air-heating collectors. During 1976 and 1977, six different collectors were tested outdoors in accordance with the Standard or slight variations of the procedures in the Standard. The main conclusions of the study are:

1. The three primary thermal tests in the Standard, the time constant, near-normal-incidence efficiency, and incident angle modifier tests

can be carried out with little difficulty on flat-plate liquid-heating and air-heating collectors. The three day pre-conditioning test was not evaluated during this study for any collectors.

2. The time constant and near-normal-incidence efficiency tests can be carried out on an evacuated tubular water-heating collector and on a tracking, concentrating collector having a low concentration ratio with little difficulty. For collectors with large time constants (on the order of 20-30 min.) such as the evacuated tubular collector, the near-normal-incidence efficiency curve is more difficult to obtain because of the fewer test points that can be obtained during a single test day due to problems of stability and larger test intervals.

3. The incident angle modifier test as currently specified in Section 8.3.3 of the Standard is only applicable for flat-plate collectors. An entirely different procedure is required for other types of collectors and it will vary depending upon the optical characteristics of the collector. For example, a single-axis tracking collector should have the incident angle modifier determined as a function of the angle between the outward drawn normal to the plane of the collector aperture and the direct solar beam in a direction parallel to the axis of the collector. In contrast, a stationary evacuated tubular collector should have two incident angle modifier curves determined; one as a function of the incident angle in a direction parallel to the tubes and one perpendicular to the tubes.

4. The procedure for conducting the time-constant test in Section 8.3.1, Method (1) of the Standard, which involves suddenly shading the collector during an outdoor test, is much easier to complete and hence preferable to Method (2), which involves suddenly changing the entering fluid temperature during an indoor test.

5. The procedure for conducting the incident angle modifier test in Section 8.3.3, Method (2) of the Standard, which involves keeping the test stand stationary facing due south and gathering all the data in one all-day test, is preferable to Method (1), which requires the test stand to be rotated and data collected across solar noon. Method (1) requires several test days to complete and can produce erroneous results for collectors with large time constants (10-30 minutes).

6. A class 1 pyranometer, as classified by the World Meterological Organization [7], is required to insure reasonably accurate test results.

7. It is necessary to collect thermal efficiency data symmetrically with respect to solar noon in order to eliminate collector-heat-capacity effects and to insure an accurate near-normal-incidence efficiency curve.

8. Since the near-normal-incidence efficiency data is always collected on clear sunny days with the incident solar radiation in the plane of the collector near 945 W/m^2 (300 $Btu/h \cdot ft^2$), it is not necessary to allow data to be taken at levels as low as 630 W/m^2 (200 $Btu/h \cdot ft^2$) as currently specified in Section 5.1.4 of the Standard. Such low levels may result in additional unnecessary scatter in the data.

9. The definition of gross collector area and aperture area in the Standard allows too much interpretation to be made by the testing organization and consequently the possibility for error and misuse. In addition, the aperture or absorber area should be used in the computation of collector efficiency since it is more closely related to the performance of the collector than gross area. When gross area is used, the y intercept and slope of the near-normal-incidence efficiency curve are $\frac{A_a}{A_g} F_R(\tau\alpha)_e$ and $\frac{A_a}{A_g} F_R U_L$, respectively. The subscripts a and g refer to aperture and gross, respectively. This fact must be realized when relating the experimental data to the theoretical characteristics of the collector as described in [14]. This possible confusion would be eliminated if aperture area were used.

10. In the testing of air heaters to obtain efficiency values, care should be taken to eliminate air leakage in the test loop and to properly handle air leakage in the collector. If the collector is tested under positive pressure, the air flow rate should be measured downstream of the collector. If the collector is tested under negative pressure, the air flow rate should be measured on both sides of the collector.

11. If a single module of an air heater is tested and the collector is normally installed with two or more modules in series, it is possible to adjust the test results to predict the performance of the field-installed array by techniques outlined in this report.

12. The all-day collector performance of flat-plate collectors on clear sunny days can be predicted with reasonable accuracy using the test results obtained in accordance with the Standard.

13. The turbine flow meter used in one of the test loops for water-heating collectors was found to drift in calibration by 2.5% over a period of one year.

14. If any significant amount of collector testing is to be done, an automatic data logger with a magnetic tape drive recording system is preferable to the use of strip chart recorders and hand recording of data.

15. An accurate measurement of ambient air temperature is just as important as an accurate measurement of the transfer fluid entering the collector. Both affect the abscissa value on the plot of near-normal-incidence efficiency in the same way.

16. An open loop is preferable to a closed loop in testing air heaters, since it's easier to maintain steady inlet temperature to the collector.

17. The technique of determining the fraction of the incident solar radiation which is diffuse by periodically shading the pyranometer gave results comparable within 2% to using a pyheliometer and obtaining the diffuse fraction by deduction.

18. For flat-plate collectors having a time constant of less than five minutes, the three primary thermal tests can be completed in six complete test days using a stationary south-facing test stand. One each for the time constant and incident angle modifier tests and four to obtain the near-normal-incident efficiency data. It may be possible to reduce the time to four or five days if the time constant and incident angle modifier data are taken on the same day.

19. The use of a solar simulator as specified in Section 7.3 of the Standard was not evaluated during this study.

20. The use of integrators is not essential to obtain time averages of variables such as fluid flow rate, t across the collector, and incident solar radiation when determining the near-normal-incidence efficiency. Across solar noon, each of the variables typically changes by less than 2% over a 1-minute interval and because of linearity of variation, the arithmetic average of sampled data agrees to within 1% with continuously monitored and integrated data. This does not imply that the variable should not be continuously monitored by strip chart recorders.

6. RECOMMENDATIONS FOR FUTURE WORK

Based on the results of this study and consultation with researchers around the world doing solar collector testing, the following recommendations are made for future work to improve the state-of-the-art in collector testing:

1. A general procedure for establishing the incident angle modifier curve(s) for a variety of non-flat-plate collectors should be established.

2. A method or procedure should be developed for using the time constant as experimentally determined in accordance with the Standard for design purposes.

3. The feasibility of measuring air flow rate both upstream and downstream of an air collector during test to characterize its leakage rate should be determined.

4. The feasibility of adopting the Standard to a wide range of concentrating collectors typically used in building applications should be examined. A major part of this would be accomplished in 1. above.

5. The relationship between long-term collector performance exposed to a wide range of weather conditions and the performance indicated by the tests of the Standard should be determined.

6. It would be desirable to obtain the same performance parameters for the collector as is presently obtained by using a combination of indoor and outdoor tests (without the use of a solar simulator). This would reduce the time and costs of performing the tests, particularly in the less sunny parts of the U.S. Three different organizations have proposed the use of an indoor test and pumping hot water through the collector to determine its heat loss characteristics [29,30,31]. This would be an alternate way of establishing the slope of the near-normal-incidence efficiency curve, thus requiring only a short outdoor test to determine the ordinate intercept. This technique should be evaluated to determine if an accurate efficiency curve can be established. Work has already begun as a result of the procedure in [31] being used in a round robin testing program being conducted by the International Energy Agency (IEA) in 1978.

7. Because of the allowable range of environmental conditions in the Standard during the test to establish the near-normal-incidence efficiency curve, considerable scatter is possible in the data. A correction technique has recently been demonstrated [5,6] whereby each data point can be corrected to "standard environmental conditions" using a mathematical model of the collector. This is a potentially powerful tool for outdoor testing of collectors and should be experimentally verified and then "packaged" as a set of nomographs or computer program.

8. Several alternate testing configurations have recently been proposed [32,33] that might enable the solar collector thermal output to be determined more accurately than is now possible by the separate measurements of $\dot{m}$, c_p, and $t_{f,e} - t_{f,i}$. They basically involve inserting an electrical heater in the test loop with a measurement of Δt across the heater and eliminating the flow meter and a need for knowing the specific heat of the transfer fluid. The accuracy of this approach should be determined.

9. The liquid-heating collectors are frequently tested with one fluid and one flow rate and used in actual installations with another fluid and/ or flow rate. A correction technique for predicting performance under other than test conditions needs to be developed from first principles and verified for use in the field.

10. The potential for establishing a more accurate near-normal-incidence efficiency curve by testing the collector side by side with a "standard collector" whose characteristics are well known should be investigated.

11. Determination and evaluation of a standard instrument and test procedure for determination of effective sky temperature should be made.

12. For air-heating collectors, an additional test should be developed which will result in the determination of how collector performance varies with transfer fluid flow rate. This would enable a designer to more easily select the optimum flow rate for his system.

7. REFERENCES

1. Hill, J.E. and T. Kusuda, "Methods of Testing for Rating Solar Collectors Based on Thermal Performance," NBSIR 74-635, December, 1974.

2. Hill, J.E., Streed, E.R., Kelly, G.E., Geist, J.C., and T. Kusuda, "Development of Proposed Standards for Testing Solar Collectors and Thermal Storage Devices," NBS Technical Note 899, February, 1976.

3. Hill, J.E., and E.R. Streed, "A Method of Testing for Rating Solar Collectors Based on Thermal Performance," Solar Energy, Vol. 18, No. 5, 1976.

4. "Methods of Testing to Determine the Thermal Performance of Solar Collectors," ASHRAE STANDARD 93-77, ASHRAE, 345 East 47th Street, New York, New York, 10017, 1977.

5. Streed, E.R., Thomas, W.C., Dawson, A.G., Wood, B.D., and J.E. Hill, "Results and Analysis of a Round Robin Test Program for Liquid-Heating Flat-Plate Solar Collectors," NBS Technical Note 975, August, 1978.

6. Streed, E.R., Thomas, W.C., Dawson, A.G., Wood, B.D., and J.E. Hill, "Results and Analysis of a Round Robin Test Program for Liquid Heating Flat-Plate Solar Collectors," Solar Energy, accepted for publication, 1978.

7. Guide to Meteorological Instrumentation and Observing Practices, Secretariet of the World Meteorological Organization, Geneva, Switzerland, 4th Edition, 1971.

8. Klein, S.A., Beckman, W.A., and J.A. Duffie, "A Design Procedure for Solar Heating Systems," Solar Energy, Vol. 18, No. 2, 1976.

9. Klein, S.A., Beckman, W.A., and J.A. Duffie, "A Design Procedure for Solar Air Heating Systems," Solar Energy, Vol. 19, No. 5, 1977.

10. Yass, K., and H.B. Curtis, "Low-Cost Air Mass 2 Solar Simulator," NASA TM X-3509, presented at the United States Section Meeting of the International Solar Energy Society, held in Cleveland, Ohio, October 3-4, 1973.

11. Simon, F.F., and P. Harlamert, "Flat-Plate Collector Performance Evaluation, the Case for a Solar Simulator Approach," NASA TM X-71427, presented at the United States Section Meeting of the International Solar Energy Society, held in Cleveland, Ohio, October 3-4, 1973.

12. Ramsey, J.W., Borzoni, J.T., and T.H. Holland, "Development of Flat-Plate Collectors for Heating and Cooling of Buildings," NASA CR-13804 June, 1975.

13. Klein, S.A., Duffie, J.A., and W.A. Beckman, "Transient Considerations of Flat-Plate Solar Collectors," ASME Journal of Engineering Power, Vol. 96A, p. 109, 1974.

14. Duffie, J.A., and W.A. Beckman, Solar Energy Thermal Processes, John Wiley and Sons, 1974.

15. Simon, F.F., "Flat-Plate Solar-Collector Performance Evaluation with a Solar Simulator as a Basis for Collector Selection and Performance Prediction," NASA TMX-71793, presented at the 1975 International Solar Energy Society Meeting, held in Los Angeles, California, July 29-August 3, 1975.

16. Wijeysundera, N.W., "Response Time of Solar Collectors," Solar Energy, Vol. 18, pp. 65-68, 1976.

17. Simon, F.F., and E.H. Buyco, "Outdoor Flat-Plate Collector Performance Prediction from Solar Simulator Test Data," NASA TM-71707, presented at the 10th AIAA Thermal Physics Conference, held in Denver, Colorado, May 27-29, 1976.

18. "Solar Thermal Electric Power Systems-First Quarter Progress Report," Report No. NSF/RANN/SE/GI - 37815/PR/74/1, Colorado State University, April, 1974.

19. Flowers, E., "Test and Evaluation of the Performance of Solar Radiation Sensors at Inclinations from the Horizontal Under Laboratory and Field Conditions," Department of Energy Report DSE/1041-1, September, 1977.

20. Pendleton, R.L., "Evaluating a Solar Energy Concentrator," ASHRAE Journal, pp. 47-50, November, 1976.

21. Thomas, W.C., "Thermal Efficiency Test Procedures and Results for a Cyclindrical Concentrating Collector," Proceedings of the ERDA Concentrating Solar Collector Conference, held in Atlanta, Georgia, September 26-28, 1977.

22. Johnson, S.M., "Standardized Performance Tests of Collectors of Solar Thermal Energy-A Flat-Plate Copper Collector with Parallel Mylar Stripping," NASA TM X-73553, November, 1976.

23. Close, D.J., and M.B. Yosoff, "The Effects of Air Leaks on Solar Air Collector Behaviour," Solar Energy, Vol. 20, No. 6, pp. 459-463, 1978.

24. Farber, E.A. and C.A. Morrison, "Clear Day Design Values," Chapter IV of Applications of Solar Energy for Heating and Cooling of Buildings, ASHRAE Publication GRP 170, 1977.

25. Zerlaut, G.A., Dokos, W.T., and R.F. Heiskell, "The Use of ASHRAE Standard 93-77 in Predicting All-Day Performance of Flat-Plate Collectors," Proceedings of the 1977 Flat-Plate Solar Collector Conference, held in Orlando, Florida, February 28-March 2, 1977.

26. Tleimat, B.N., Howe, E.D., and R.E. Buckland, "A Proposed Method of Rating the Thermal Performance of Solar Collectors," presented at the Joint Conference of the International Solar Energy Society and the Solar Energy Society of Canada, held in Winnepeg, Canada, August 15-20, 1976.

27. Simon, F.F., and Miller, D.M., "A Generalized Correlation of Experimental Flat-Plate Collector Performance," NASA TM X-71832, presented at the Conference on Standards for Solar Heating and Cooling, held in Philadelphia, Pennsylvania, October 14-15, 1975.

28. Miller, R., "Performance Correlations of Five Solar Collectors Tested Simultaneously Outdoors," NASA TM X-73546, presented at the Joint Conference of the International Solar Energy Society and the Solar Energy Society of Canada, held in Winnipeg, Canada, August 15-20, 1976.

29. Smith, C.C., and T. Weiss, "Design Application of the Hottel-Whiller-Bliss Equation," presented at the 1975 International Congress, "Solar Use Now-A Resource for People," held in Los Angeles, California, July 28 - August 1, 1975.

30. Symons, J.G., "The Direct Measurement of Heat Loss from Flat-Plate Solar Collectors on an Indoor Testing Facility," CSIRO, Division of Mechanical Engineering, Technical Report No. TR 7, 1976.

31. "Guidelines and Directions for Determining the Feasibility of Utilizing Solar Collectors, A. Efficiency Tests of Solar Collectors," A Proposed Method of BSE, The German Solar Energy Industries Association, September, 1976.

32. Carroll, J. and D. Wald, "Improved Instrumentation for Performance Testing of Solar Collectors," unpublished note, Santa Clara Solar Research Institute, Santa Clara, California, 1978.

33. Reed, K.A., "Interim Solar Collector Test Plan," Proceedings of the ERDA Concentrating Solar Collector Conference, held in Atlanta, Georgia, September 26-28, 1977.

34. Kusuda T., "NBSLD, The Computer Program for Heating and Cooling Loads in Buildings," NBS Building Science Series 69, July, 1976.

35. Buchberg, H., and J.L. Cairns, "A Convective Conductance Meter: Design and Evaluation," ISA Transactions, Vol. 10, No. 3, pp. 325-330, 1971.

36. Ito, N. Kumura K., and J. Oko, "A Field Experiment Study on the Convection Heat Transfer Coefficient on Exterior Surface of a Building," ASHRAE Transactions, Vol. 78, Part I, 1972.

37. Aagard R.L., "Convection Free Instrument for Measuring Infrared Radiation in the Atmosphere," The Review of Scientific Instruments, Vol. 29, No. 11, pp. 1011-1016, November, 1958.

38. Beckman, W.A., et. al., "Units and Symbols in Solar Energy", Solar Energy, Vol. 21, pp. 65-68, 1978.

Table 1. Specifications for the Equipment and Sensors Used in the Liquid Collector Test Loops

Equipment/Sensor	Specifications
Temperature measurement section/temperature well	Outer shell assembly is constructed from 1.27 cm (0.5 in.) i.d., 0.317 cm (0.125 in.) wall hard-drawn copper tubing and fittings; 0.952 cm (0.375 in.) o.d., 0.081 cm (0.032 in.), wall capped brass tube provides for a thermopile well while a 0.474 cm (0.187 in.) compression fitting with teflon ferrule allows for insertion of sheathed temperature probes; flow rate and flow configuration produces turbulent flow and fluid swirling after passing through one right angle bend (See Figure 15.)
Water-to-air heat exchanger	Vega automative radiator; effective surface area of 1.85 m^2 (20 ft^2); U_A value of 181.5 W/(m^2•°C) (32 Btu/(h•ft^2•°F))
Water-to-water heat exchanger	Single-pass counter-flow heat exchanger
Storage tank	37.8ℓ (10 gal.) glass-lined domestic hot water tank; 1500 W (5118 Btu/h) immersion heater
Pressure relief valve	2.06 x 10^3 Pa (30 psi) spring-loaded valve
Filter	5 micron cartridge filter for hot water applications
Electric Heater	500 W (1705 Btu/h), rod resistance immersion heater
Temperature Controller	Adjustable proportional set point controller; 1000 W (3410 Btu/h) load capability using a triac assembly and a type-T thermocouple sensor

Table 1 (Cont.)

Equipment/Sensor	Specifications
Pump	Self-priming, eccentric-disc positive-displacement pump; variable pumping capacity of 0-3.45 x 10^{-4} m^3/s (0-5 gal./min.), forward or reverse and a static pressure head of 3.44 x 10^4 Pa (50 psi)
Flow meters	Turbine meter; Paddle-wheel type incorporating an orifice upstream and downstream providing a linear span of 0-6.3 x 10^{-5} m^3/sec (0-1 gal./min.) using ball bearings and a magnetic pick-up; specially linerized to within $\pm$ 0.9% over the intended ranges of temperature and flow rates
	Positive Displacement meter; oval-gear positive-displacement incorporating an active RF pickup functional over the flow range of 1.07 x 10^{-5} to 6.30 x 10^{-5} m^3/s (0.17 to 1 gal./min.)
Temperature sensors	100 ohm, 3 wire platinum resistance thermometers interfaced with linear bridge amplifiers for a 1 mv/°C output
	Thermocouples, type-T, 24 gauge incorporating stainless steel or copper sheathing with and without grounded thermocouple junctions
Temperature difference sensors	Platinum resistance thermometers - same as for absolute temperature measurement
	Thermopile, type-T, 6 junctions formed from 30 gauge wire with each junction individually insulated with shrink tubing
Pressure drop sensor	Inverted U-tube manometer; 0.635 cm (0.25 in.) i.d. and 25.4 cm (10 in.) long filled with water and allowing the upper U to be trapped with air

Table 2. Specifications for the Equipment and Sensors Used in the Air Collector Test Loop

Equipment/Sensor	Specification
Nozzle	Aluminum ASME long-radius nozzle; factory-calibrated and traceable to NBS standards; nozzle diameters of 5.1, 6.4, 7.6, and 10.2 cm (2.0, 2.5, 3.0, 4.0 in.)
Blower	Industrial centrifugal blower; rated at 0.47 m^3 (1000 ft^3/min.) at 2500 Pa (10 in. H_2O); 746 W 2500 (3 hp) electric motor
Duct heaters	On/off; 39 kW in 3 kW increments
	Proportionally-controlled; 6 kW
Temperature sensors	Thermocouples; laboratory-fabricated from premium-grade type-T 24 gauge thermocouple wire
Temperature difference sensors	Six junction thermopile; laboratory fabricated from premium-grade type-T 24 gauge thermocouple wire
Pressure sensors	Nozzle pressure drop; 0 to 1000 Pa (0 to 4 in. H_2O) inclined manometer; 5 P_a (0.02 in.H_2O) smallest scale division; also 0 to 1250 Pa (0 to 5 in. H_2O) elastic diaphram pressure transducer
	Nozzle gauge pressure; 0 to 2500 Pa (0 to 10 in. H_2O) vertical manometer; 25 Pa (0.10 in. H_2O) smallest scale division
	Pitot tube pressure; 0 to 1250 Pa (0 to 5 in. H_2O) vertical manometer; 5 Pa (0.02 in.H_2O) smallest scale division

Table 3. Specifications for the Instrumentation Used to Make the Meteorlogical Measurements

Measurement	Specification
Ambient air temperature	Calibrated type-T, 24 gauge thermocouple or precision platinum resistance thermometer housed within a vented weather shelter
Wind speed	Standard 3-cup wind anemometer incorporating a d.c. generator; output of 0.0581 volts/m/s (0.026 volts/mph) directly proportional to wind velocity
Wind direction	Direction vane with a two-wiper potentiometer (0-540°)
Total solar radiation incident on the collector tilted surface	Precision spectral pyranometer utilizing an all black thermopile detector and temperature compensation; class 1 pyranometer as classified by the World Meteorological Organization
Diffuse component of the solar radiation incident on the collector tilted surface	10 cm (3.93 in.) shadow disc attached to a 1 m (3.28 ft) long support rod
Direct beam solar radiation	Normal incident pyrheliometer with a collimated view of 5.7° and an automatic tracker
Sky temperature	Pyrgeometer; precision infrared radiometer capable of undirectional measurement of either incoming or outgoing long wave terrestrial radiation; a modification of the precision spectral pyranometer using a silicon hemisphere with a transmittance of 0.50 from 0.35 to 50 μm
Incident angle between sun's direct beam and the outward drawn normal to the plane of the collector aperture	Shadow protractor; see Figure 27 and accompanying description

Table 4. NBS Pyranometer Intercomparison Clear Sunny Conditions

Date / 8-48 pyranometer	Pyranometer Inclination: Horizontal		22°		45°		56°	
	PSP Reading W/m^2	8-48 Deviation %	PSP Reading W/m^2	8-48 Deviation %	PSP Reading W/m^2	8-48 Deviation %	PSP Reading W/m^2	8-48 Deviation %
8/5/76/No. 1	869	+ 1.2	996	- 5.1	909	- 7.4	-	-
8/5/76/No. 2	869	+ 0.11	996	- 4.1	909	- 5.3	-	-
8/6/76/No. 1	820	+ 1.5	885	- 3.8	803	- 5.8	681	- 6.2
8/6/76/No. 2	820	+ 0.6	885	- 3.2	803	- 3.9	681	- 4.2

Table 5. Specifications for Strip-Chart Recorders, Integrators, and the Data Logger

Strip-Chart Recorders

2 Pen - Multi Range Input Span
- Uncertainty: ±0.25% of span
- Input Impedance: 0 - 5 V, 30 megohms; 5 V - 10 V, 2.5 megohms
- Time Constant: 0.5s
- Input Spans: 0.1 mV - 10 V, multiple range
- Type Inputs Monitored: thermopiles, pyranometers, flow rates

2 Pen - Fix Input Span
- Uncertainty: ±0.05% of reading
- Input Impedance: 5 megohms
- Time Constant: 0.75s
- Input Span: 0 - 5 mV
- Type Inputs Monitored: referenced thermocouples

3 Pen - Fixed Input Spans
- Uncertainty: ±0.5% of span
- Input Impedance: 5 megohms
- Time Constant: 1s
- Input Spans: 0 - 5 mV, 0 - 100 mV, 0 - 5 V
- Type Inputs Monitored: thermopiles, flow rates, resistance thermometers

Integrators

Uncertainty: ±0.5% of reading, ±2 digits/h
Input Impedance: 1 megohm
Input Span: 0 - 30 mV
Type Inputs Monitored: thermopiles, pyranometers

Data Logger

Uncertainty: ±0.01 mV, Max Error: 0.005% FS, ±0.2 °C
Input Imedance: 100 megohms
Input Ranges: 0 - 400 mV; type-T thermocouples
Type Inputs Monitored: All input data thermocouples, 0 - 100 °C; analog signals, 0 - 400 mV
Special Features: 16 channel arithmetic averager with separate averaging time base
Magnetic Tape Drive: Incremental tape drive, 800 bpi, 9 track with a DTL/TTL plus voltage true interface

Table 6. Description of Solar Collectors Tested

Collector No.	Heat Transfer Fluid	Aperture Area m^2	Gross Collector Area, m^2	Absorber	Glazing	Back Insulation	Miscellanous
1	water	1.61	1.68	aluminum roll-bond, black paint	double-glass	7.6 cm glass fiber	
2	water	1.40	1.66	steel plate with copper tubing, black chrome selective surface	double-glass, anti-reflective coating on three glass surfaces	8.5 cm semi-rigid fiber board	
3	water	1.79	1.96	steel, black-chrome selective surface	single-glass	7.0 cm glass fiber	
4	water	5.04	5.98	concentric glass, selective surface	single-glass, evacuated air space		white-painted surface mounted 10 cm behind tubes; 48 tubes; exposed tube length = 1.05 m; tube diameter = 5.1 cm; space between the tubes = 5.0 cm.
5	water	1.8	3.1	copper, black-chrome selective surface	linear Fresnel lens	3.2 cm glass fiber side insulation in cavity; 6.4 cm glass fiber insulation behind tube	tracking concentrating collector; 2 collectors; collector aperture = 0.3 m by 3.0 m; t to t spacing = 0.9 m
6	air	6.25	7.25	steel, black paint	double-glass	9 cm glass fiber	air flow is beneath absorber in 1.6 cm deep channel.

Table 7. Time Constants for the Liquid-Heating Collectors Tested

Collector No.	Transfer Fluid Flow Rate m^3/s	Time Constant min.
1	3.2×10^{-5}	1.7
2	2.8×10^{-5}	1.6
3	3.5×10^{-5}	1.8
4	3.8×10^{-5}	20.3
5	5.0×10^{-5}	0.9

Table 8. Computation of All-Day Solar Collector Efficiency

Calculation Steps	Hour of the Day, Solar Time[1]												Daily Total
	6-7	7-8	-	-	-	-	-	-	-	4-5	5-6		
1. Inlet fluid temperature to the collector, $t_{f,i}$, °C													
2. Ambient air temperature, t_a, °C													
3. Incident solar radiation of a horizontal surface, I_h, W/m^2													
4. Ratio of total incident solar radiation on the tilted surface (normal to the collector plane) to that on a horizontal surface, R[2]													
5. Incident solar radiation on the collector plane, I, W/m^2, line 3 x line 4[3]													
6. Collector thermal efficiency at normal incidence determined in accordance with Sections 8.3.2 and 8.5 of ASHRAE Standard 93-77 and using data from lines 1, 2, and 5													
7. Incident angle between the direct solar beam and outward drawn normal to the collector plane, θ[4]													
8. Incident angle modifier, determined in accordance with Sections 8.3.3 and 8.6 of ASHRAE Standard 93-77 and using the value of θ from line 7													
9. Energy output from the collector, W/m^2, line 5 x [line 6 + $F_R(\tau\alpha)_{e,n}$ x ($K_{\alpha\tau}$ - 1)]													
10. Collector thermal efficiency, line 9/line 5													

[1] to convert standard time to solar time, see reference [14], pp. 18-19.

[2] to compute R, see reference [14], pp. 48-55.

[3] can be determined by direct measurement using data from reference [24] or other accepted methods.

[4] to compute θ, see reference [14], pp. 14-18.

Table 9. A Comparison of Measured and Predicted All-Day Collector Efficiency

Collector	$\overline{t_{f,i}-t_a}$ °C	$\text{day}\int Id\tau$ kJ	Measured Daily Collected Energy kJ	Predicted Daily Collected Energy kJ	Measured Daily Efficiency %	Predicted Daily Efficiency %
2	21	33,400	18,500	19,200	55.4	57.5
2	52	34,800	15,800	15,840	45.4	45.5
2	64	34,100	15,800	14,900	46.3	43.7
3	19	41,700	28,300	27,000	67.8	64.7
3	52	42,600	22,100	21,300	51.9	50.0
3	64	44,100	18,800	19,800	42.6	44.9

APPENDIX A

Calculation of Air Flow Rate Using a Nozzle and Pressure Difference Measurements

The air flow rate through the nozzle apparatus is calculated by:

$$Q_{mi} = 1.41\ C_N\ A_N\ (\Delta p_N\ \upsilon'_N)^{0.5} \qquad (1)$$

where

Q_{mi} = measured air flow rate, m^3/s

C_N = nozzle discharge coefficient

A_N = nozzle throat cross-sectional area, m^2

Δp_N = static pressure difference across the nozzle, Pa

υ'_N = specific volume of the air at the nozzle, m^3/kg dry air

The nozzle discharge coefficient C_N, is determined from the following table:

Reynolds Number N_{Re}	Discharge Coefficient C_N
20,000	0.96
50,000	0.97
100,000	0.98
150,000	0.98
200,000 and above	0.99

Alternately, a value of C_N can be calculated from the following equation for $20{,}000 \leq N_{Re} \leq 200{,}000$:

$$C_N = 0.95 + 3.7 \times 10^{-7}\ N_{Re}\ \left(1 - \frac{N_{Re}}{4.0 \times 10^5}\right) \qquad (2)$$

The nozzle Reynolds Number is calculated from:

$$N_{Re} = f_t \, V_a \, D_N \qquad (3)$$

where

V_a = velocity of the air at the nozzle throat, m/s

D_N = nozzle throat diameter, m

f_t = temperature factor for equation (2) above

f_t is determined from the following table:

Temperature °C	Temperature Factor f_t
-6.7	78275
+4.4	72075
+15.6	67425
+26.7	62775
+37.8	58125
+48.9	55025
+60.0	51925
+71.1	48825

V_a can be determined from the velocity pressure measured at the nozzle throat with a pitot tube or calculated from the following equation:

$$V_a = 1.40 \, (\Delta p_N \, \upsilon'_N)^{0.5} \qquad (4)$$

The nozzle throat cross-sectional area, A_N, is determined by measuring its diameter in four places approximately 45 degrees apart around the nozzle in each of two planes; one at the exit and the other in the straight section up in the nozzle. The nozzle pressure difference Δp_N, is measured as specified in the body of the report; with both an inclined manometer as well as an electronic pressure transducer.

The specific volume of the air at the nozzle, υ'_n, is calculated from:

$$\upsilon'_n = 10.1 \times 10^4 \, \upsilon n / [P_N \, (1 + W_n)] \qquad (5)$$

where

υ_n = specific volume of the air at the wet bulb and dry bulb temperature existing at the nozzle but at standard barometric pressure, m^3/kg dry air

P_N = absolute pressure at the nozzle throat, Pa

W_N = humidity ratio of the air at the nozzle, kg H_2O/kg dry air

Alternately, υ_n' can be calculated for:

$$\upsilon_n' = \frac{R_a\ T_N\ (1 + 1.608\ W_N)}{P_N} \qquad (6)$$

where

R_a = gas constant for dry air, $(P_a \cdot m^3)/(kg \cdot °K)$

T_N = absolute temperature of the air at the nozzle, °K

Both υ_n and W_N are determined from a psychrometic chart or simplified psychrometic computer routines such as those on pp. 150a - 158a of reference [34]. The wet bulb and dry bulb temperature are measured together at only one point in the test loop; W_N is computed based on those measurements, and it is assumed to be constant throughout the loop. The absolute pressure at the nozzle throat is calculated as the sum of the barometric pressure and the nozzle discharge gauge pressure, p_N. p_N is measured as indicated in the body of the report using a vertical manometer.

Once the air flow rate, Q_{mi}, is calculated, the following equation issued to calculate the flow rate, $Q_{mi,s}$ in m^3/s at standard temperature and pressure:

$$Q_{mi,s} = Q_{mi}/(1.2\ \upsilon_n') \qquad (7)$$

APPENDIX B

Description of a Radiometer to Determine Sky Temperature

If an electronically-heated plate mounted in a frame with the upper surface exposed, is placed outdoors and allowed to reach steady-state conditions, the following energy balance applies:

the rate of electrical energy input to the heater	+	the rate of incident solar radiation absorbed by the heater	=	
the rate of heat transfer to the ambient air by convection	+	the net rate of heat transfer to the ambient surroundings by radiation	+	the rate of heat transfer through the edges and back of the mounting frame by conduction

In equation form:

$$\frac{P}{A} + \alpha_s I = h_c(T_p - T_a) + \varepsilon\sigma(T_p^4 - T_e^4) + \frac{Q_K}{A} \qquad (1)$$

where

$\frac{P}{A}$ = rate of electrical energy input to the heater per unit of surface area, W/m^2

α_s = absorptance of the electrical heater surface to the solar radiation

I = incident solar radiation on the heater surface, W/m^2

h_c = convection heat transfer coefficient between the surface of the heater and the ambient air, $W/(m^2 \cdot °C)$

T_p = surface temperature of the electrical heater, °K

T_a = ambient air temperature, °K

ε = emittance of the surface of the electrical heater

σ = Stefan-Boltzmann Constant, 5.6697×10^{-8} $W/(m^2 \cdot °K)$

T_e = effective sky temperature, °K

$\frac{Q_k}{A}$ = rate of heat transfer through the edges and back of the mounting frame by conduction, W/m^2

Using the above principle, a number of researchers have built instruments to determine the value of one or more of the variables in equation (1) with the rest predetemined, or eliminated, or measured. In some cases, two identical electrical heaters have been built with all but one design characteristic the same and by using the heaters or sensors side-by-side exposed to the same environment, a simple relative measurement is used to determine the value of an unknown variable. Buchberg and Cairns [35] and Ito, Kimura, and Oka [36] have used the principle for determining an experimental value of the convection coefficient, h, for air flow over a surface of specific geometry. Aagard [37] adapted the principle to the determination of effective sky temperature at night with I = 0.

The radiometer designed and built by the French Building Research Center and one of the instruments being used by NBS to determine the effective sky temperature during a collector test also makes use of the principle of the balance expressed by equation (1). Two flat receivers are mounted side by side on the top of an insulating slab. Each receiver is a 0.093 m^2 (1.0 ft^2) square surface with a central area of 0.01 m^2 (0.11 ft^2) which is backed by a resistance heater. As can be seen in Figure 60, the first receiver has it outer perimeter area covered with a white surface of low absorptance and high emittance and the central heater covered with a shiney surface of low absorptance and high emittance. The second receiver is treated in just the opposite manner. A star-shaped thermopile is mounted on each receiver to detect any temperature difference between the central heated area and the perimeter surface area. A special electronics package was designed for and is used with the receivers. The electronics supplies electrical energy to the central heater of either receiver in order to keep its surface temperature equal to the surface temperature of the surrounding perimeter area. The electronics package also integrates the input electrical energy over either a 10 minute or 30 minute period. Only one of the receivers is used at a time and the particular one is selected automatically.

Writing equation (1) for both the central heated area as well as the perimeter area of a given receiver, two equations in several unknowns result. If, however, it can be assumed that the convection coefficient, h, and the back losses $\frac{Q_K}{A}$, are the same for both areas and recognizing that the surface temperatures of two areas are controlled to the same value, then the two equations can be solved simultaneously for the effective sky temperature, T_e, as a function of the following variables which are either known or are measured during the test:
$\alpha s1$, $\alpha s2$, ε_1, ε_2, T_p, I, $\frac{P}{A}$.

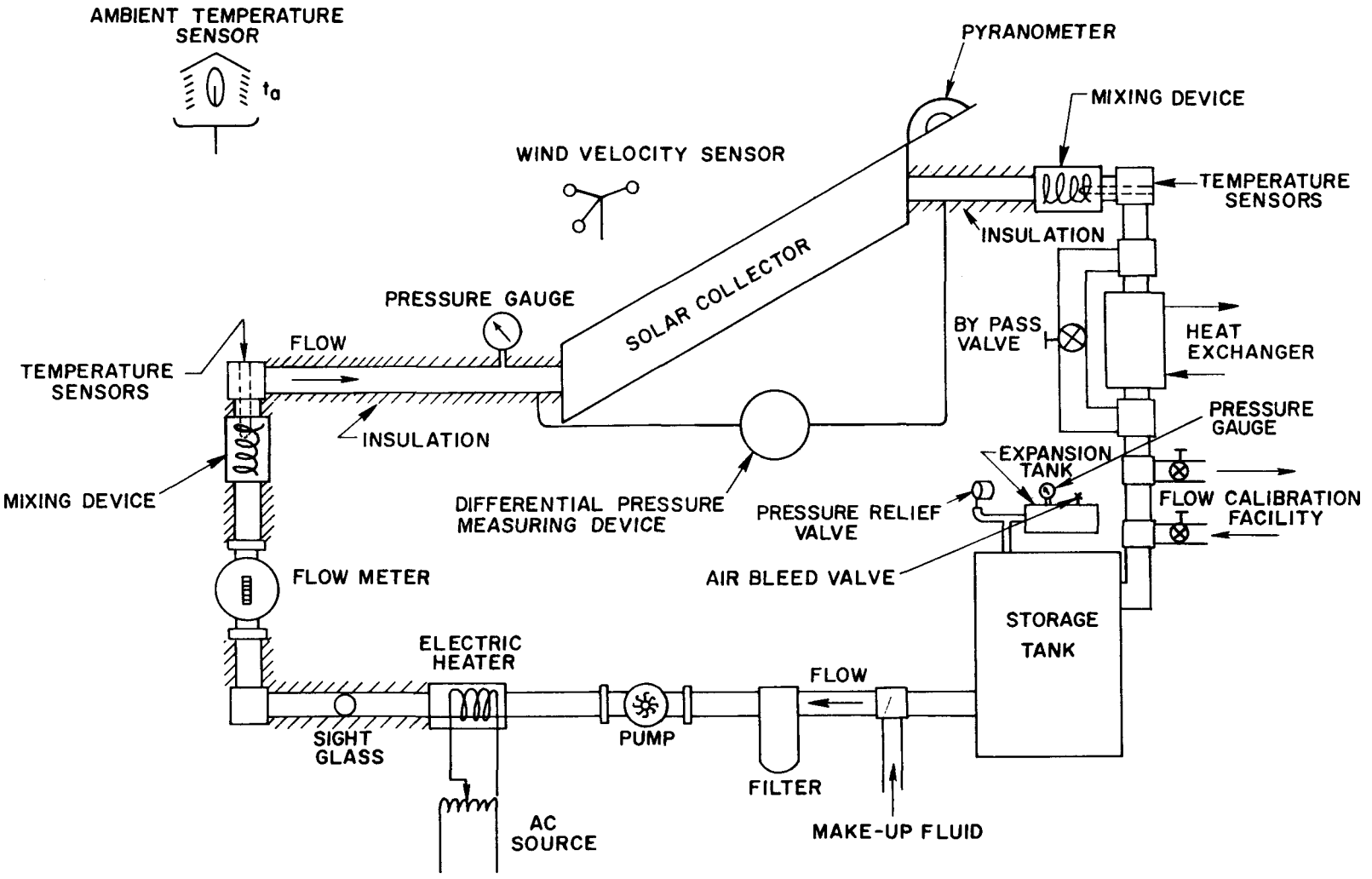

Figure 1 Closed-Loop Testing Configuration for a Solar Collector when the Transfer Fluid is a Liquid [4].

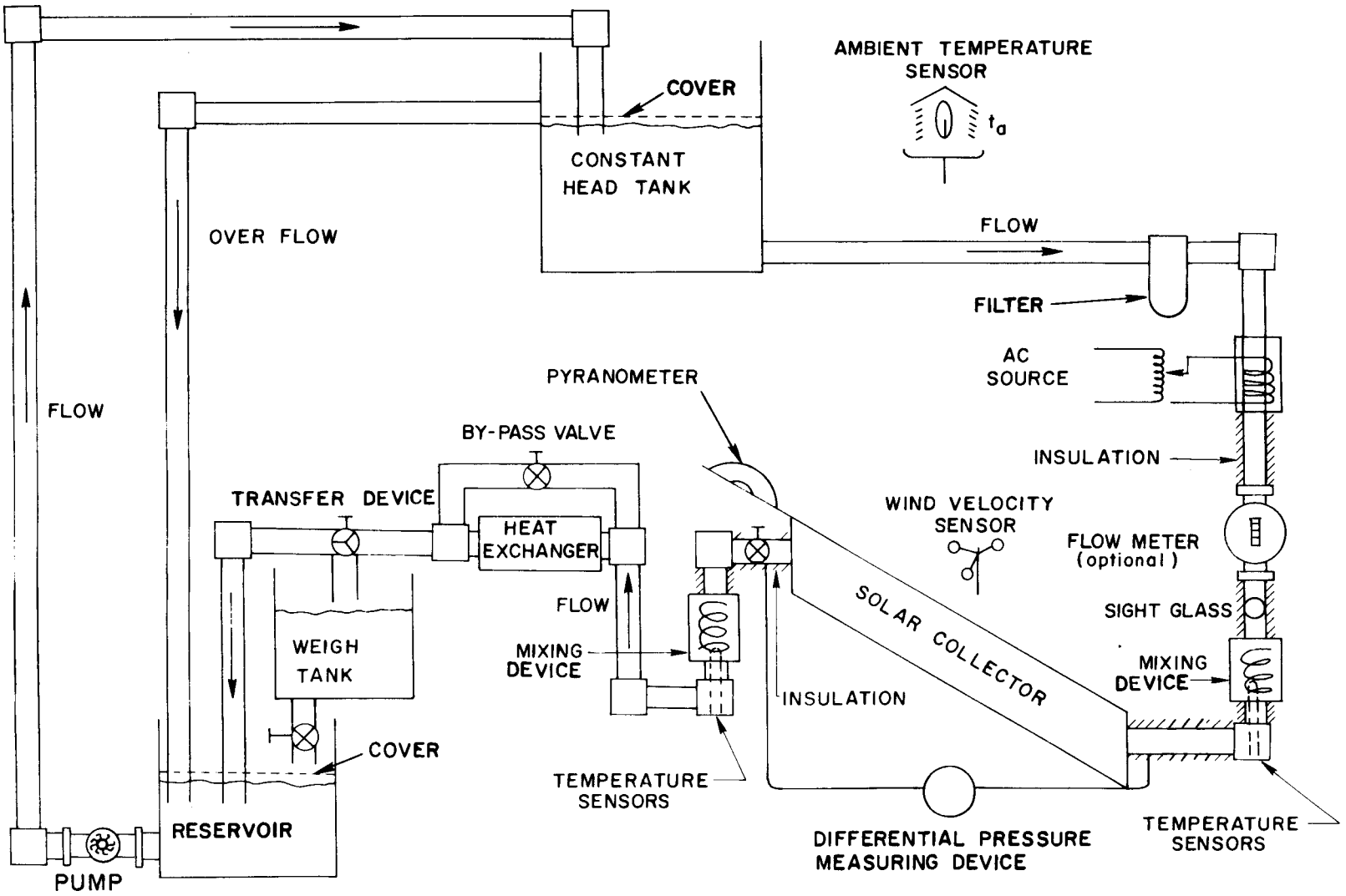

Figure 2 Open-Loop Testing Configuration for a Solar Collector when the Transfer Fluid is a Liquid [4].

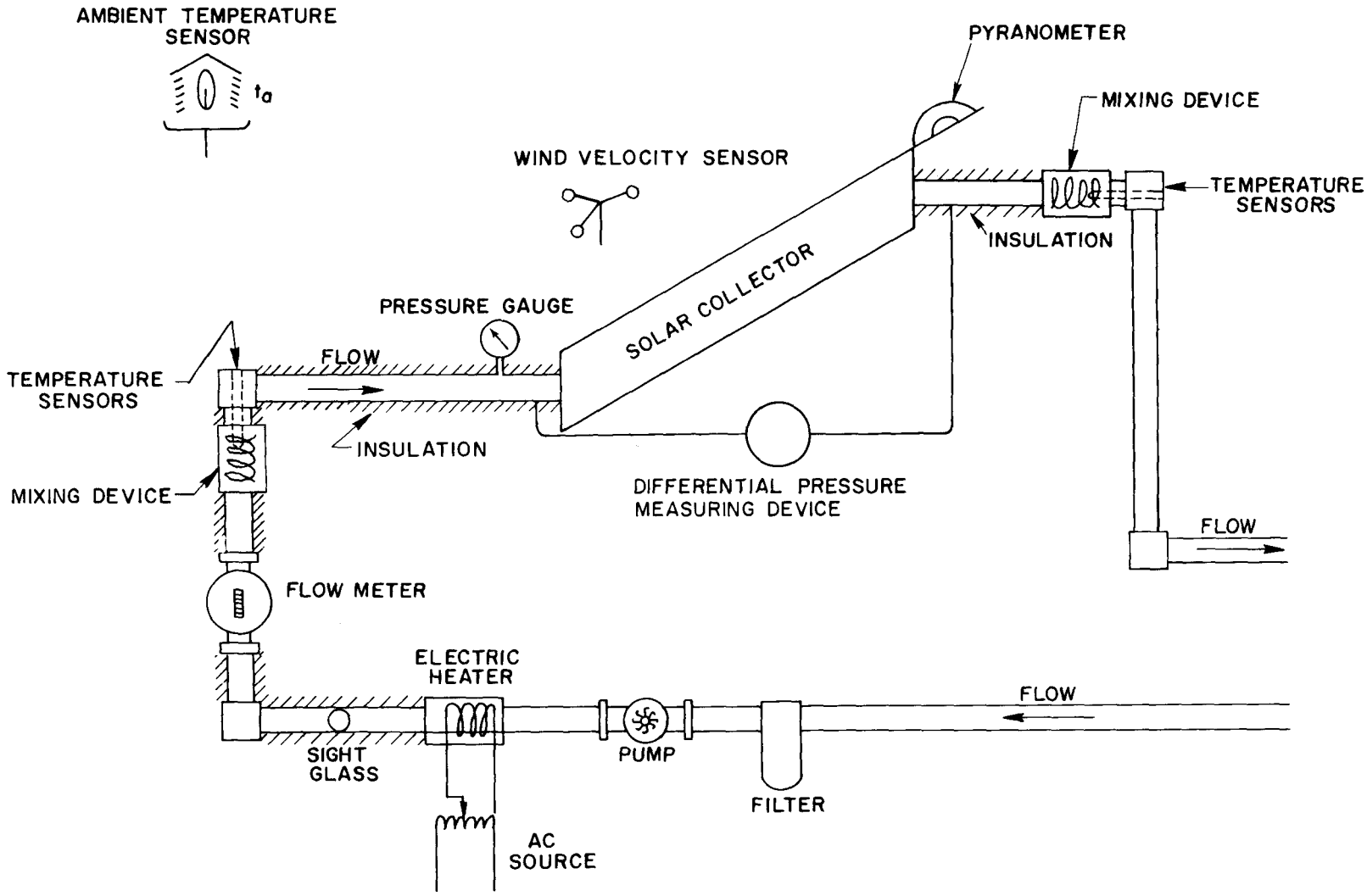

Figure 3 Open-Loop Testing Configuration for a Solar Collector when the Transfer Fluid is a Liquid and is Supplied Continuously [4].

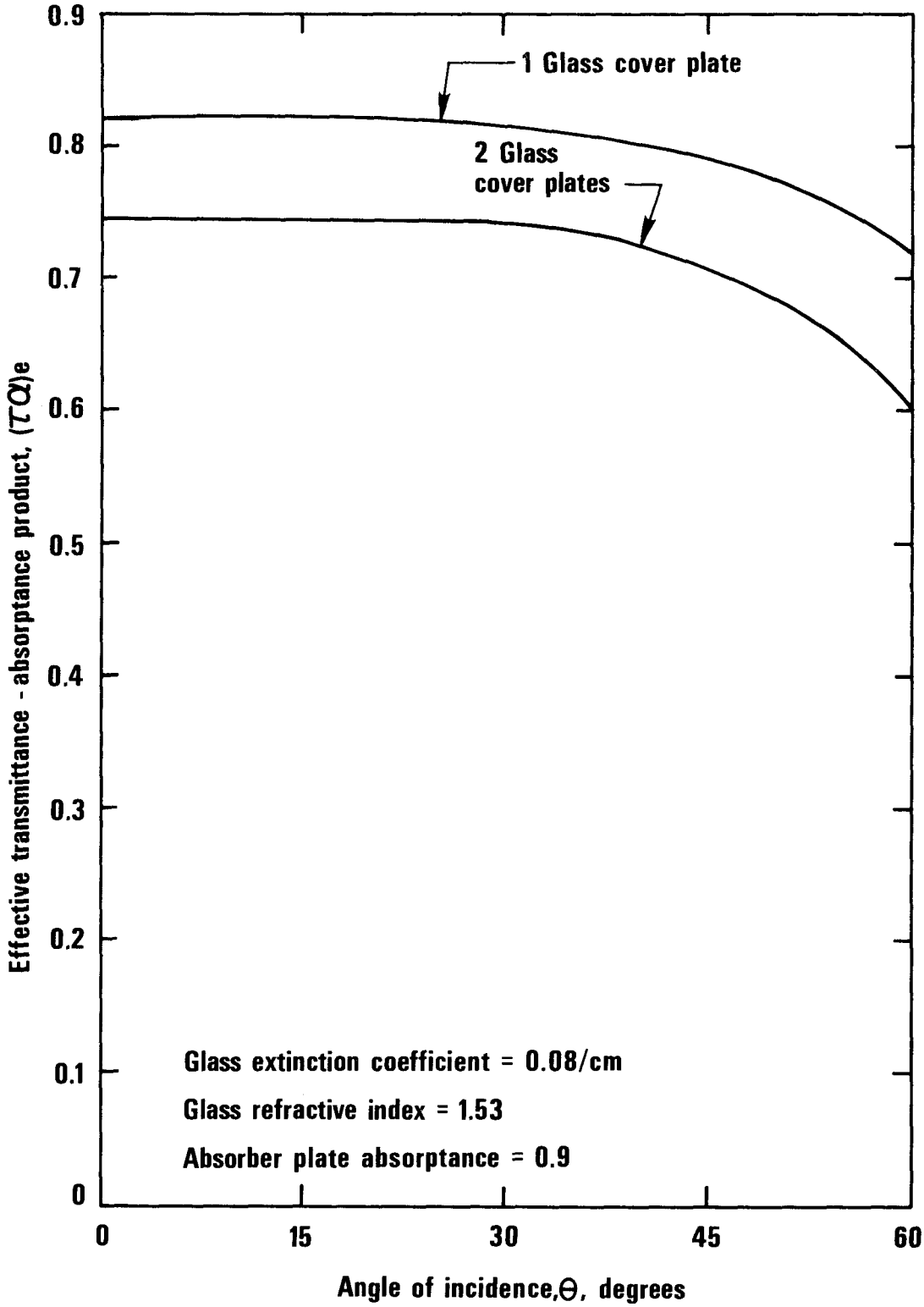

Figure 4 Effective Transmittance-Absorptance Product for Three Flat-Plate Solar Collectors with Non-Selective Coatings on the Absorber [18].

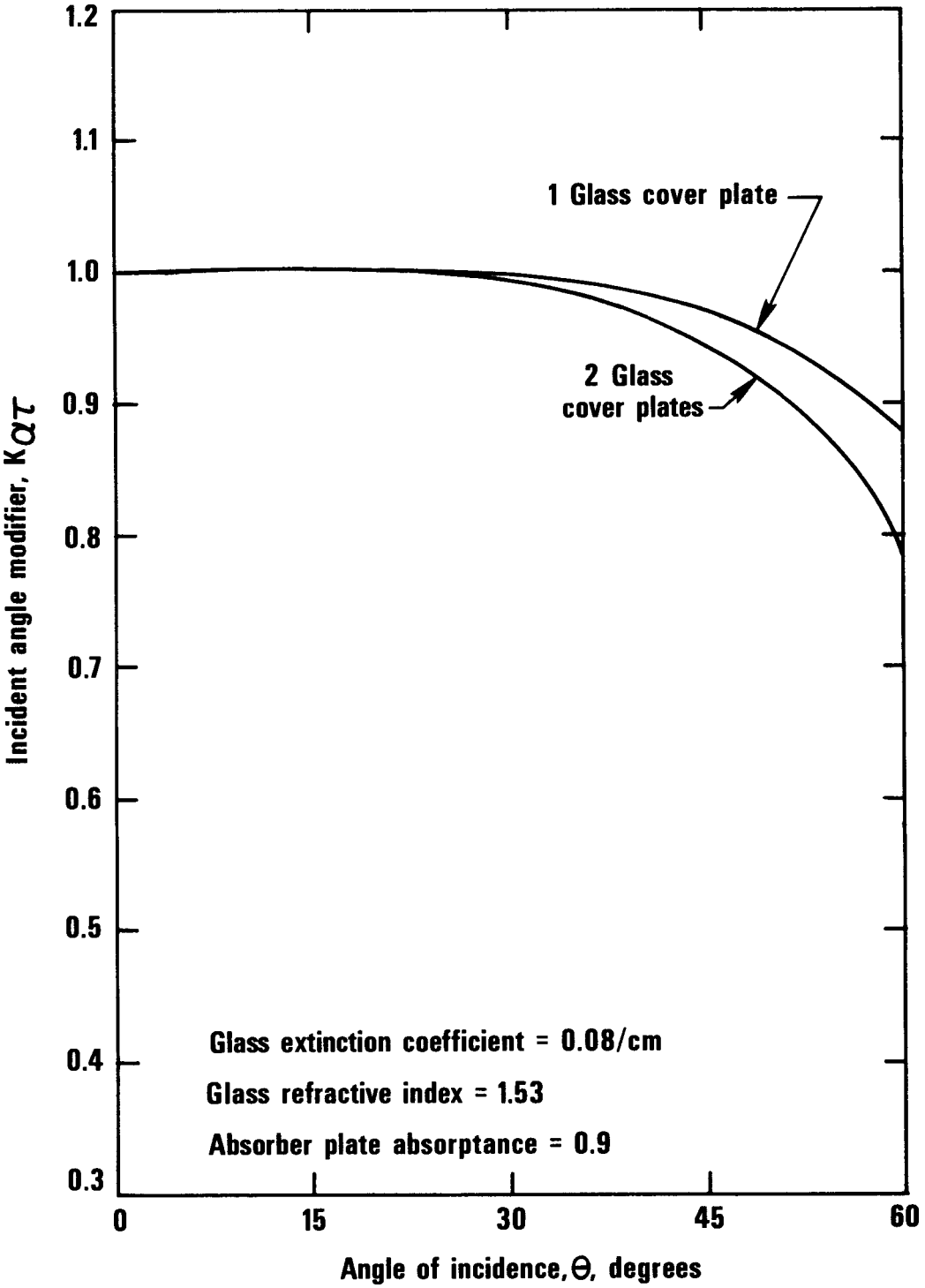

Figure 5 Incident Angle Modifier for Three Flat-Plate Solar Collectors with Non-Selective Coatings on the Absorber.

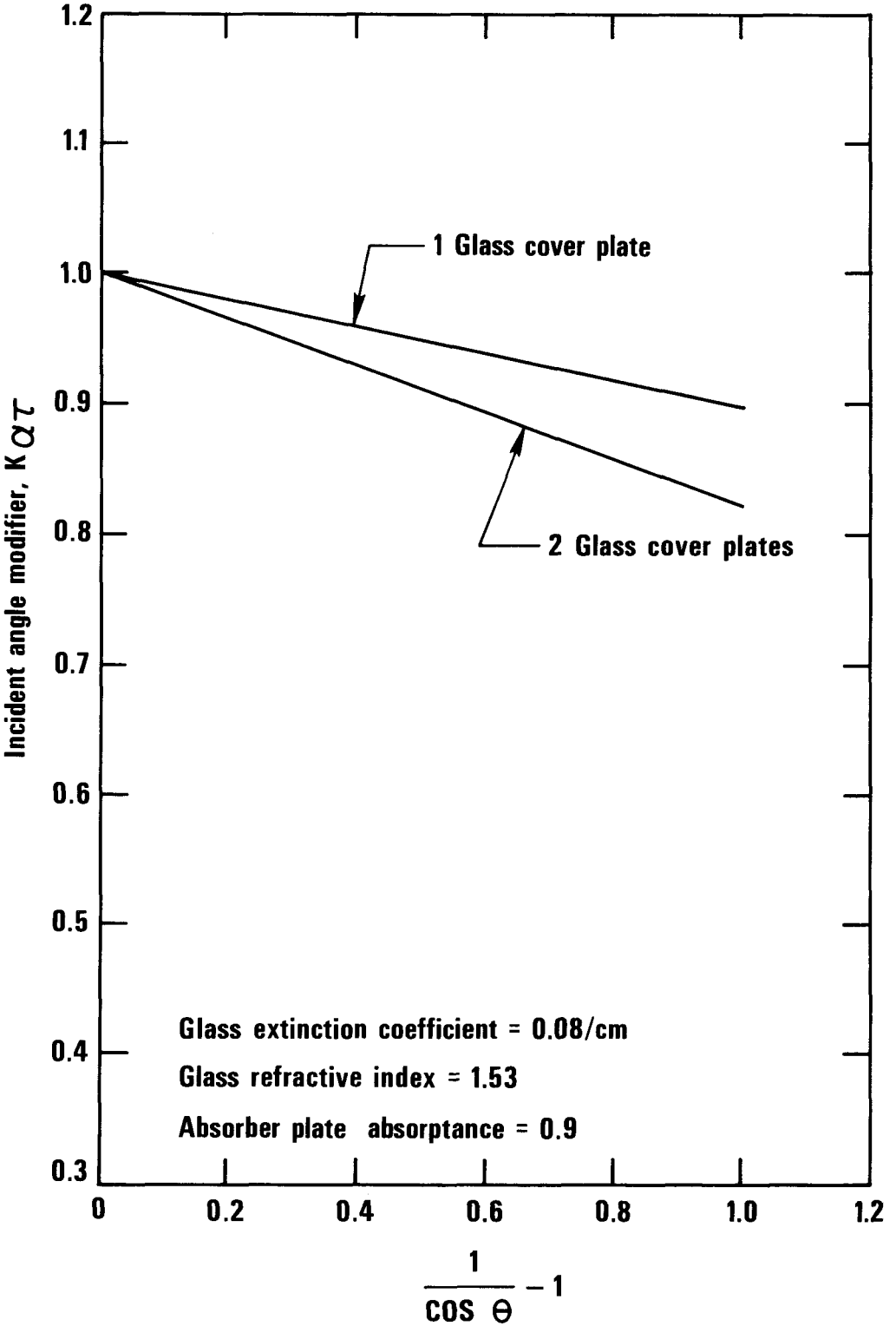

Figure 6 Incident Angle Modifier for Three Flat-Plate Solar Collectors with Non-Selective Coatings on the Absorber.

Figure 7 Elevator Door Covering an Underground Storage Bunker at the NIKI Site, NBS, Gaithersburg, Maryland.

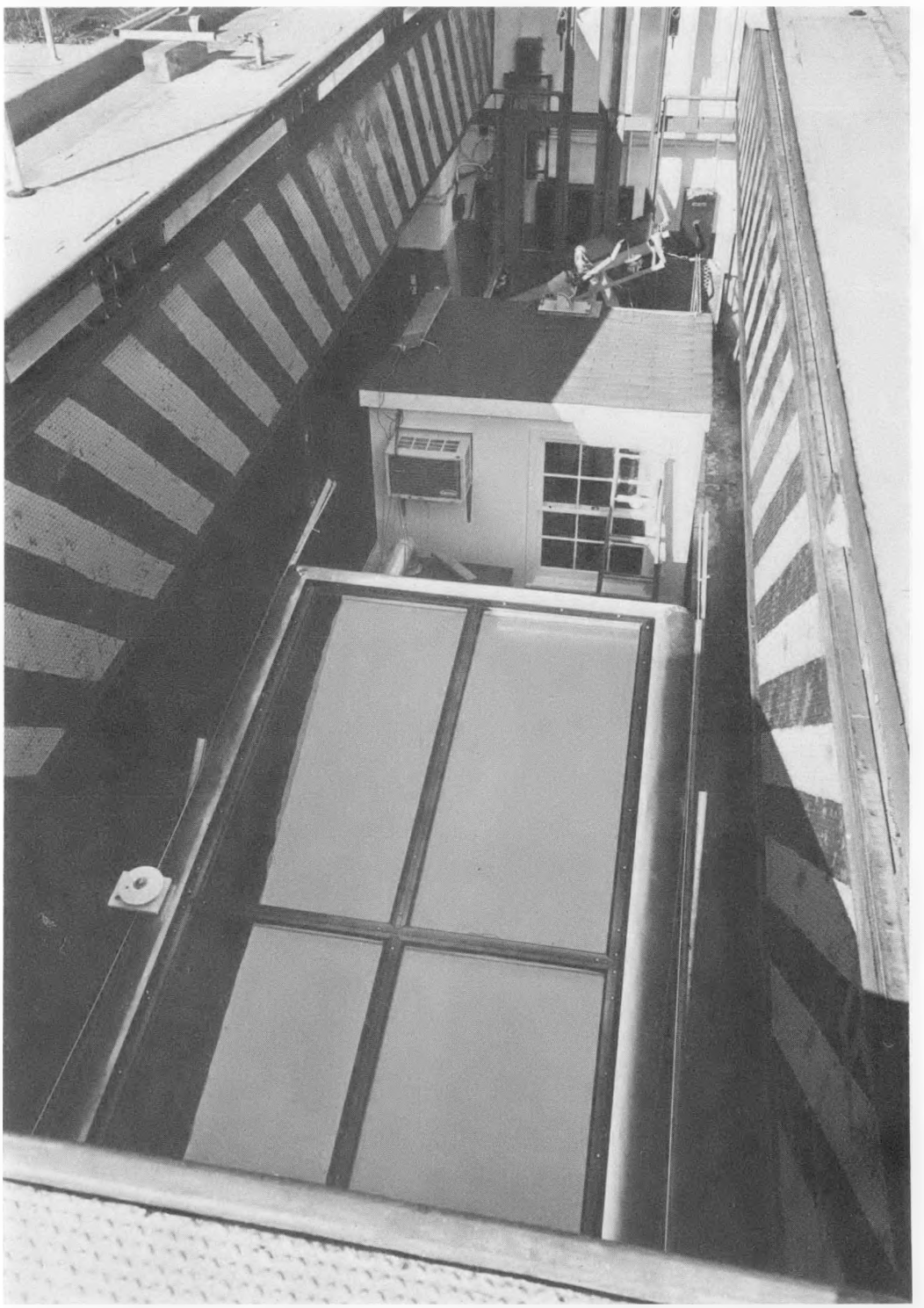

Figure 8 Solar Collector Testing Equipment Mounted on the Elevator and Lowered to the Floor of the Underground Storage Bunker at the NIKI Site, NBS, Gaithersburg, Maryland.

Figure 9 Solar Collector Testing Equipment Being Raised to Ground Level at the NIKI Site, NBS, Gaithersburg, Maryland.

Figure 10 Air Heating Solar Collector Being Cleaned Prior to Test at the NIKI Site, NBS, Gaithersburg, Maryland.

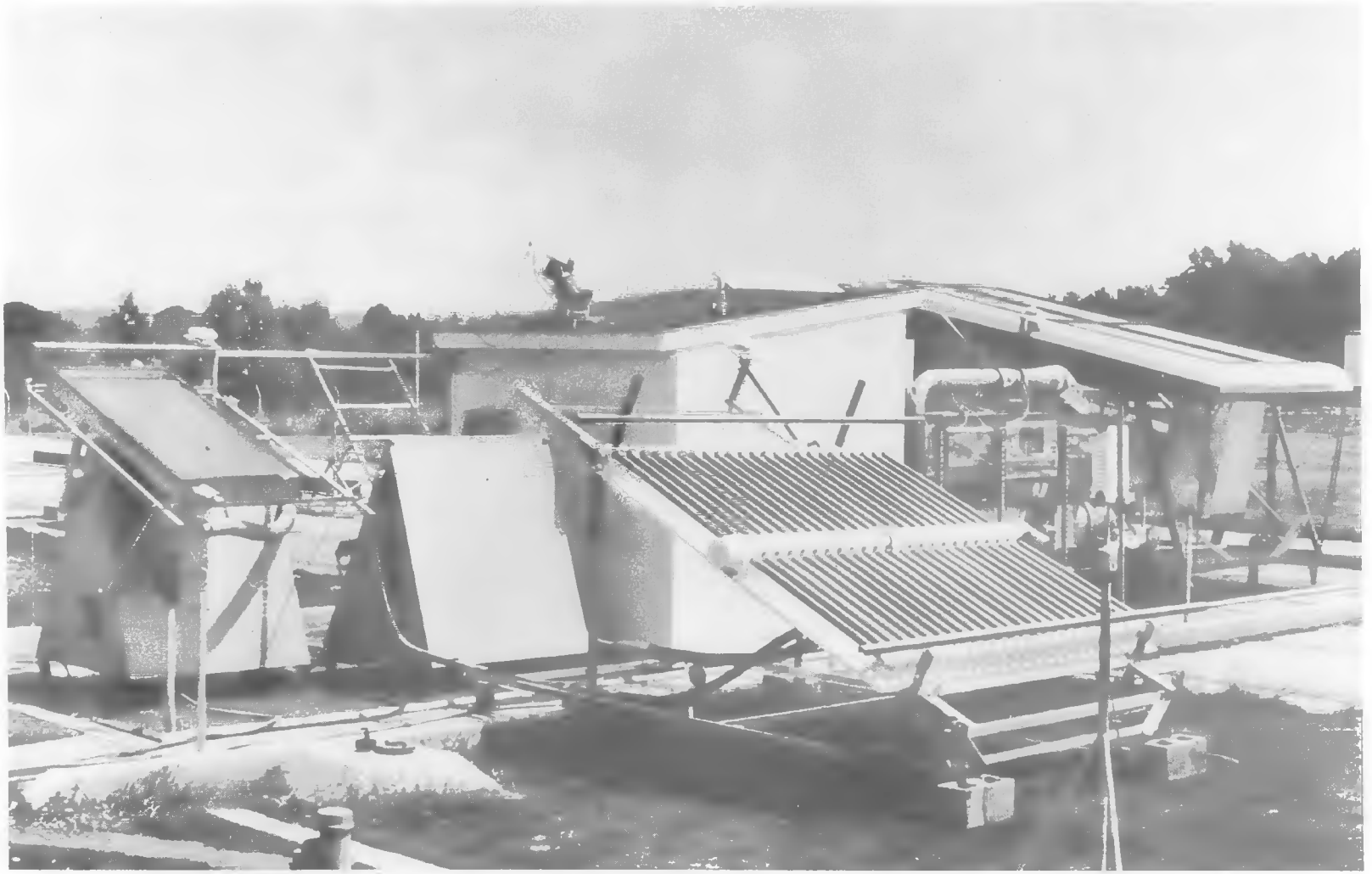

Figure 11 Solar Collector Testing Equipment in Place at the NIKI Site, NBS, Gaithersburg, Maryland.

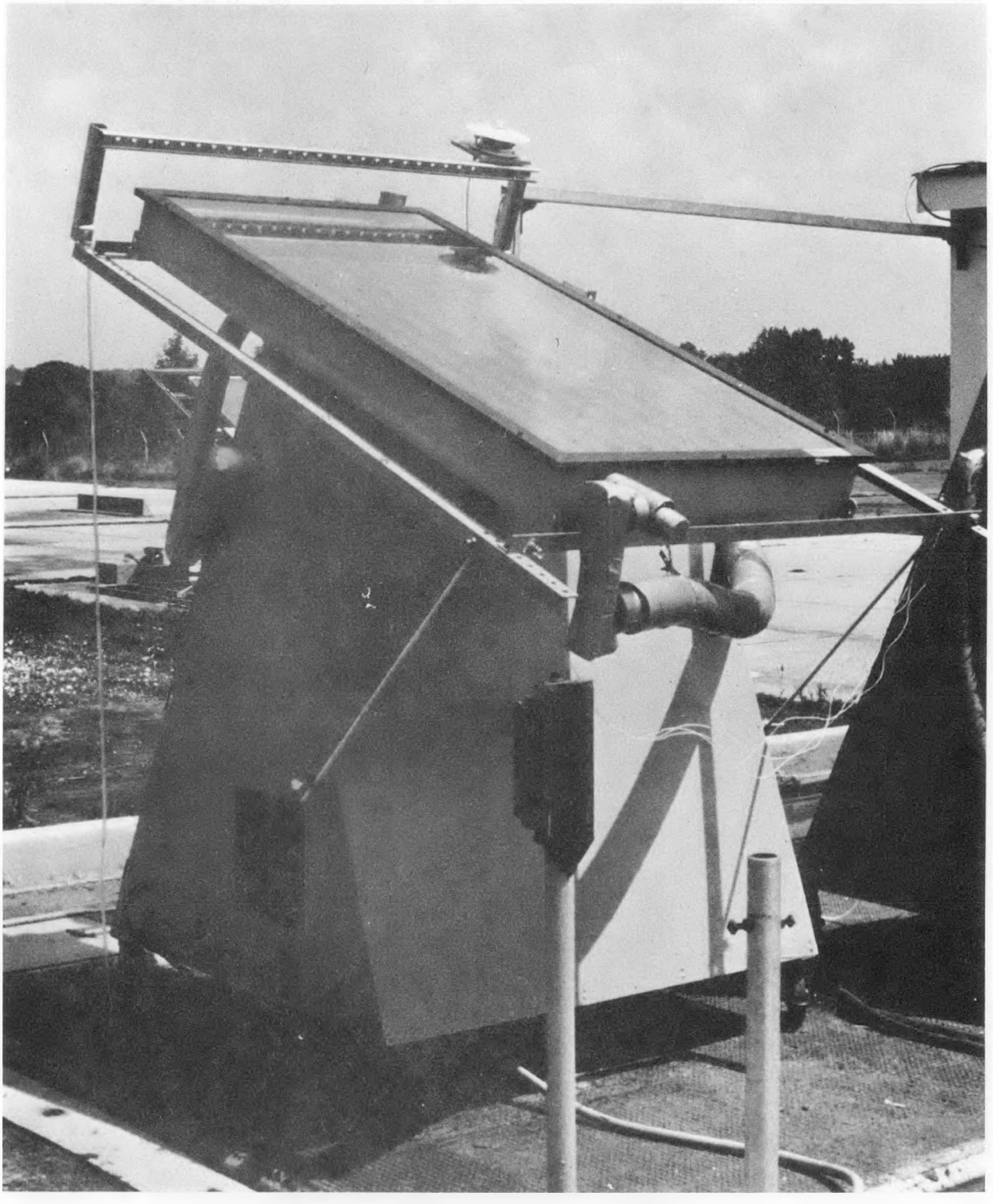

Figure 12 Test Stand for Liquid-Heating Solar Collector at the NIKI Site, NBS, Gaithersburg, Maryland.

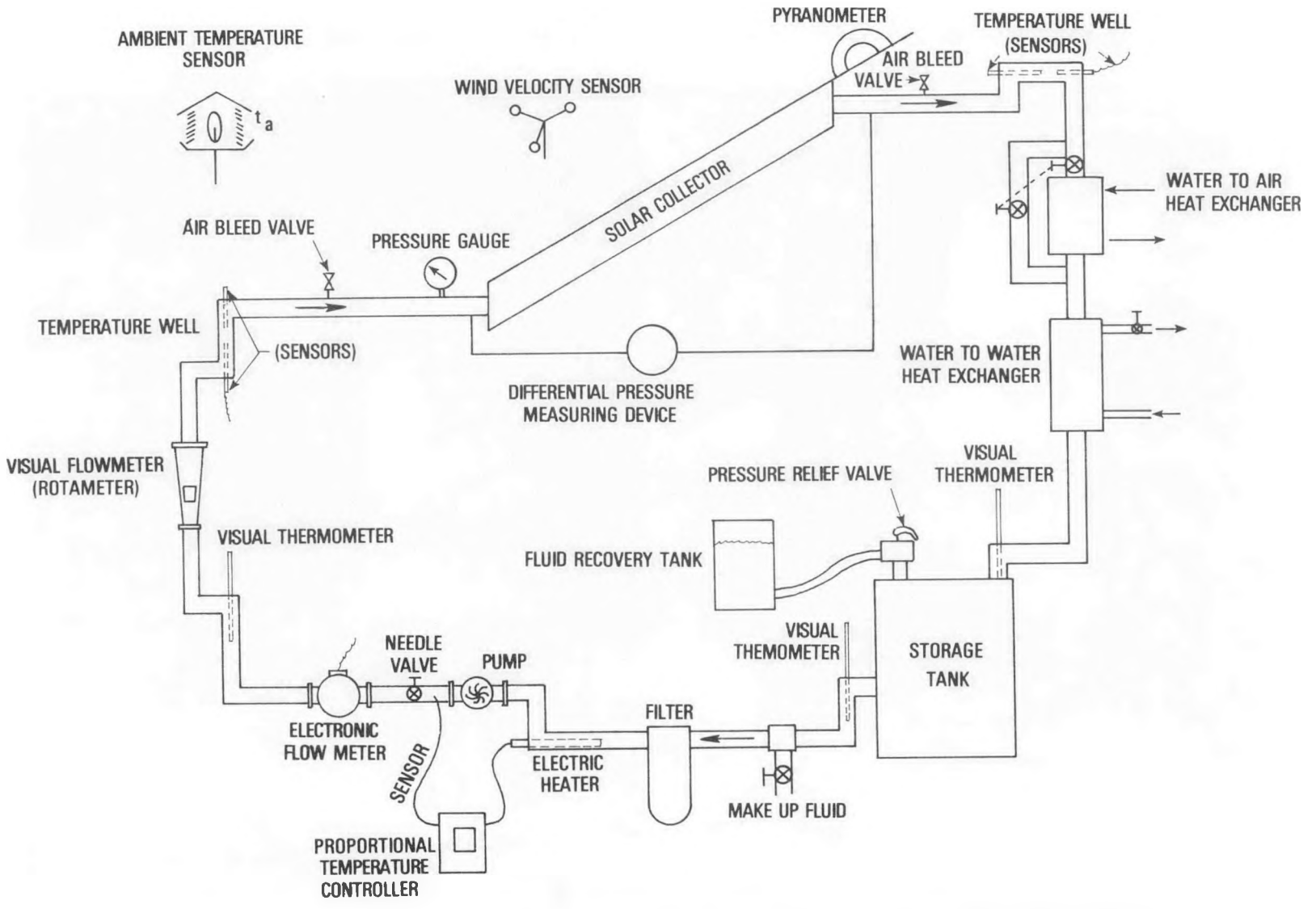

Figure 13 Schematic Diagram of an NBS Test Stand for Liquid-Heating Solar Collectors.

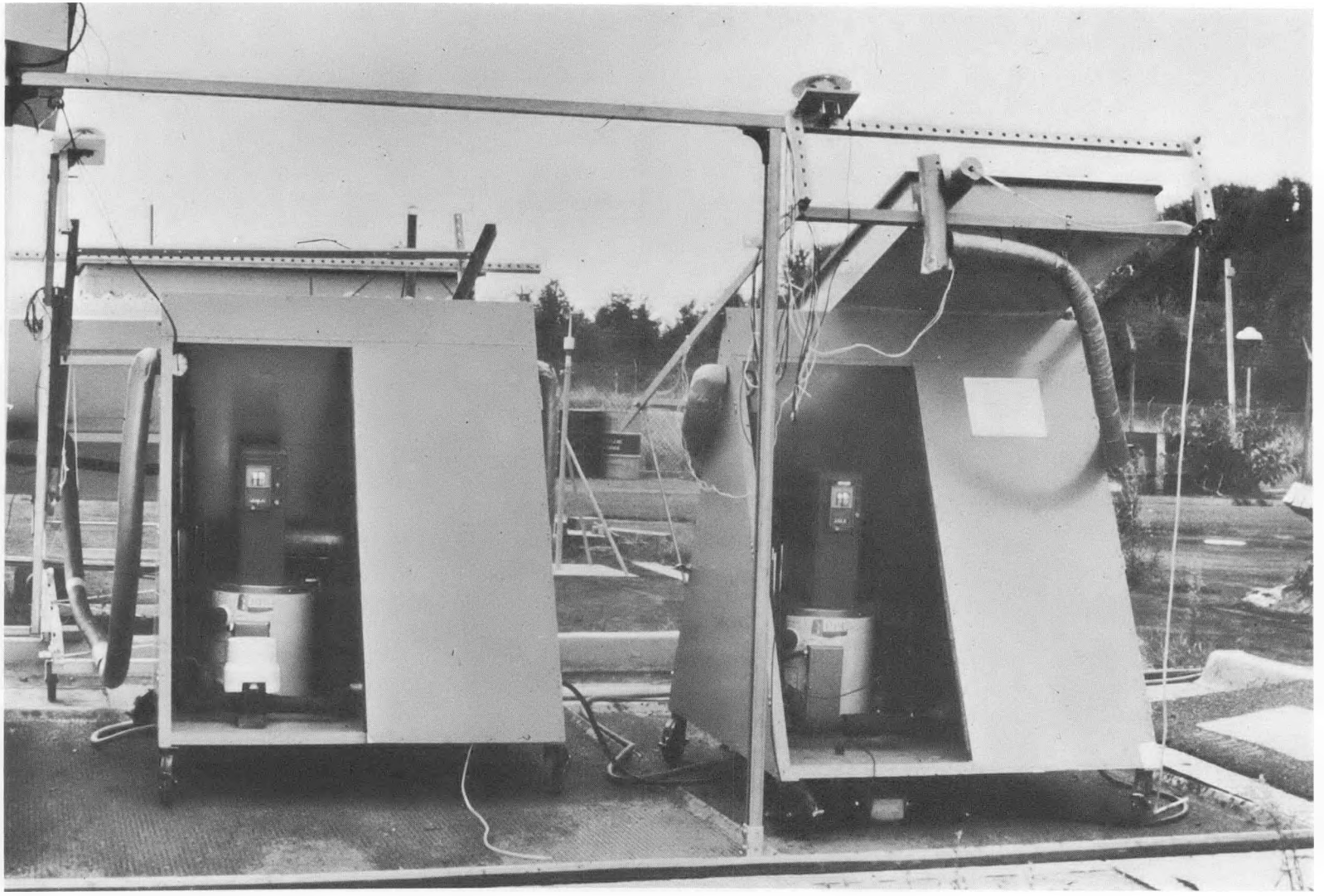

Figure 14 Test Stands for Liquid-Heating Solar Collectors as Seen from the North of the NIKI Site, NBS, Gaithersburg, Maryland.

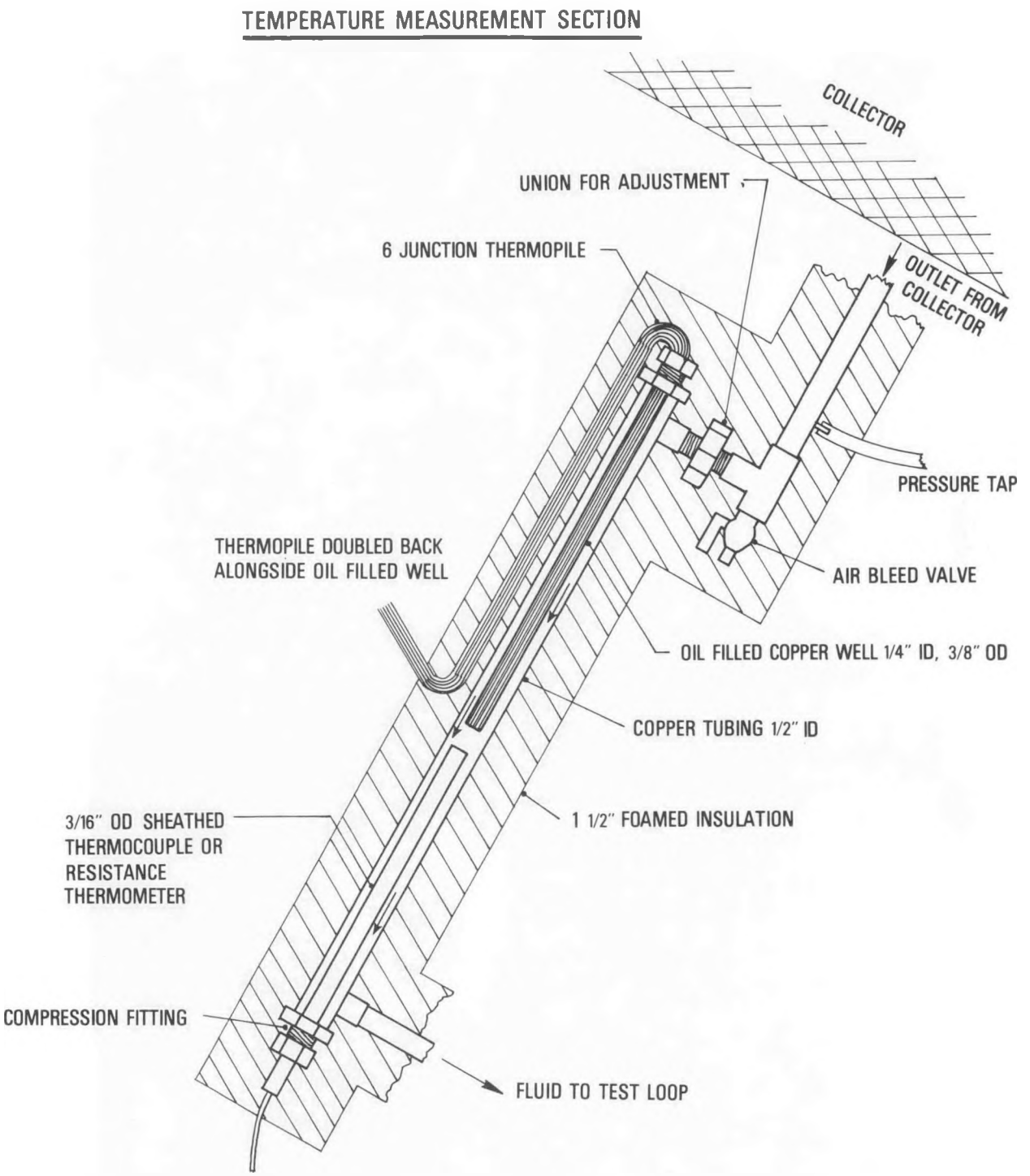

Figure 15 Schematic Diagram of the Temperature Measuring Stations in the NBS Test Stand for Liquid-Heating Solar Collectors.

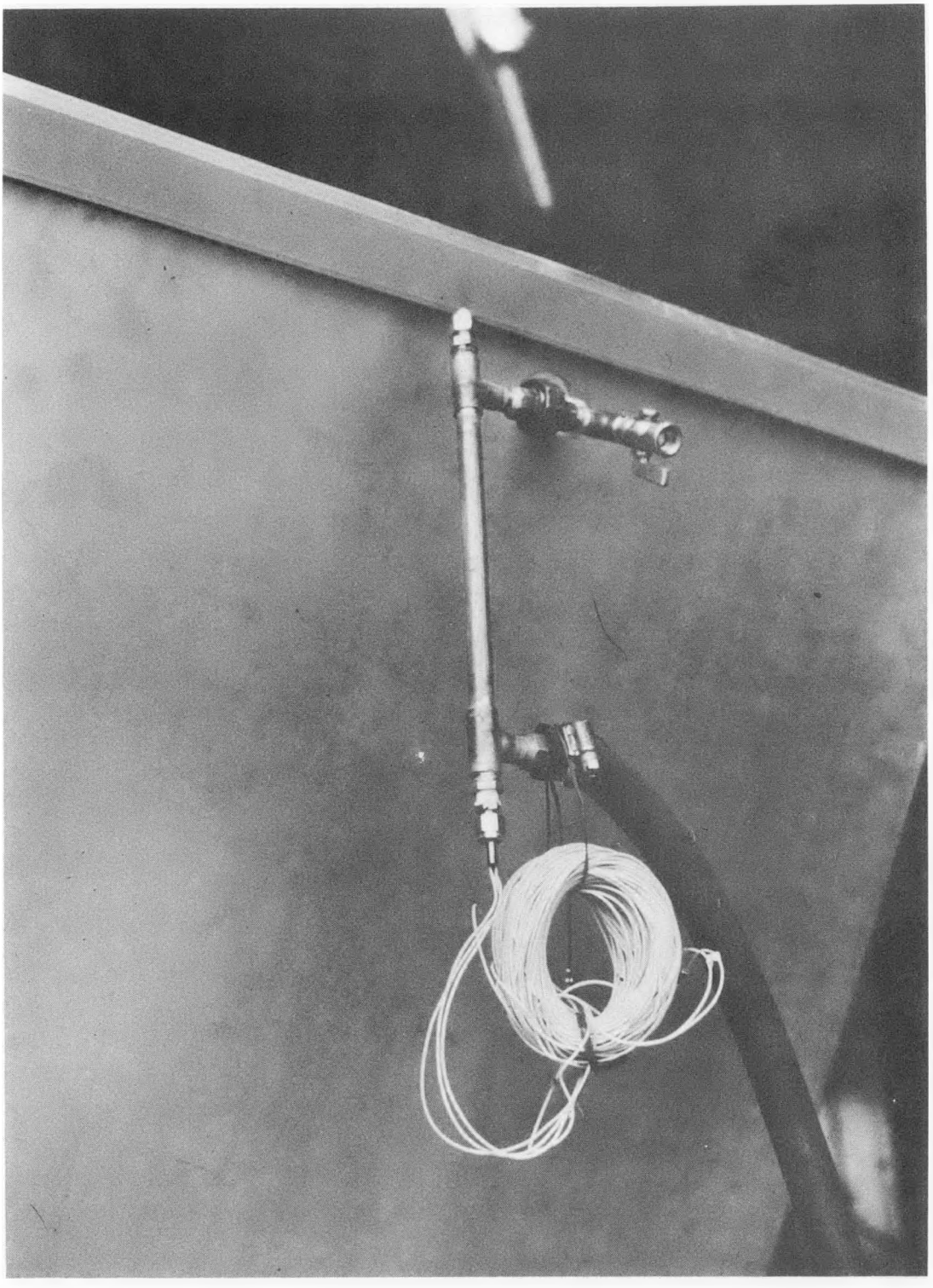

Figure 16 A Temperature Measuring Station in an NBS Test Stand for Liquid-Heating Solar Collectors.

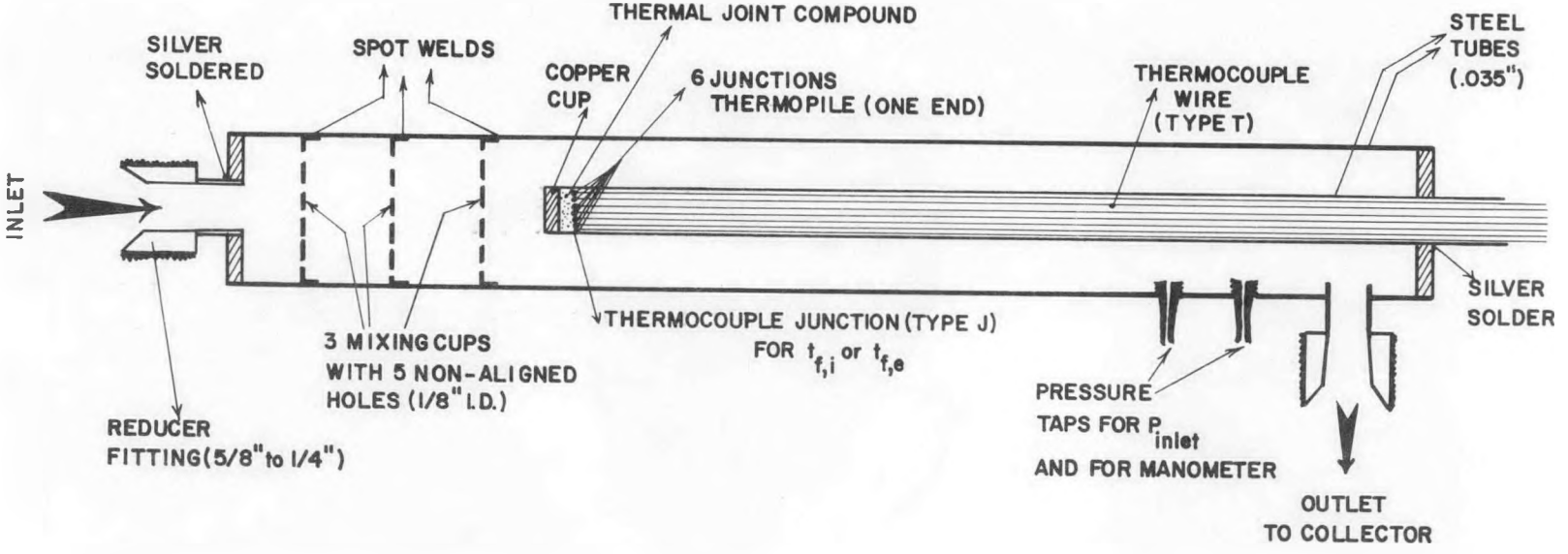

Figure 17 Schematic Diagram of an Alternate Configuration for a Temperature Measuring Station in a Test Loop for Liquid-Heating Solar Collectors.

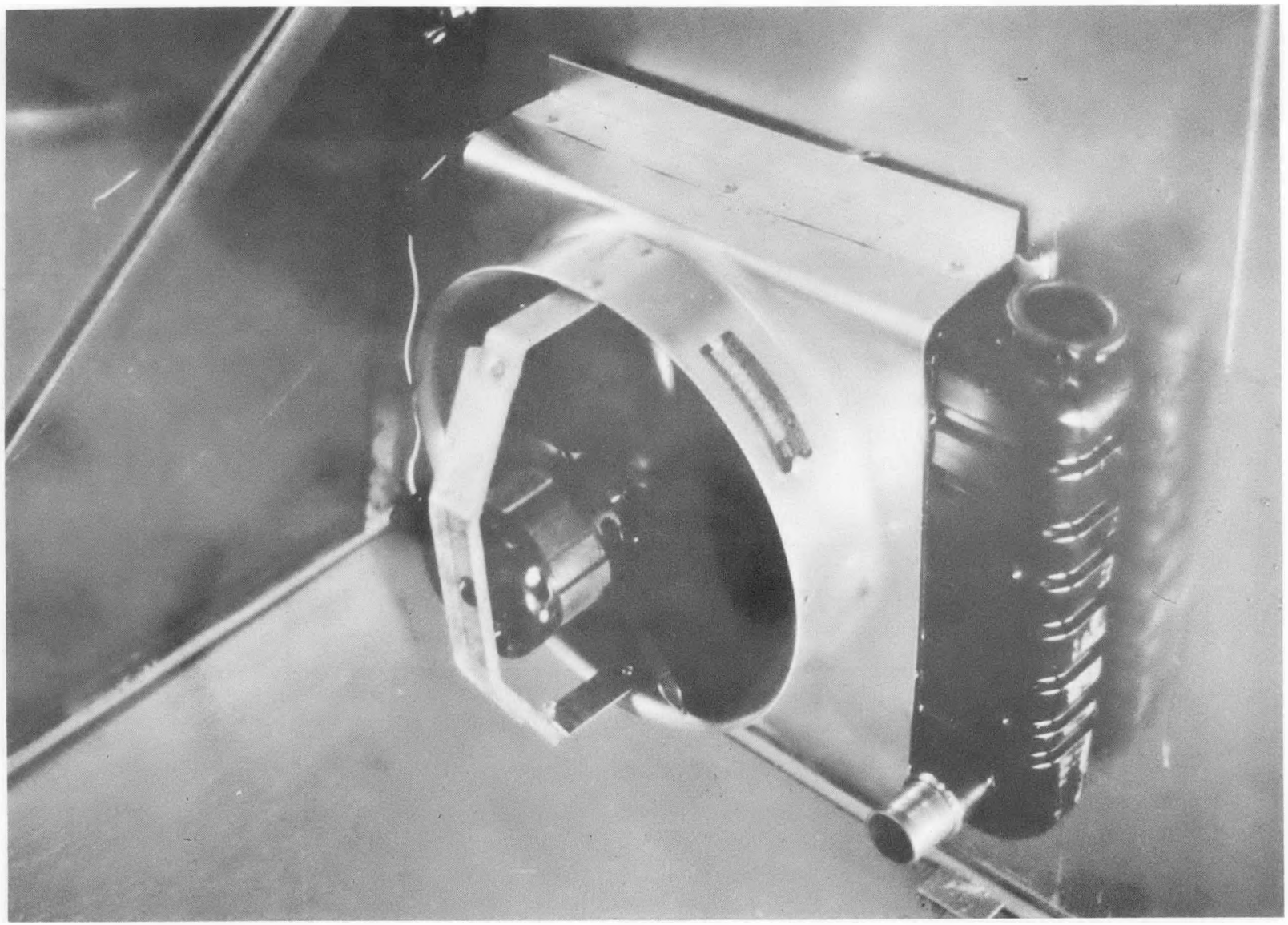

Figure 18 Water-to-Air Heat Exchanger in an NBS Test Stand for Liquid-Heating Solar Collectors.

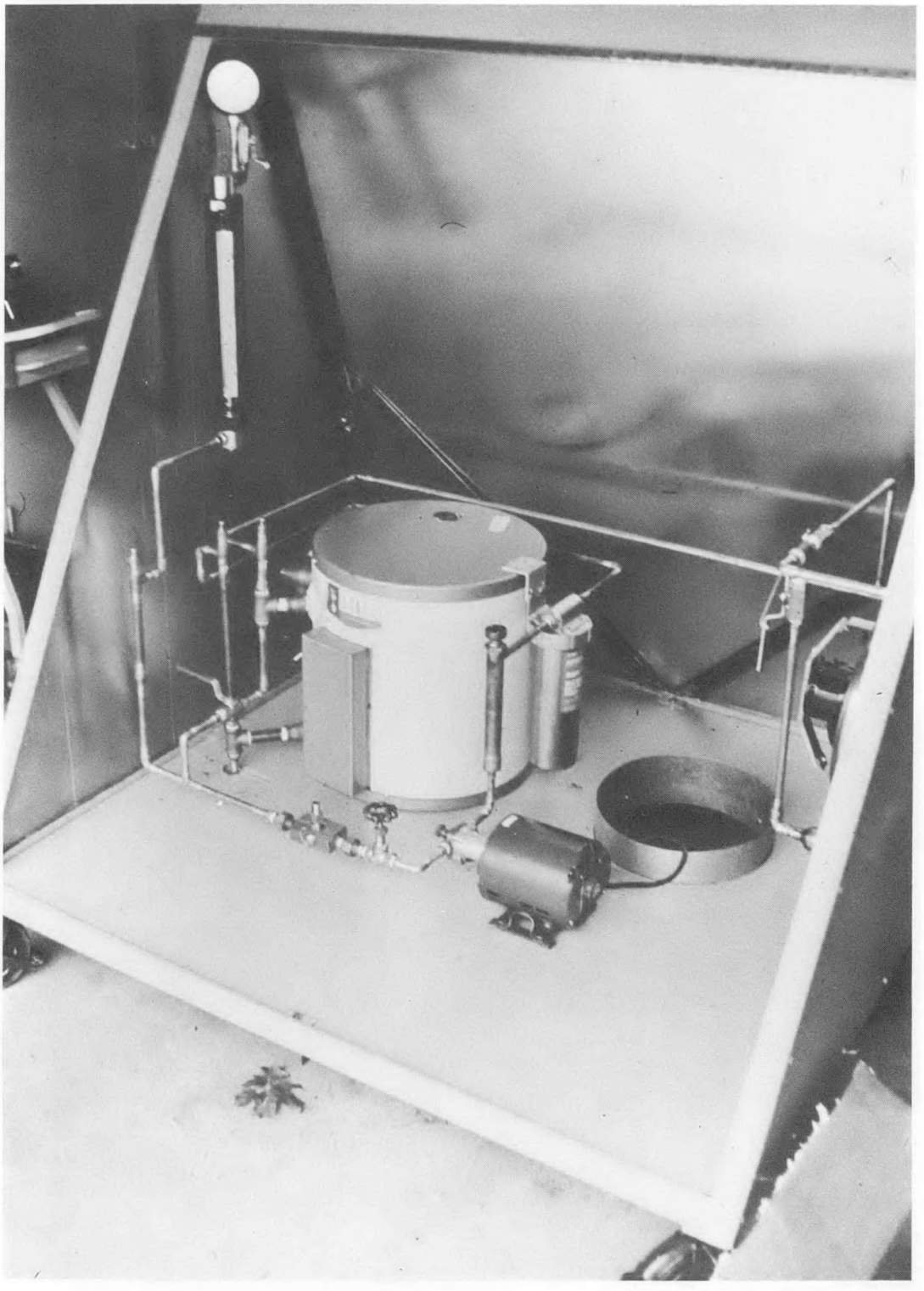

Figure 19 NBS Test Stand for Liquid-Heating Solar Collectors During Fabrication.

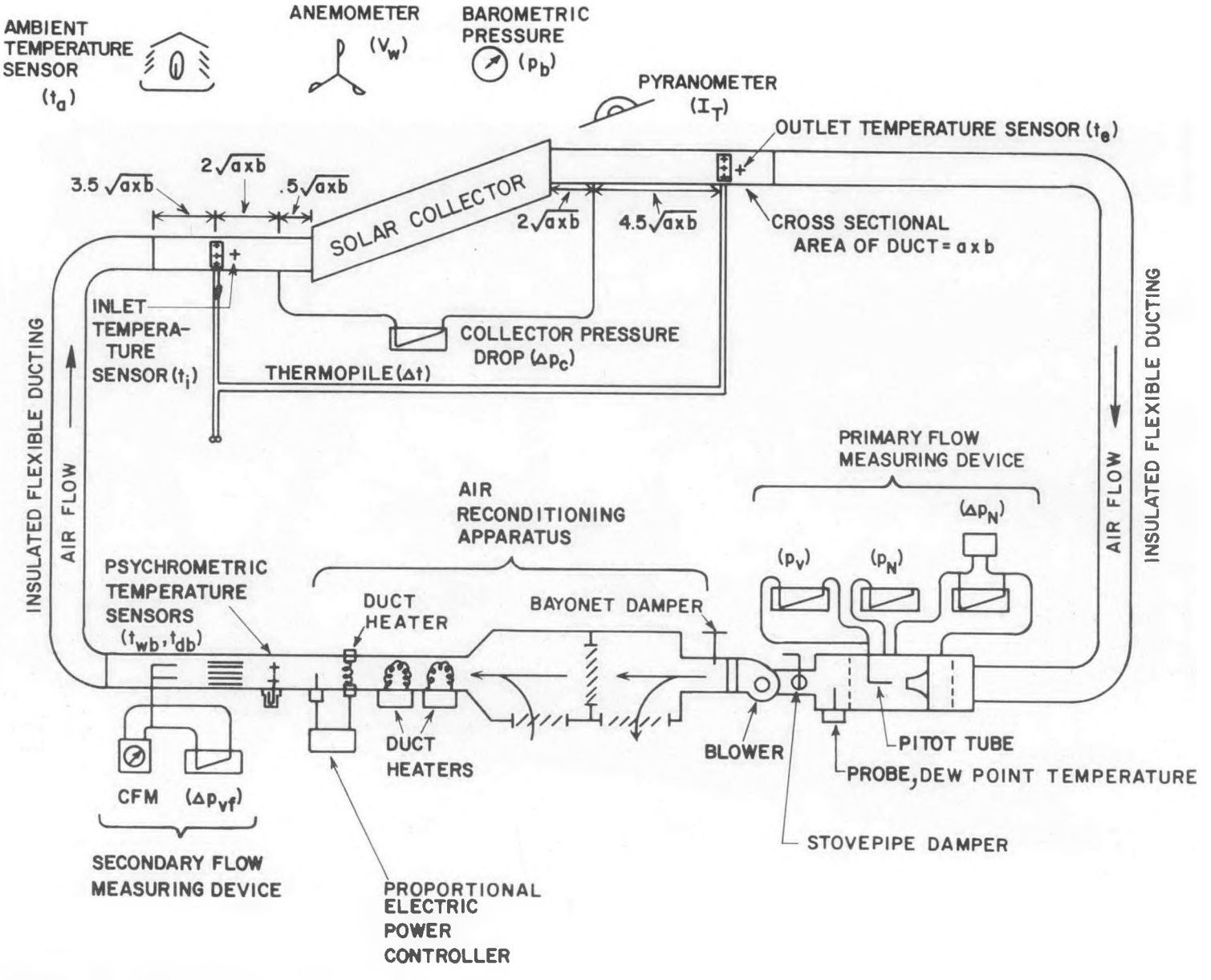

Figure 21 Schematic Diagram of the NBS Test Stand for Air-Heating Solar Collectors.

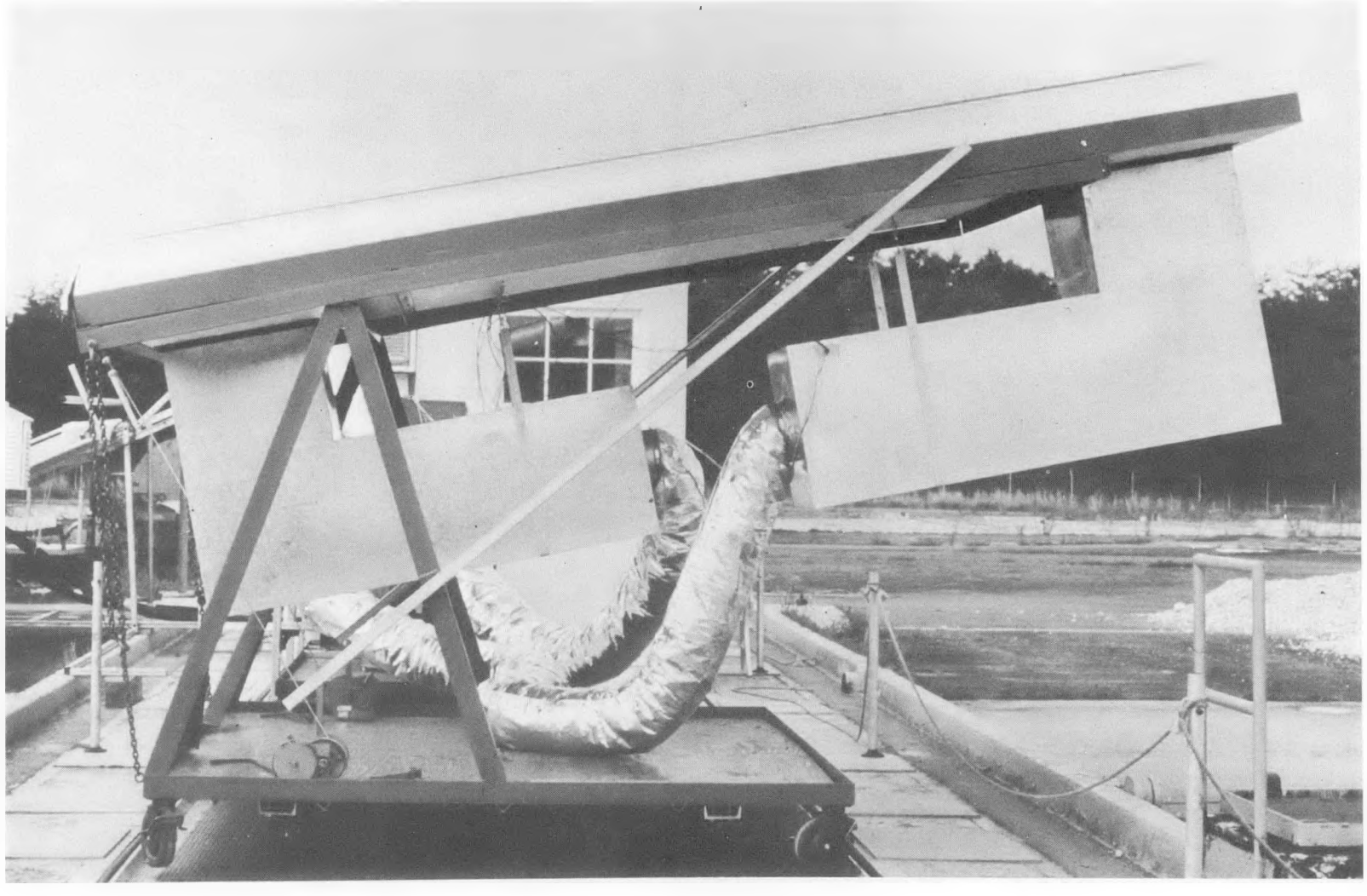

Figure 22 Test Stand for Air-Heating Solar Collectors as Seen from the Side at the NIKI Site, NBS, Gaithersburg, Maryland.

Figure 23 Test Stand for Air-Heating Solar Collectors being Turned into Position for Testing at the NIKI Site, NBS, Gaithersburg, Maryland.

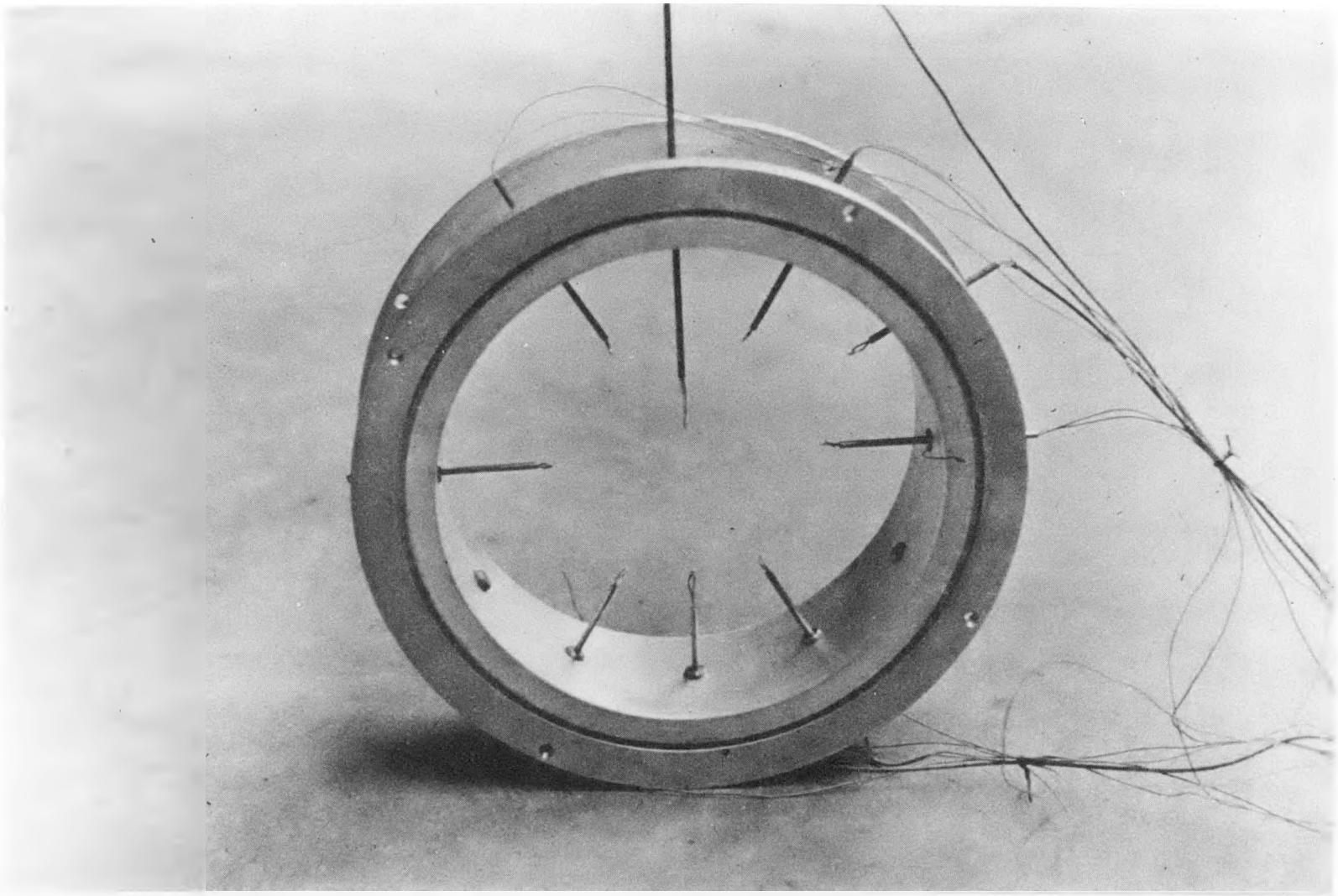

Figure 24 Framework for Temperature Sensors in the NBS Test Stand for Air-Heating Solar Collectors.

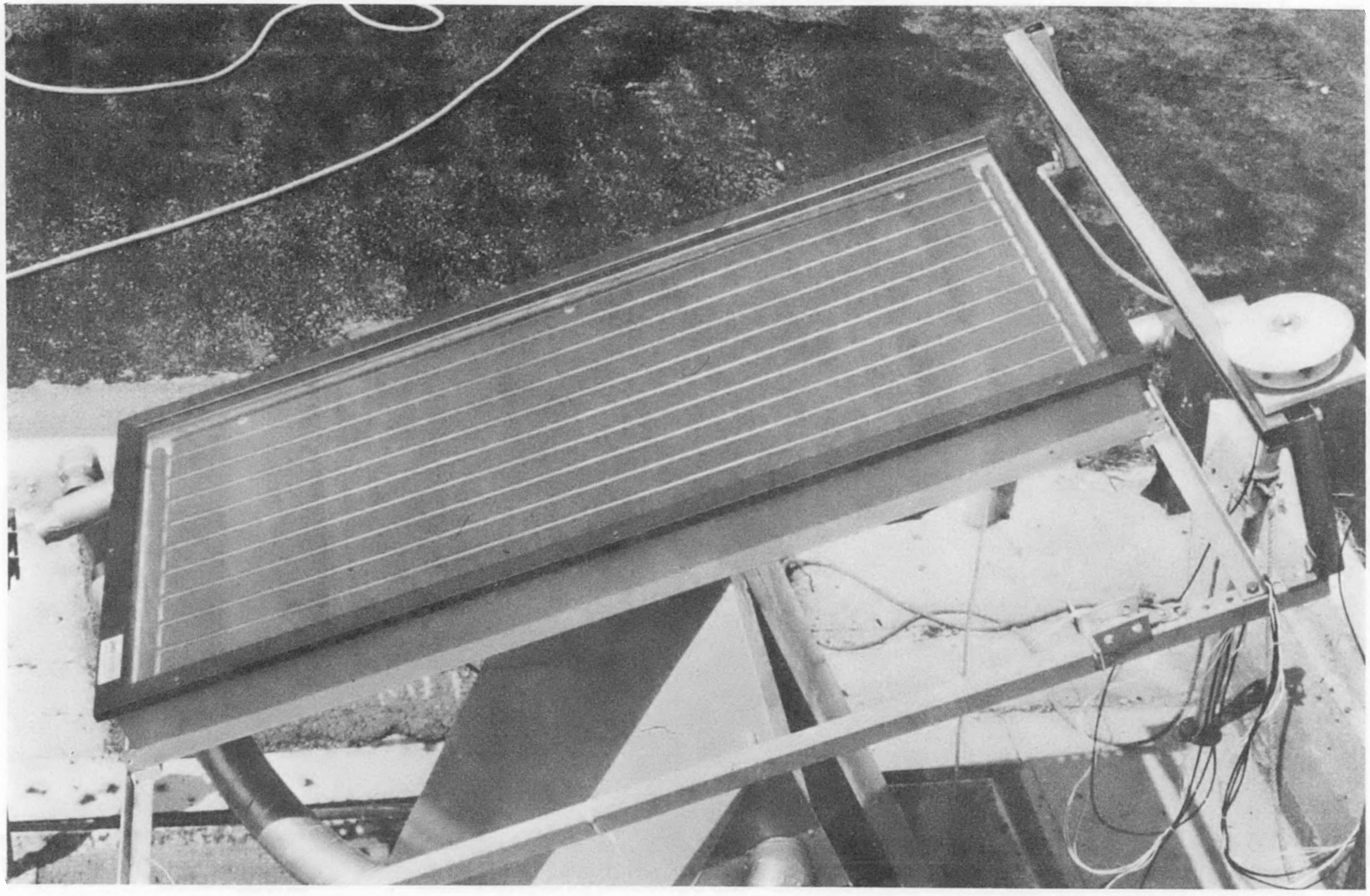

Figure 25 Collector and Pyranometer on an NBS Test Stand for Liquid-Heating Solar Collectors.

Figure 26 A Pyranometer Being Shaded During a Solar Collector Test at the NIKI Site, NBS, Gaithersburg, Maryland.

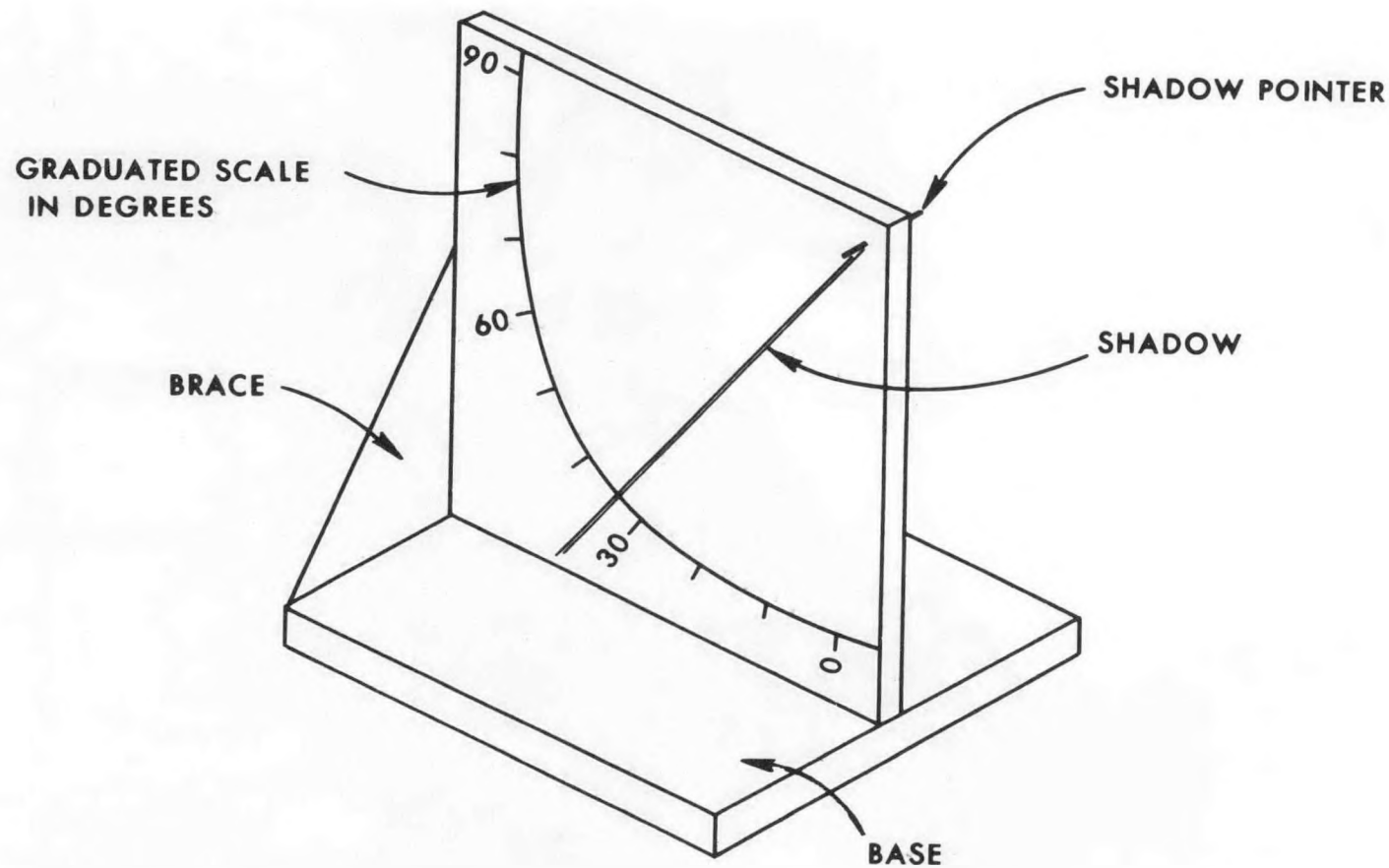

Figure 27 Instrument for Measuring the Angle of Incidence between the Outward Drawn Normal from a Surface and the Direct Solar Beam.

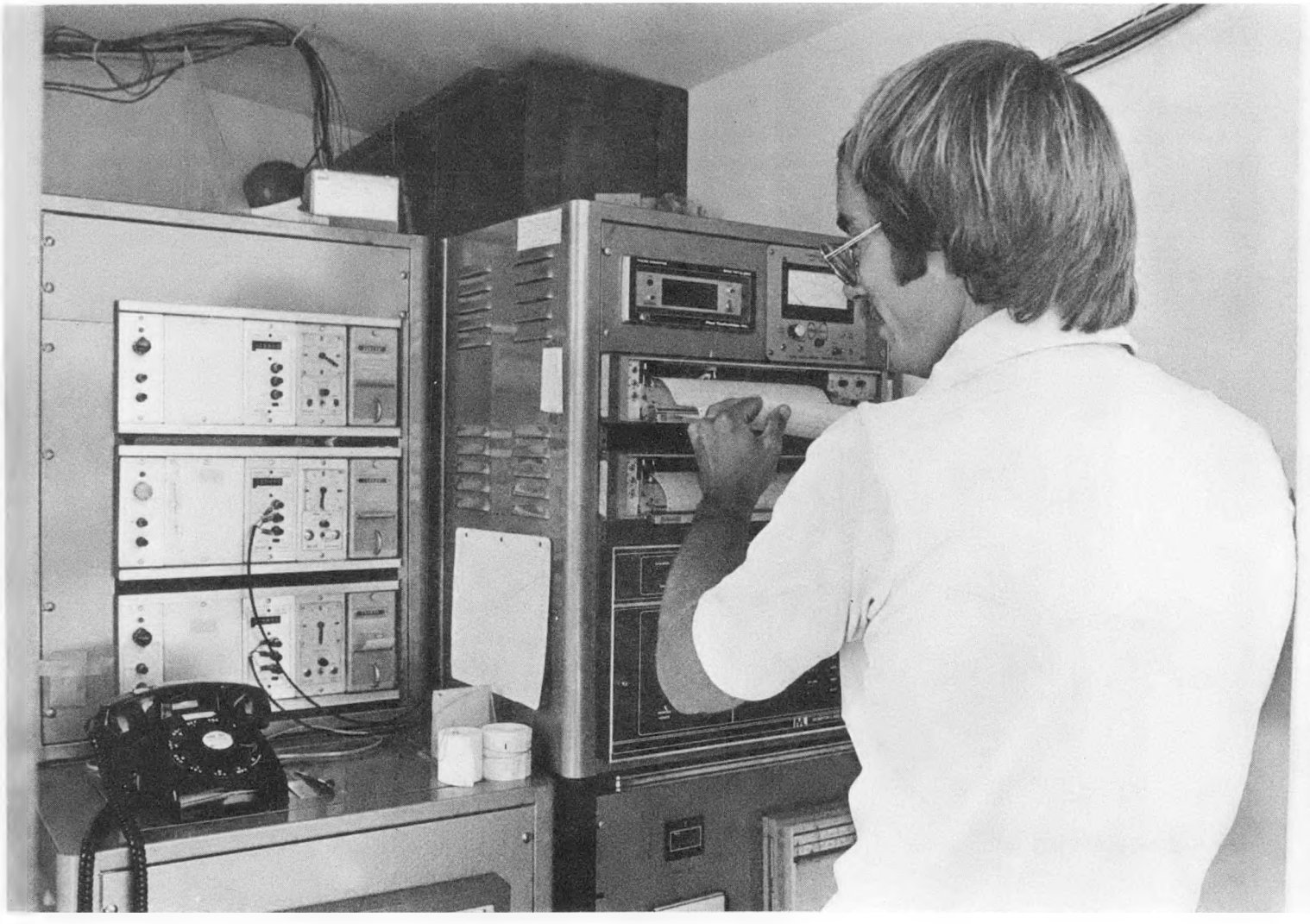

Figure 28 Data Acquisition Equipment Used with the Solar Collector Test Stands at the NIKI Site, NBS, Gaithersburg, Maryland.

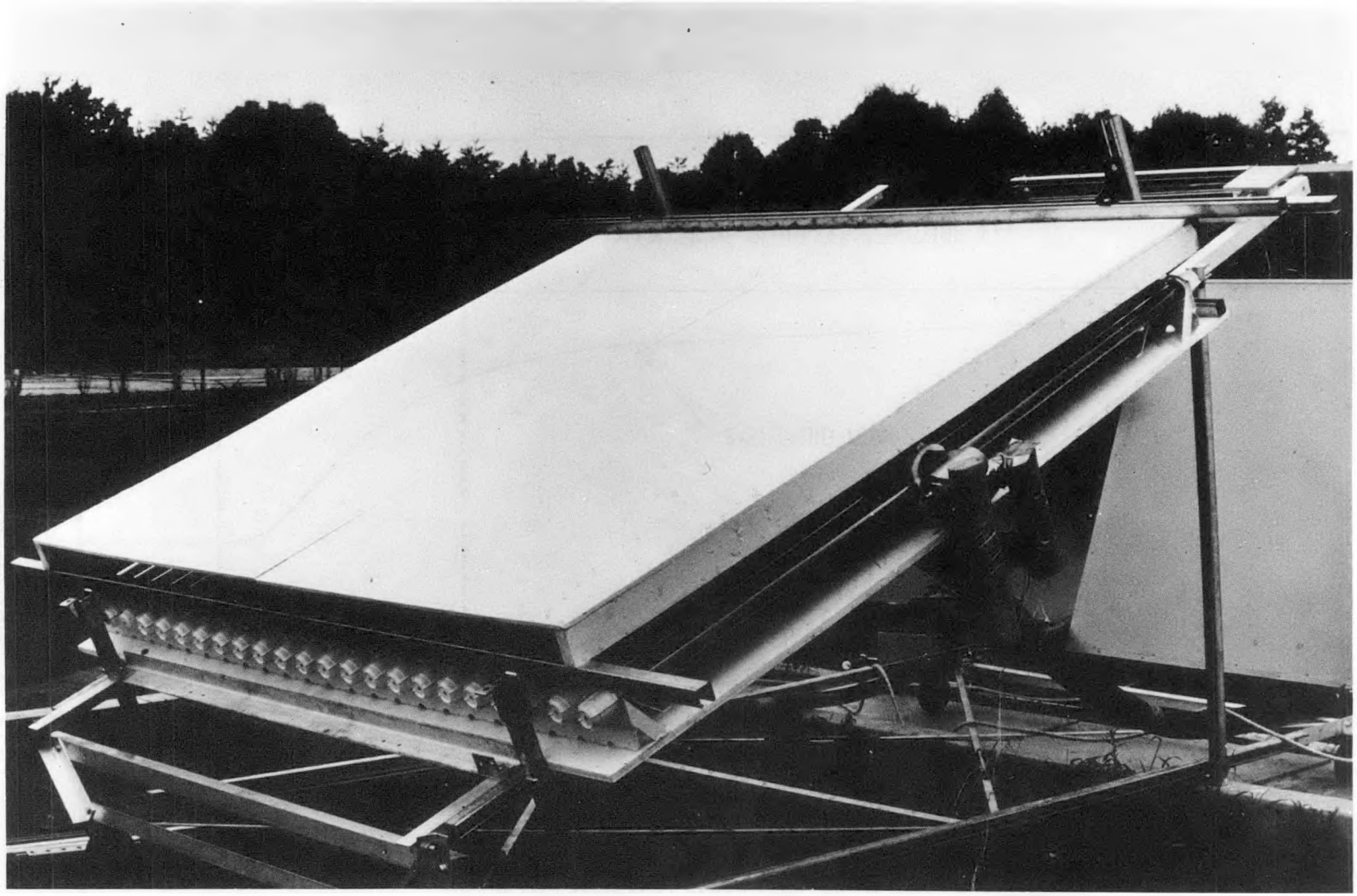

Figure 29 Evacuated Tubular Solar Collector Being Shaded During a Test to Determine the Time Constant at the NIKI Site, NBS, Gaithersburg, Maryland.

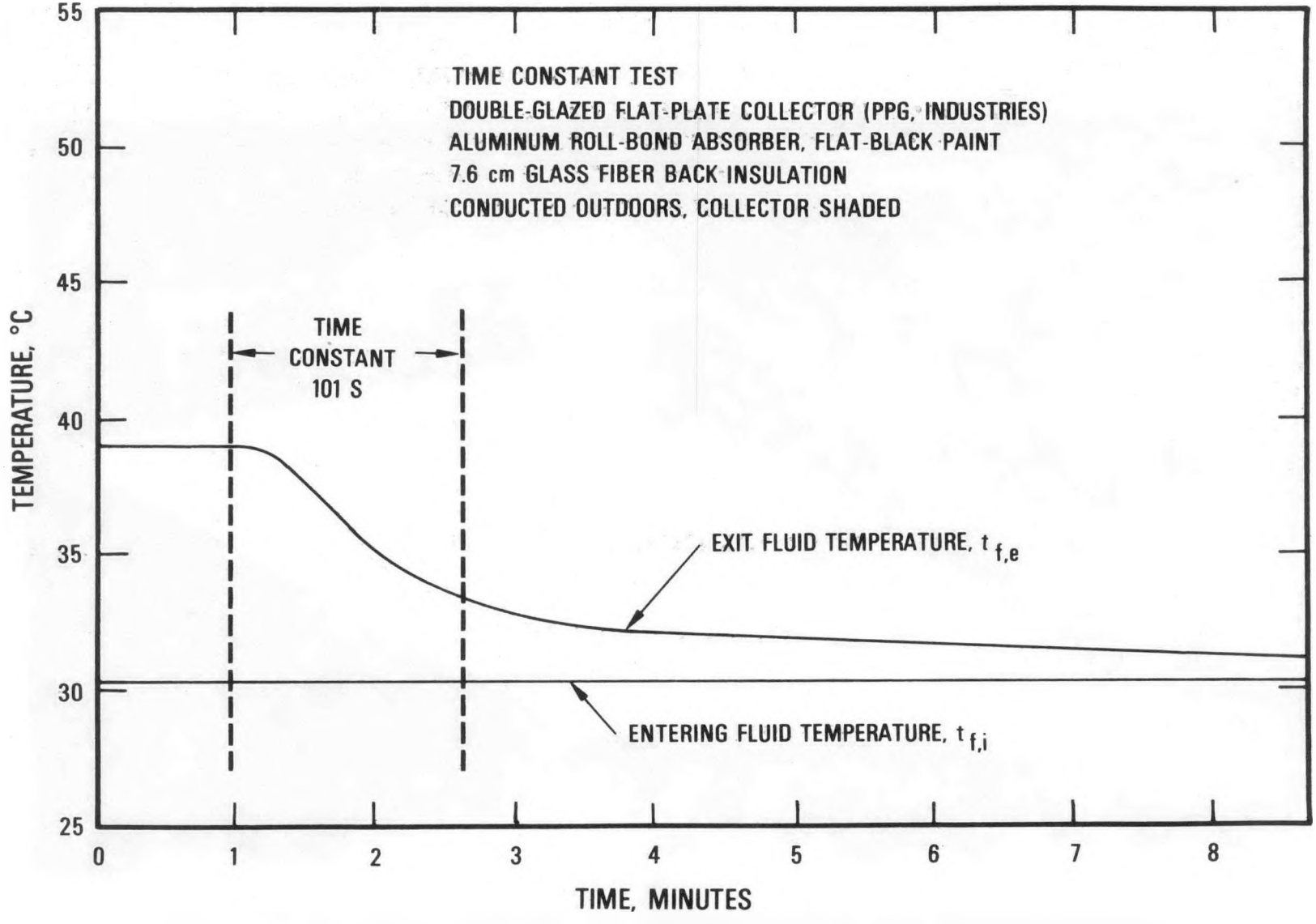

Figure 30 Experimental Results for the Time Constant Test for Water-Heating Solar Collector No. 1.

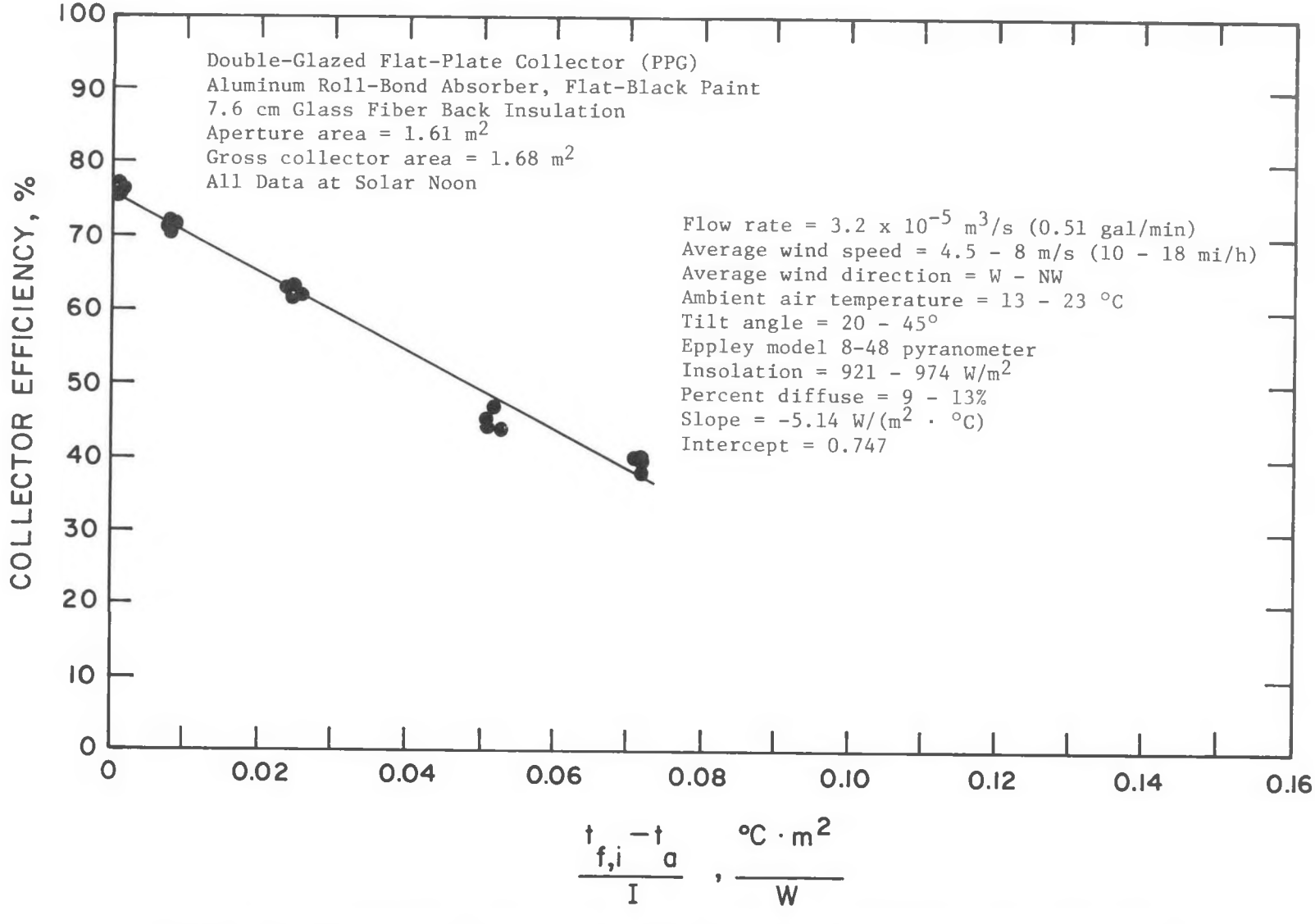

Figure 31 Experimental Results for the Near-Normal-Incidence Efficiency Test for Water-Heating Solar Collector No. 1; All Data Collected at Solar Noon.

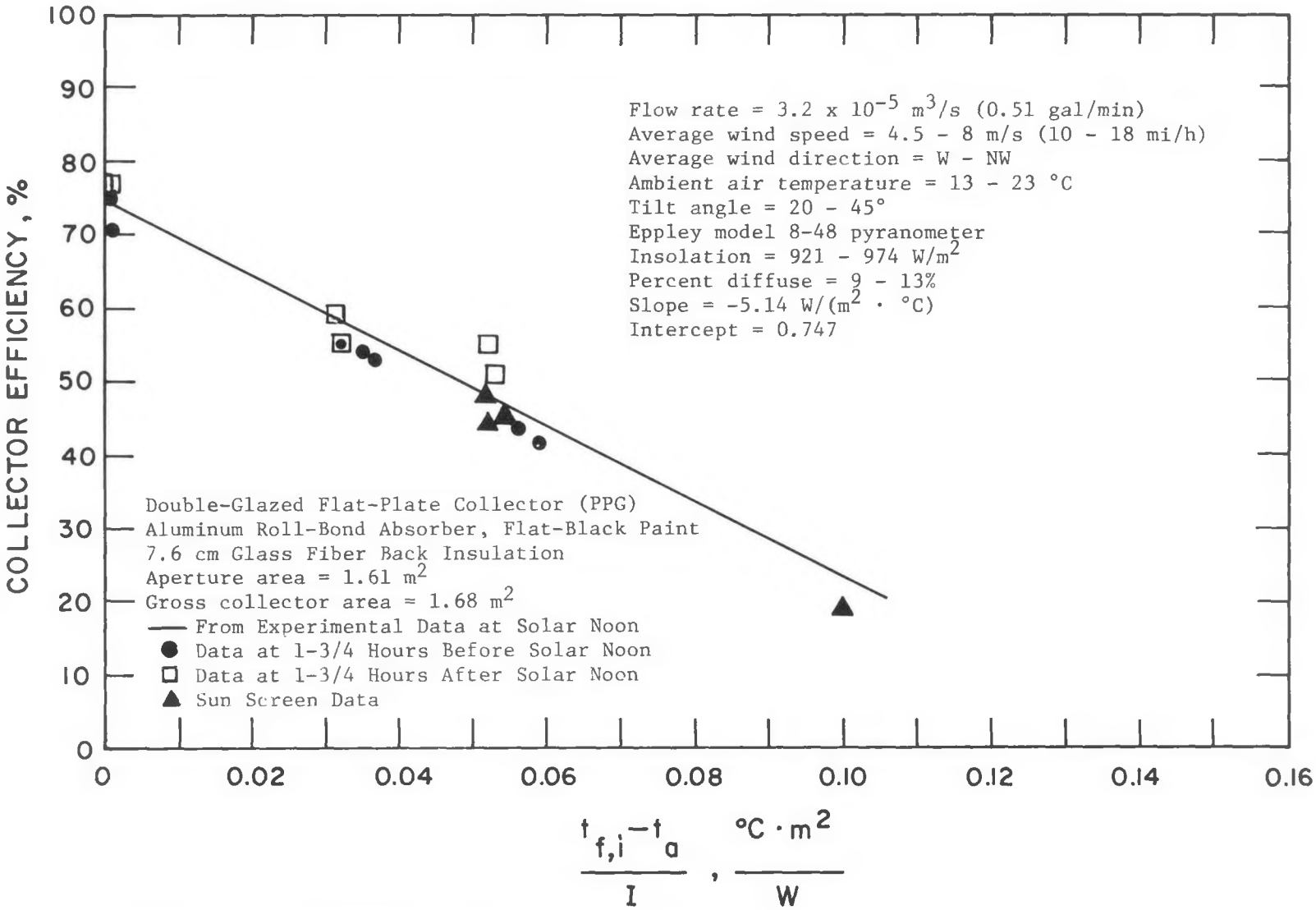

Figure 32 Experimental Results for the Near-Normal-Incidence Efficiency Test for Water-Heating Solar Collector No. 1; All Data Collected Symmetrical with Solar Noon.

Figure 33 A Solar Screen Mounted Above Water-Heating Solar Collector No. 1 During a Test to Determine the Near-Normal-Incidence Efficiency at the NIKI Site, NBS, Gaithersburg, Maryland.

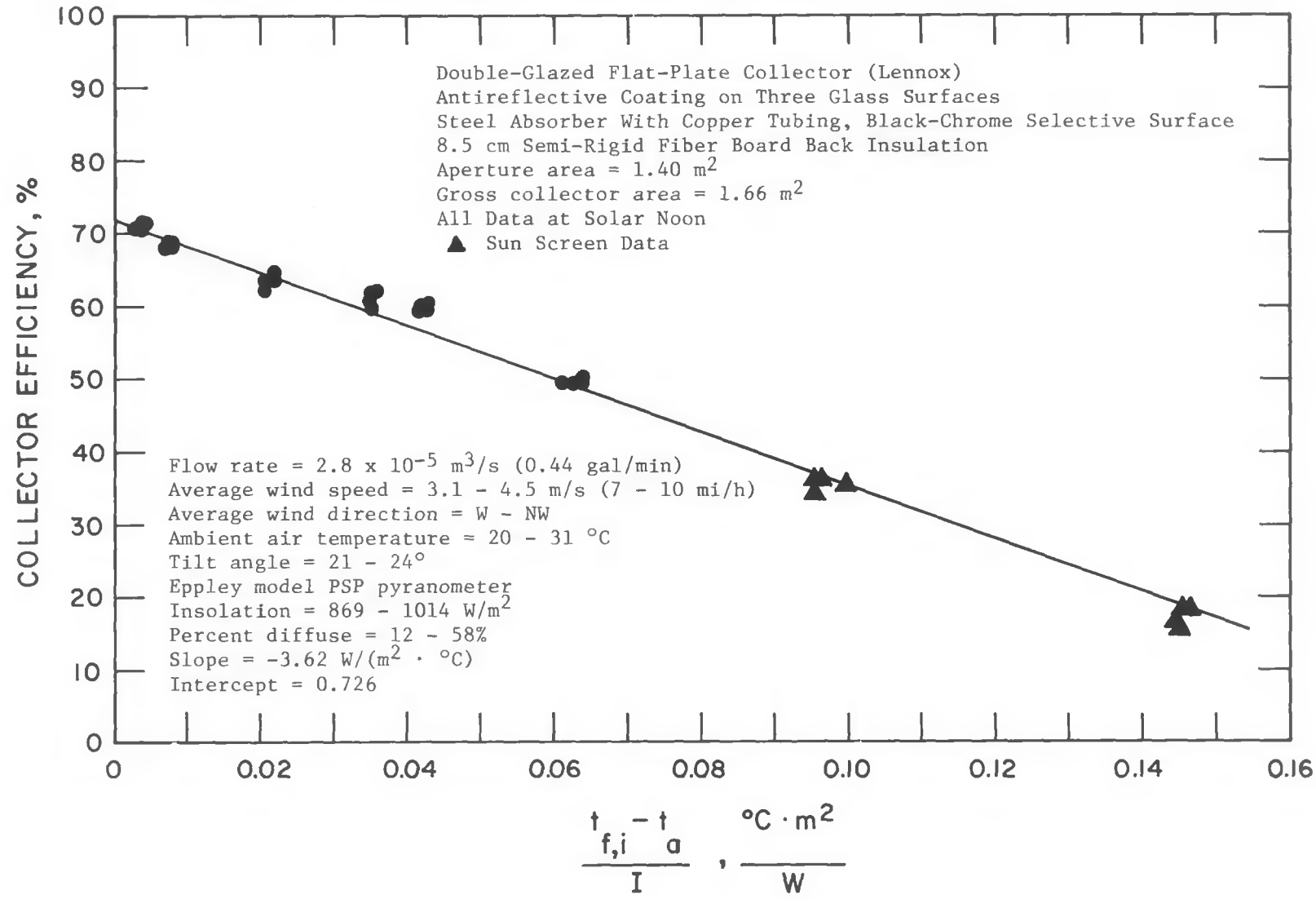

Figure 34 Experimental Results for the Near-Normal-Incidence Efficiency Test for Water-Heating Solar Collector No. 2.

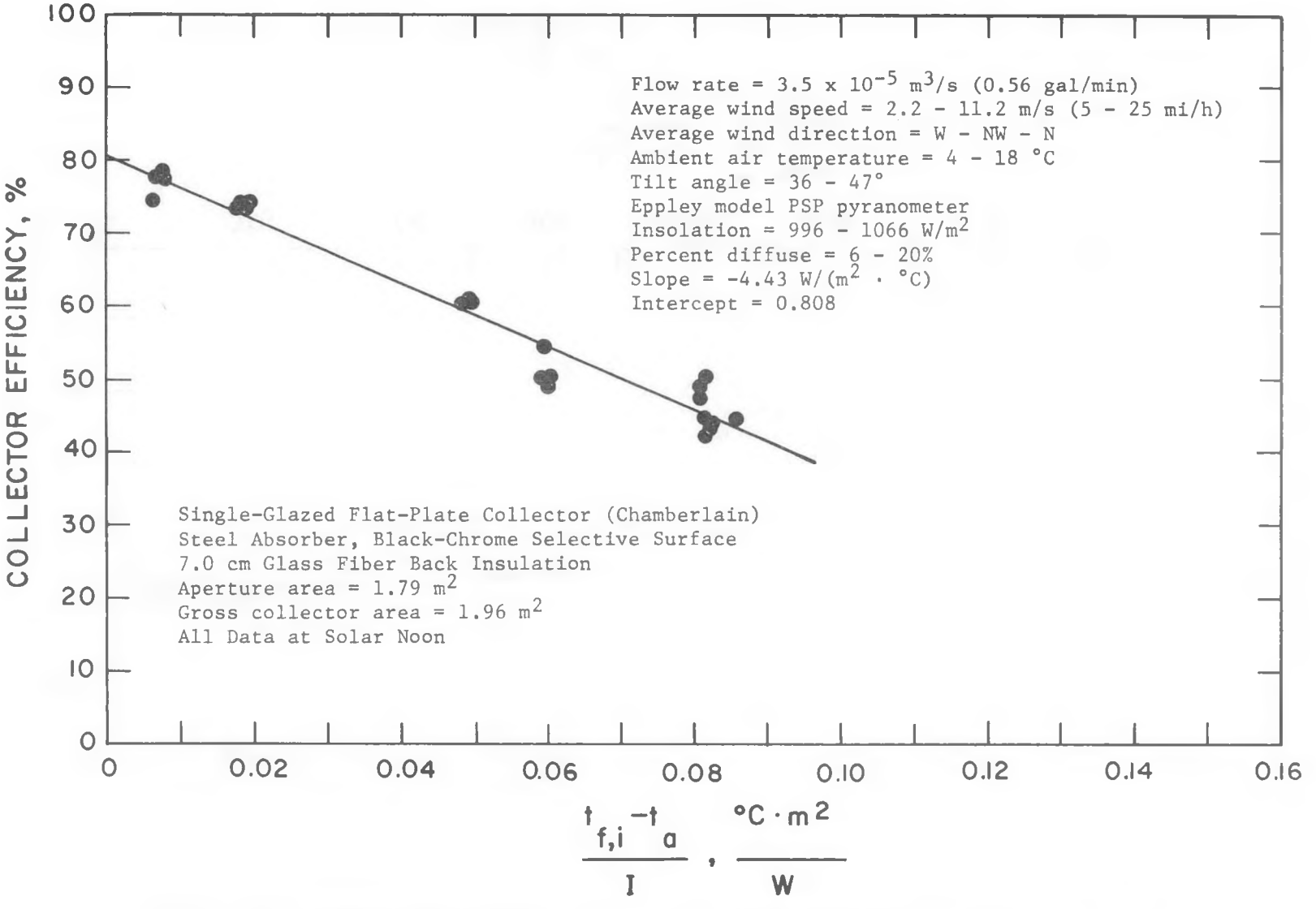

Figure 35 Experimental Results for the Near-Normal-Incidence Efficiency Test for Water-Heating Solar Collector No. 3.

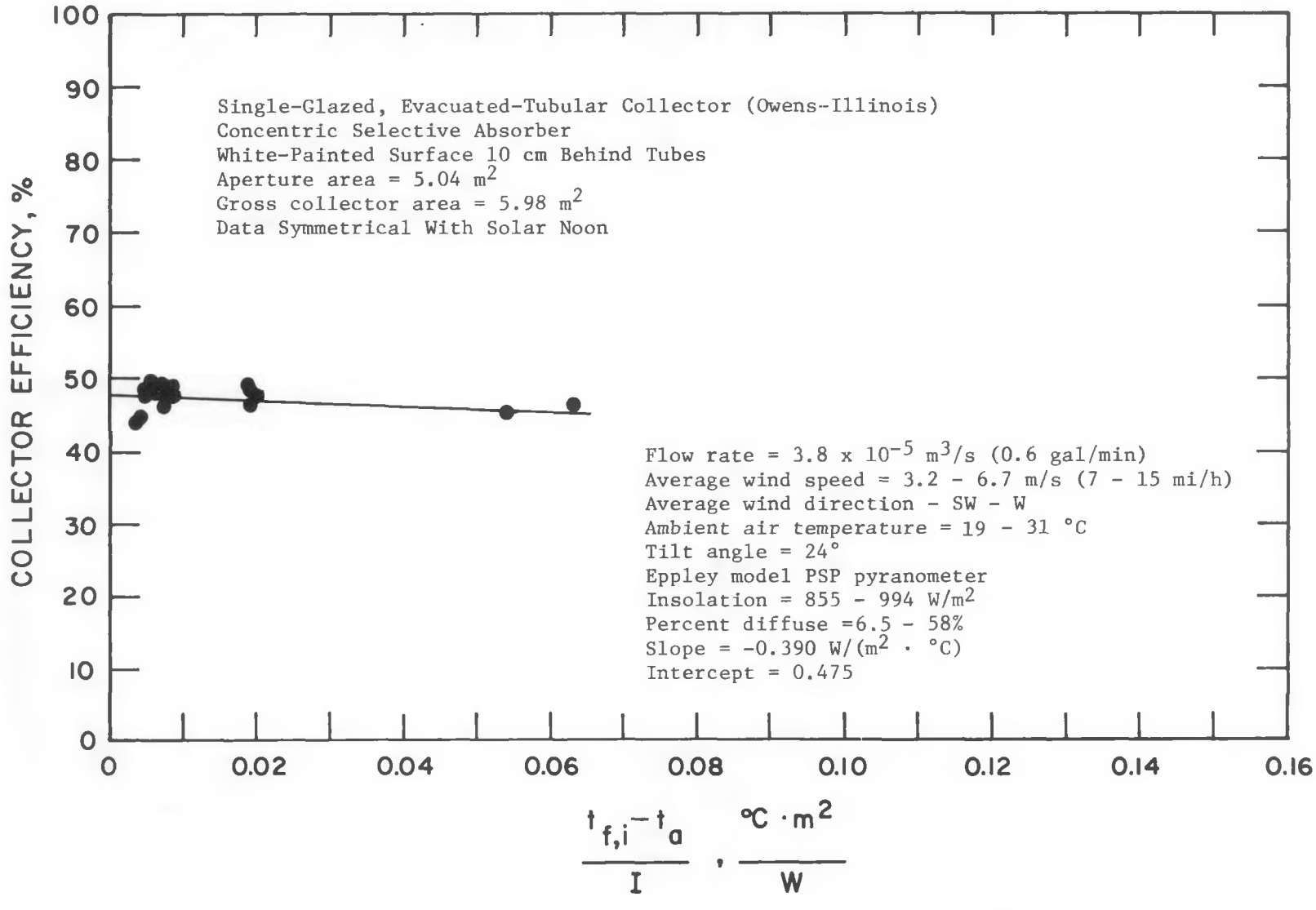

Figure 36 Experimental Results for the Near-Normal-Incidence Efficiency Test for Water-Heating Solar Collector No. 4.

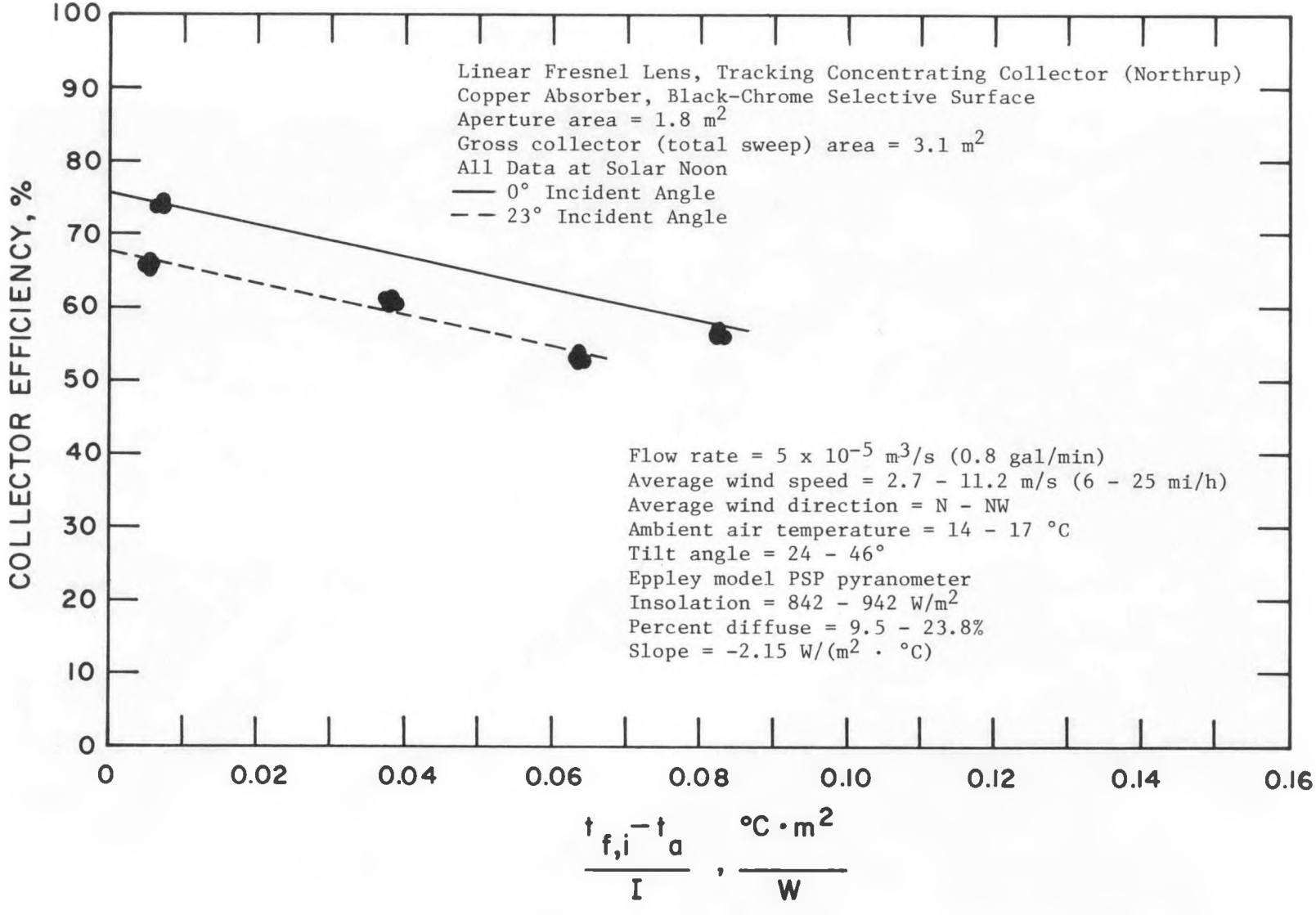

Figure 37 Experimental Results for the Near-Normal-Incidence Efficiency Test for Water-Heating Solar Collector No. 5.

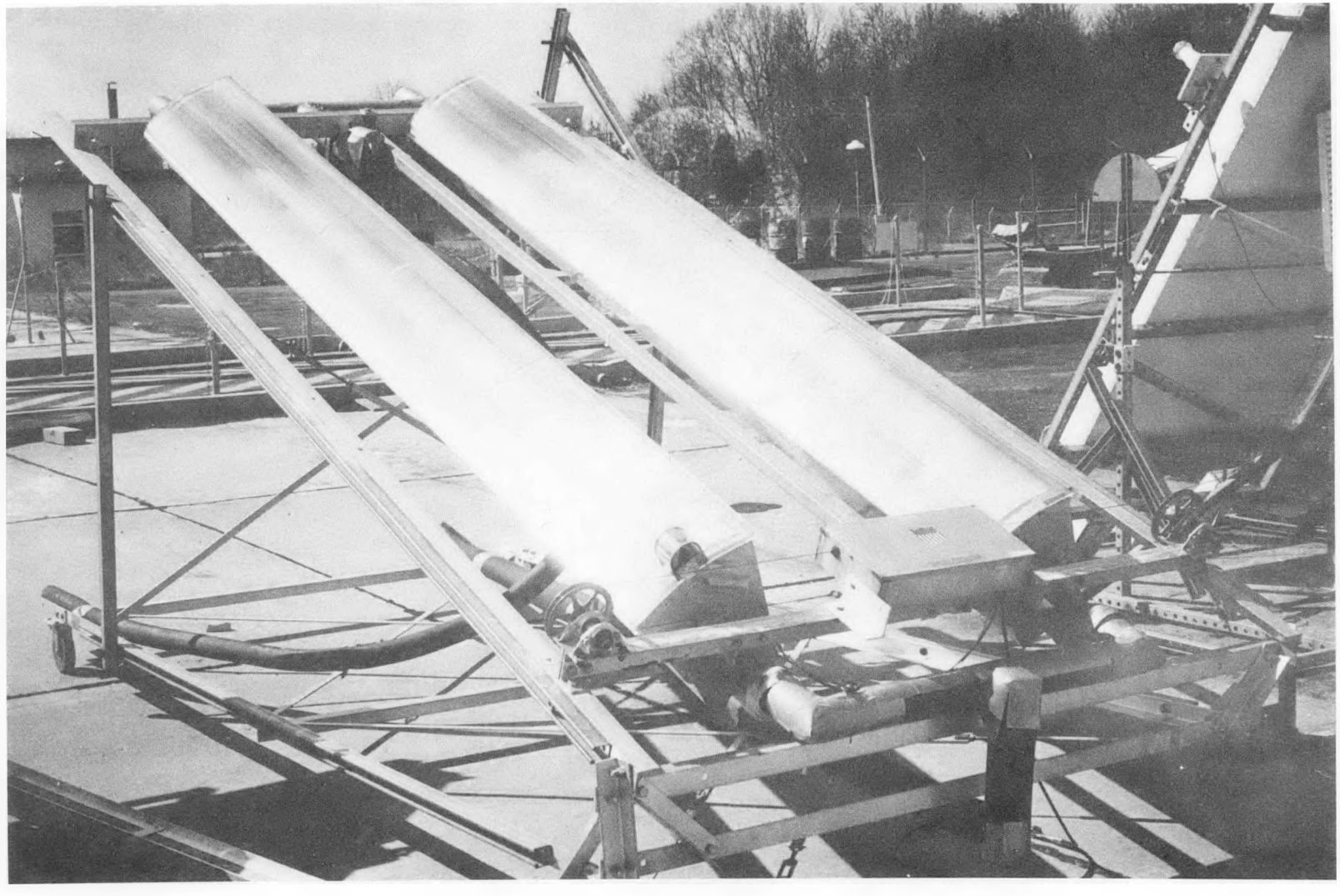

Figure 38 Tracking, Concentrating Water-Heating Solar Collector Which was Tested at the NIKI Site, NBS, Gaithersburg, Maryland.

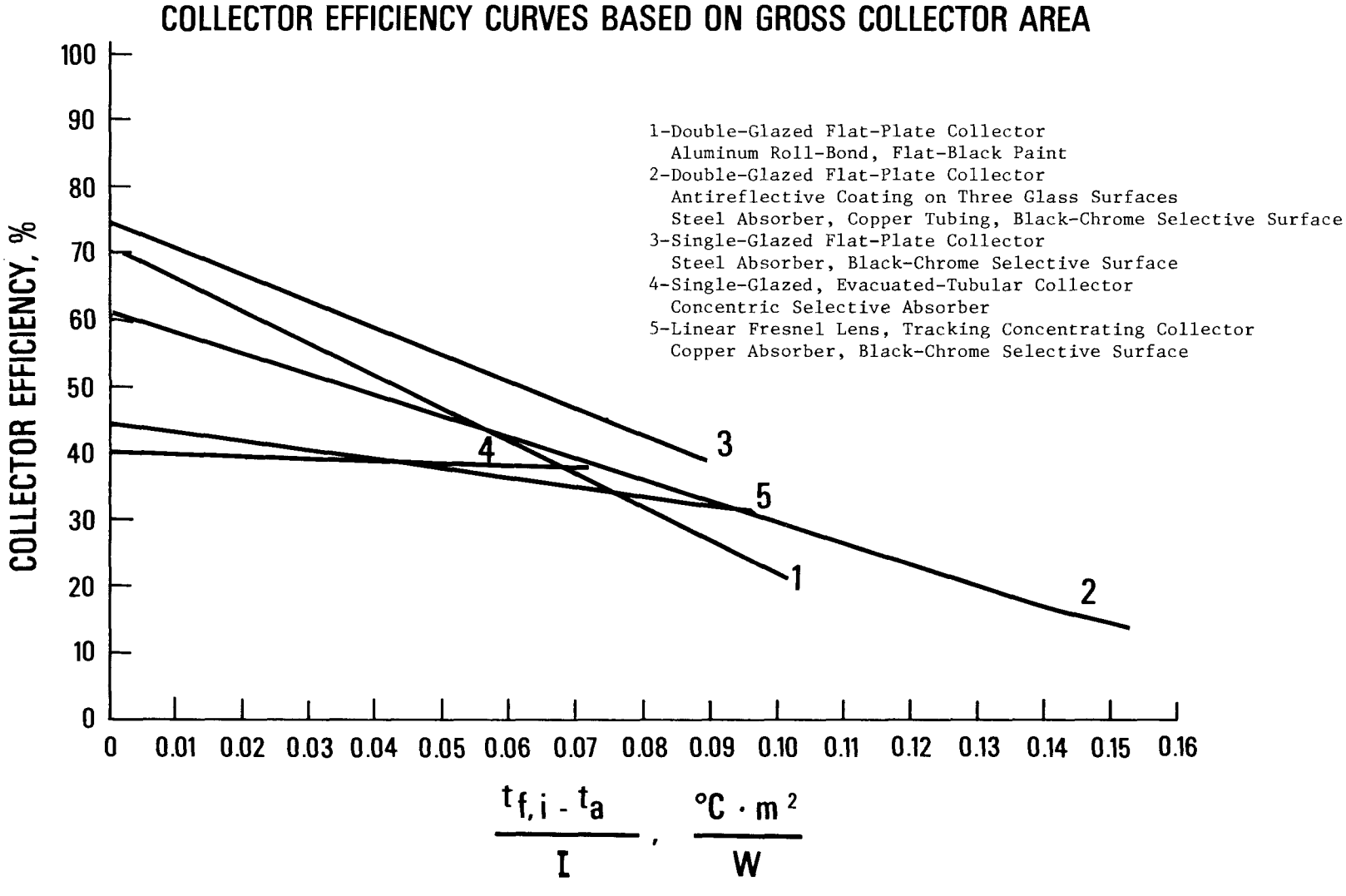

Figure 39 Near-Normal-Incidence Efficiency Based on Gross Collector Area for Selected Water-Heating Solar Collectors.

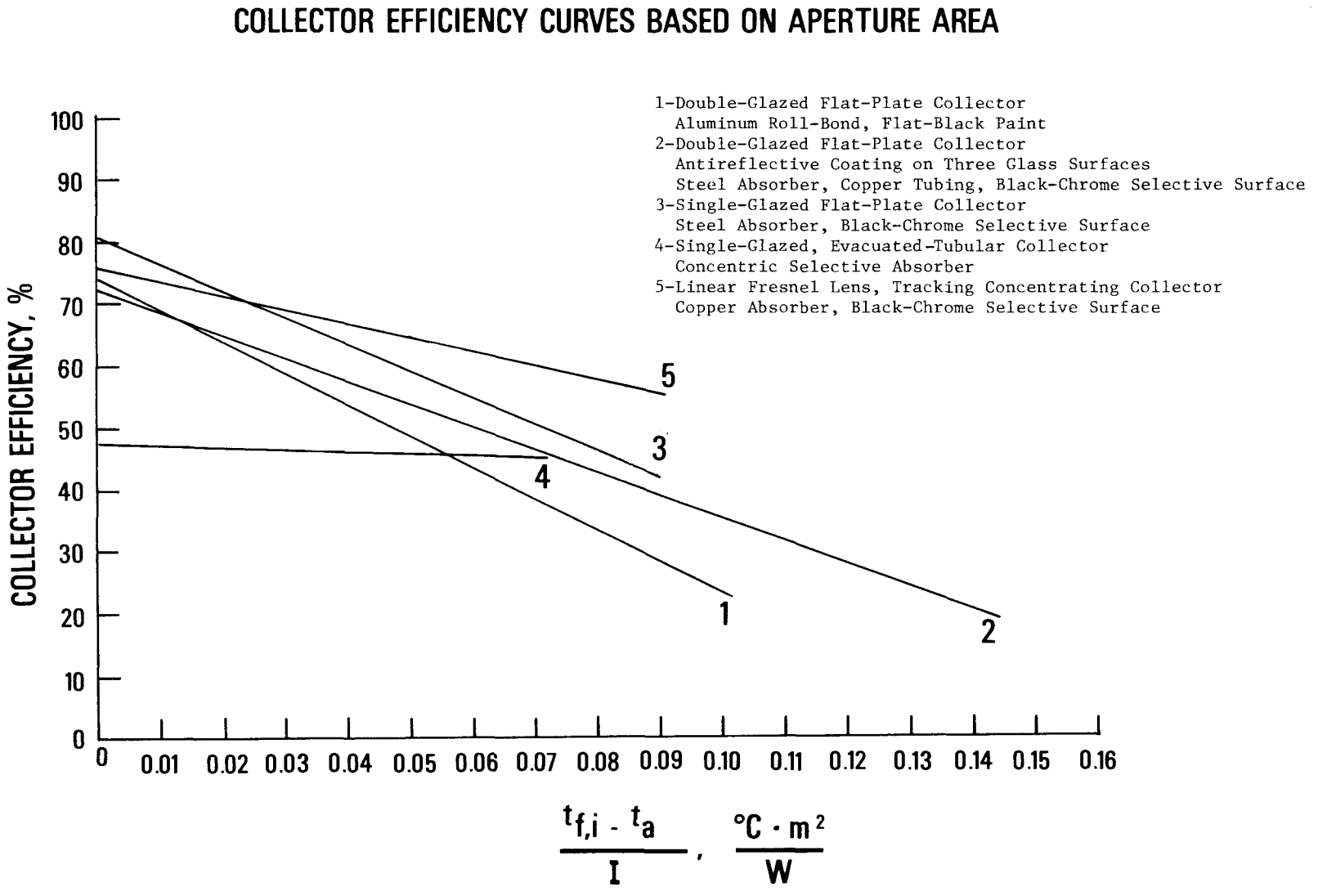

Figure 40 Near-Normal-Incidence Efficiency Based on Aperture Area for Selected Water-Heating Solar Collectors.

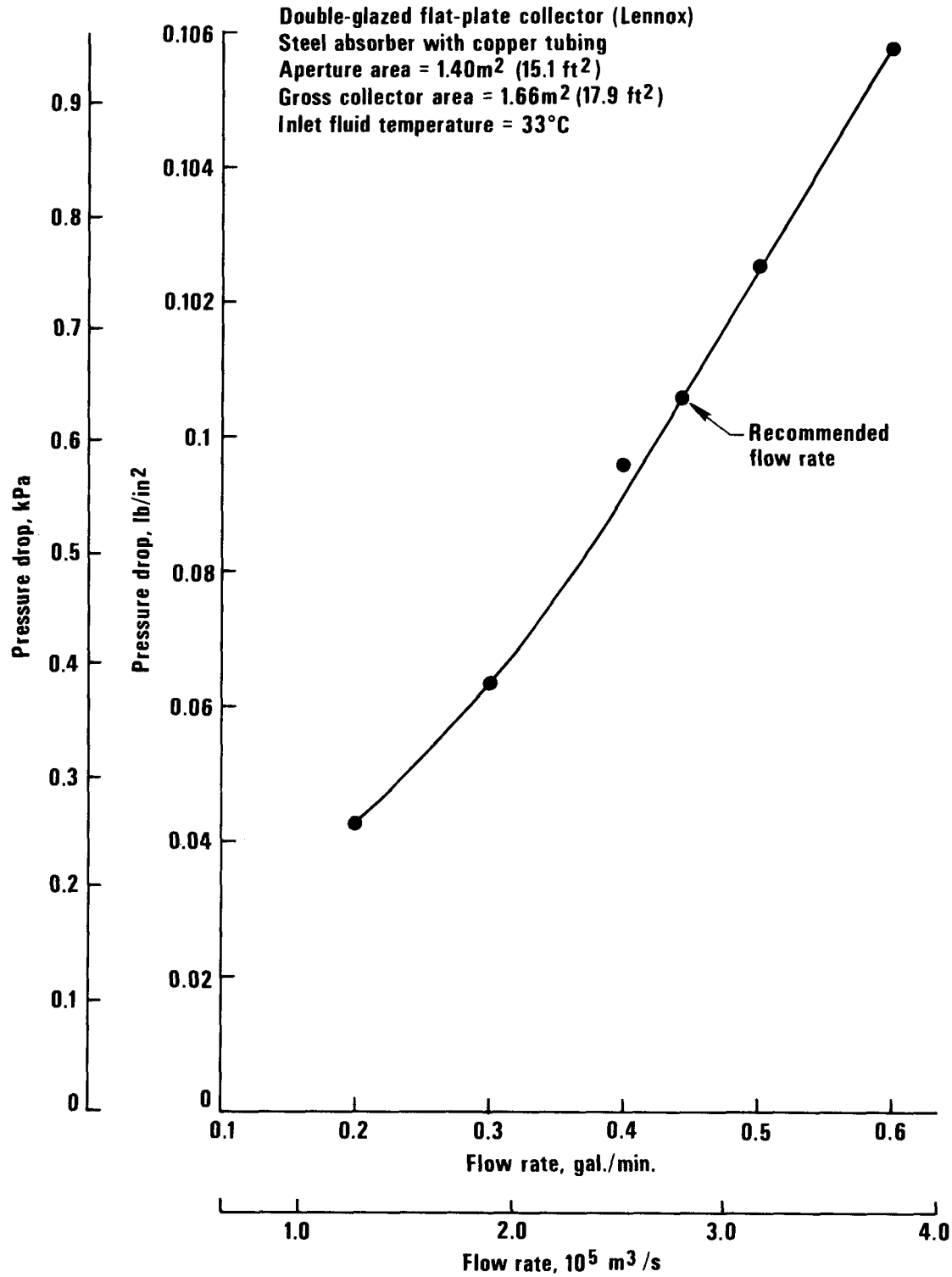

Figure 41 Pressure Drop Versus Flow Rate for Water-Heating Solar Collector No. 2.

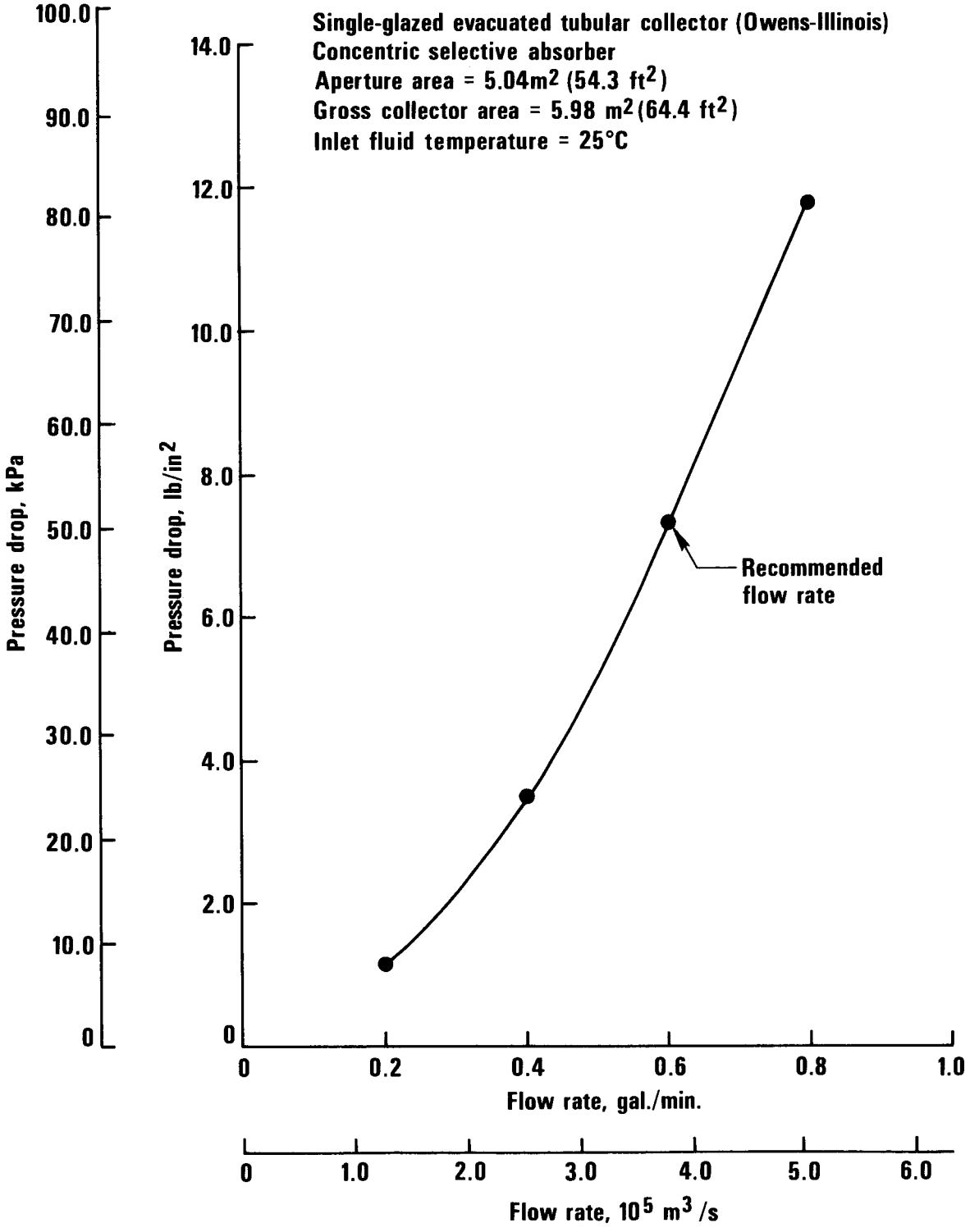

Figure 42 Pressure Drop Versus Flow Rate for Water-Heating Solar Collector No. 4.

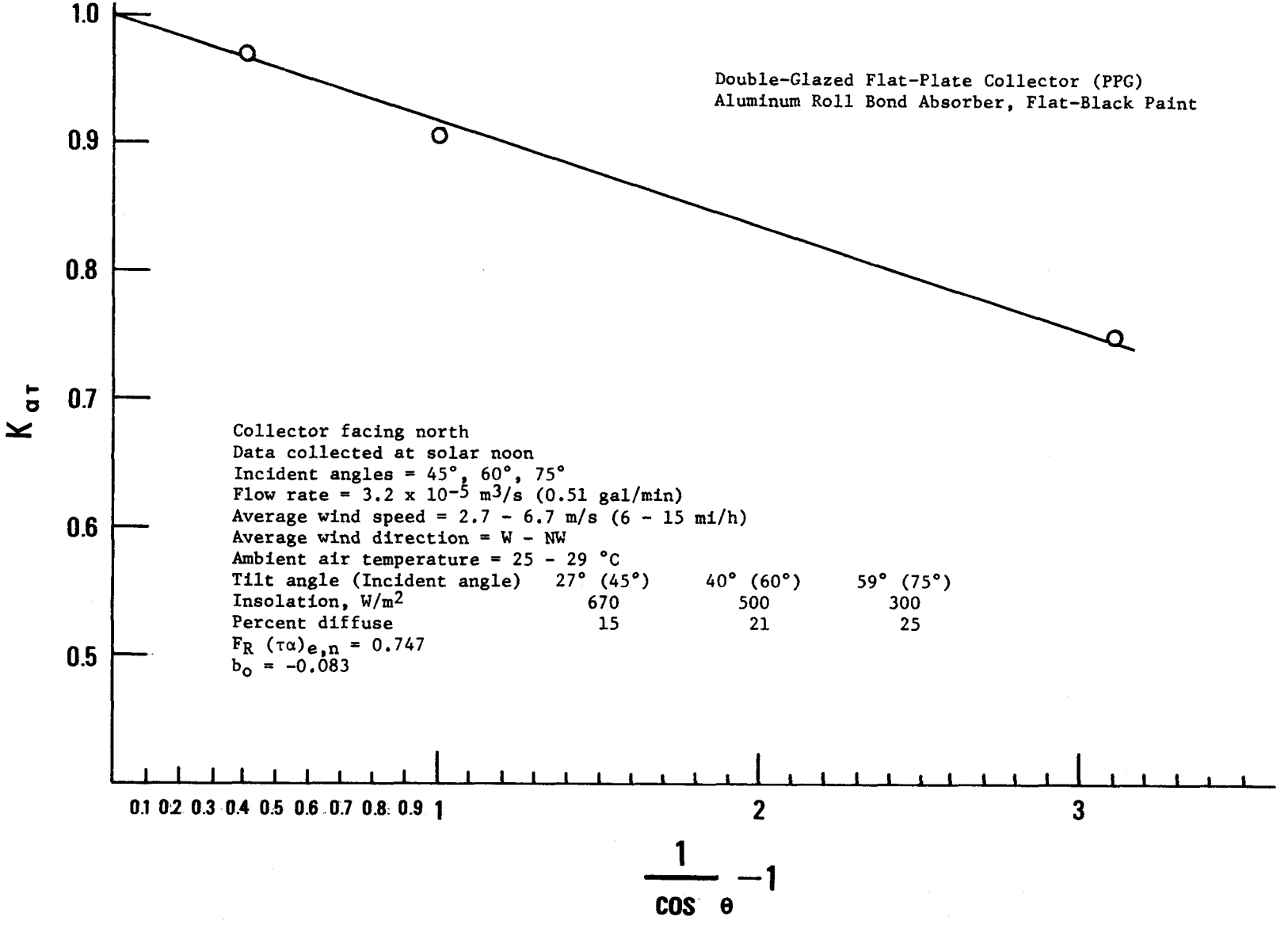

Figure 43 Experimental Results for the Incident Angle Modifier Test for Water-Heating Solar Collector No. 1.

Double-Glazed Flat-Plate Collector (Lennox)
Antireflective Coating on Three Glass Surfaces
Steel Absorber With Copper Tubing, Black-Chrome Selective Surface
8.5 cm Simi-Rigid Fiber Board Back Insulation

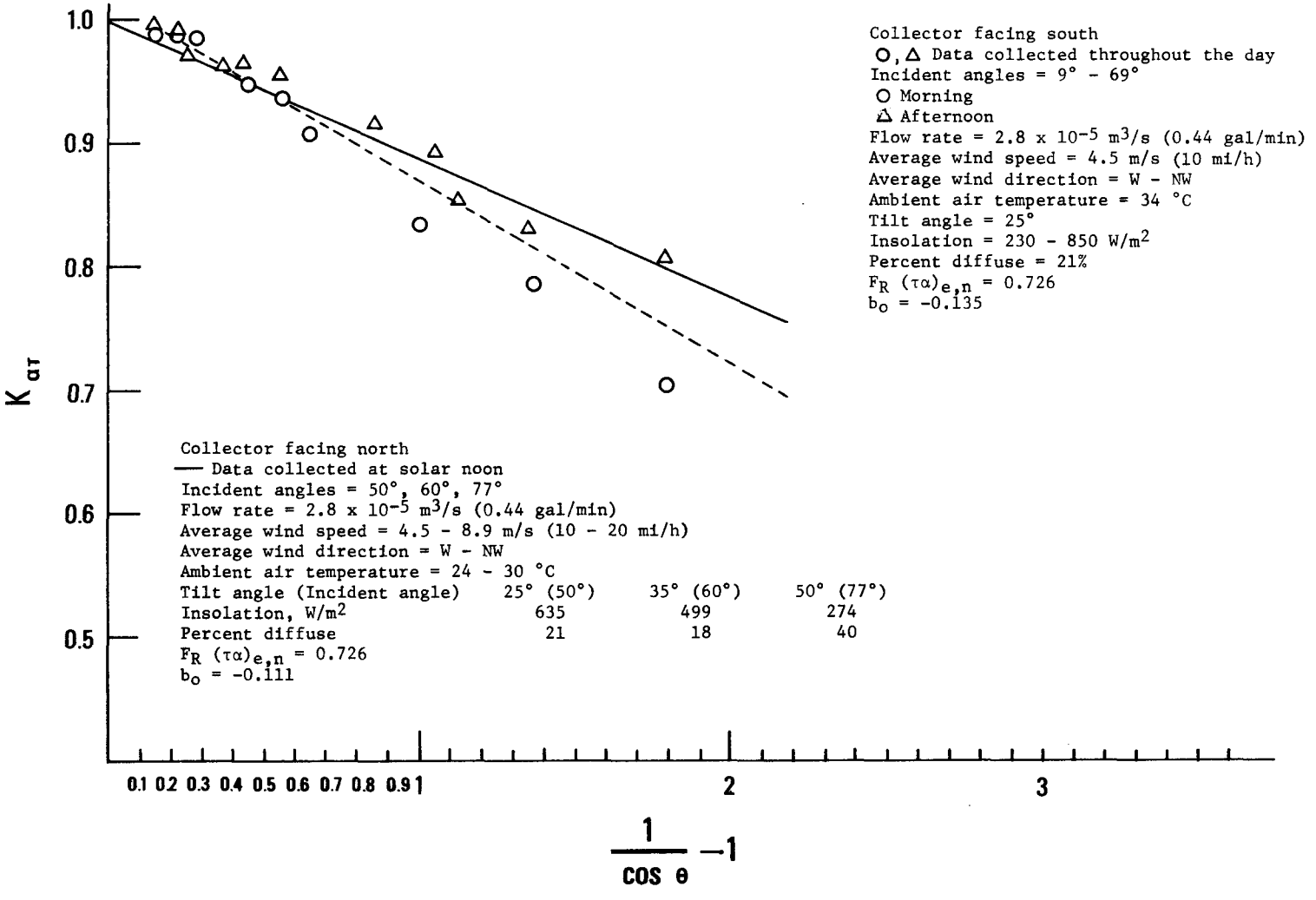

Figure 44 Experimental Results for the Incident Angle Modifier Test for Water-Heating Solar Collector No. 2.

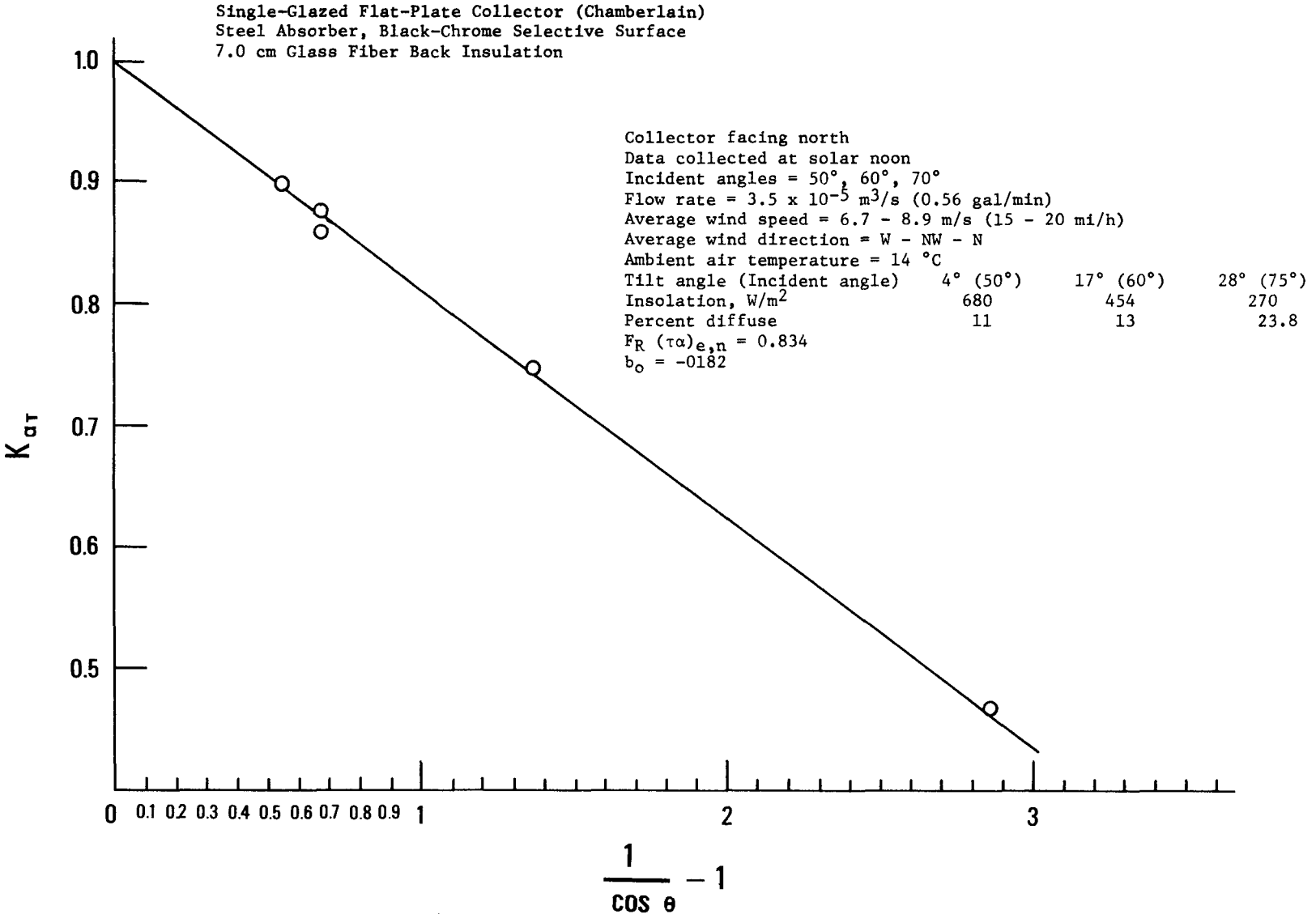

Figure 45 Experimental Results for the Incident Angle Modifier Test for Water-Heating Solar Collector No. 3.

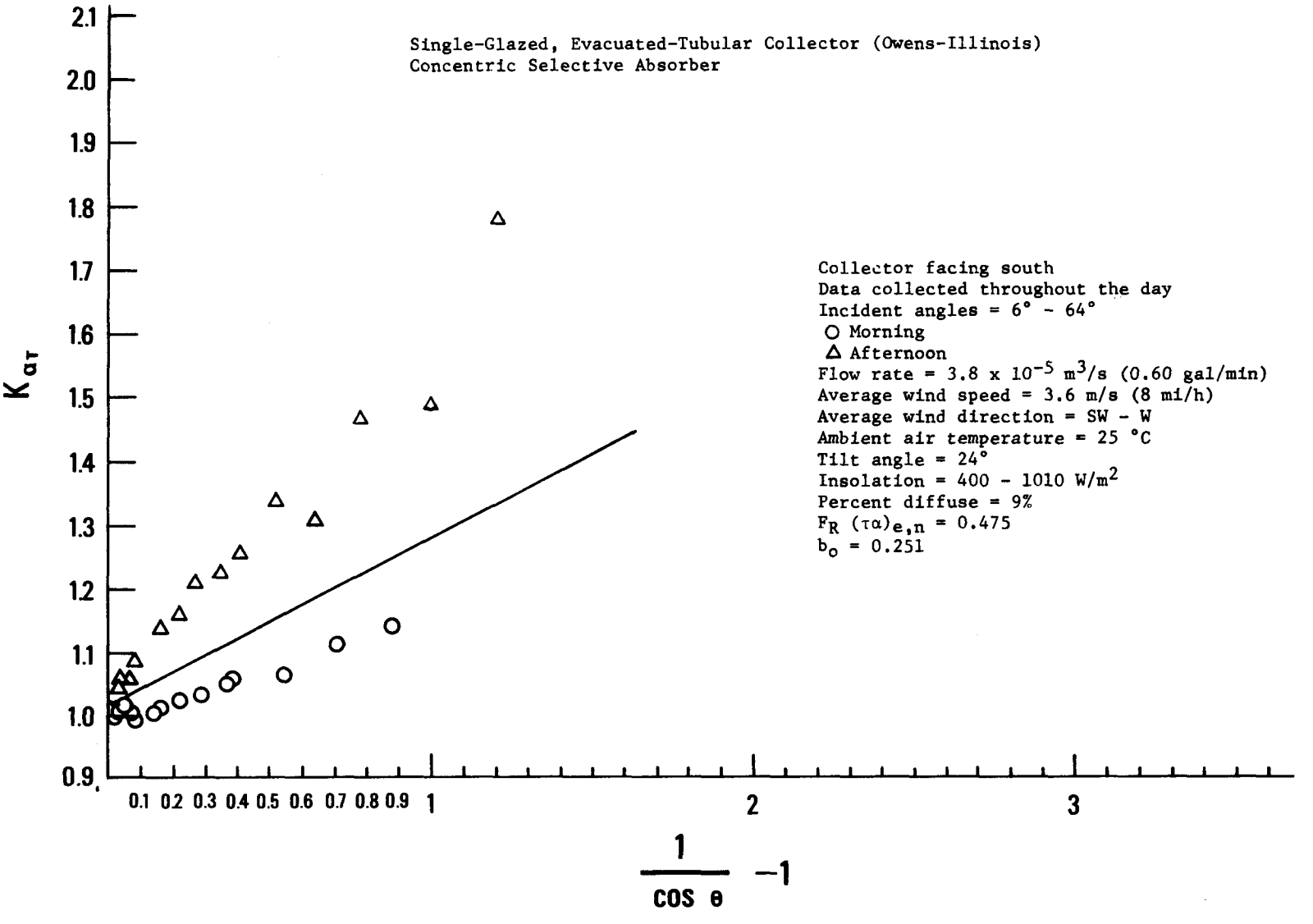

Figure 46 Experimental Results for the Incident Angle Modifier Test for Water-Heating Solar Collector No. 4.

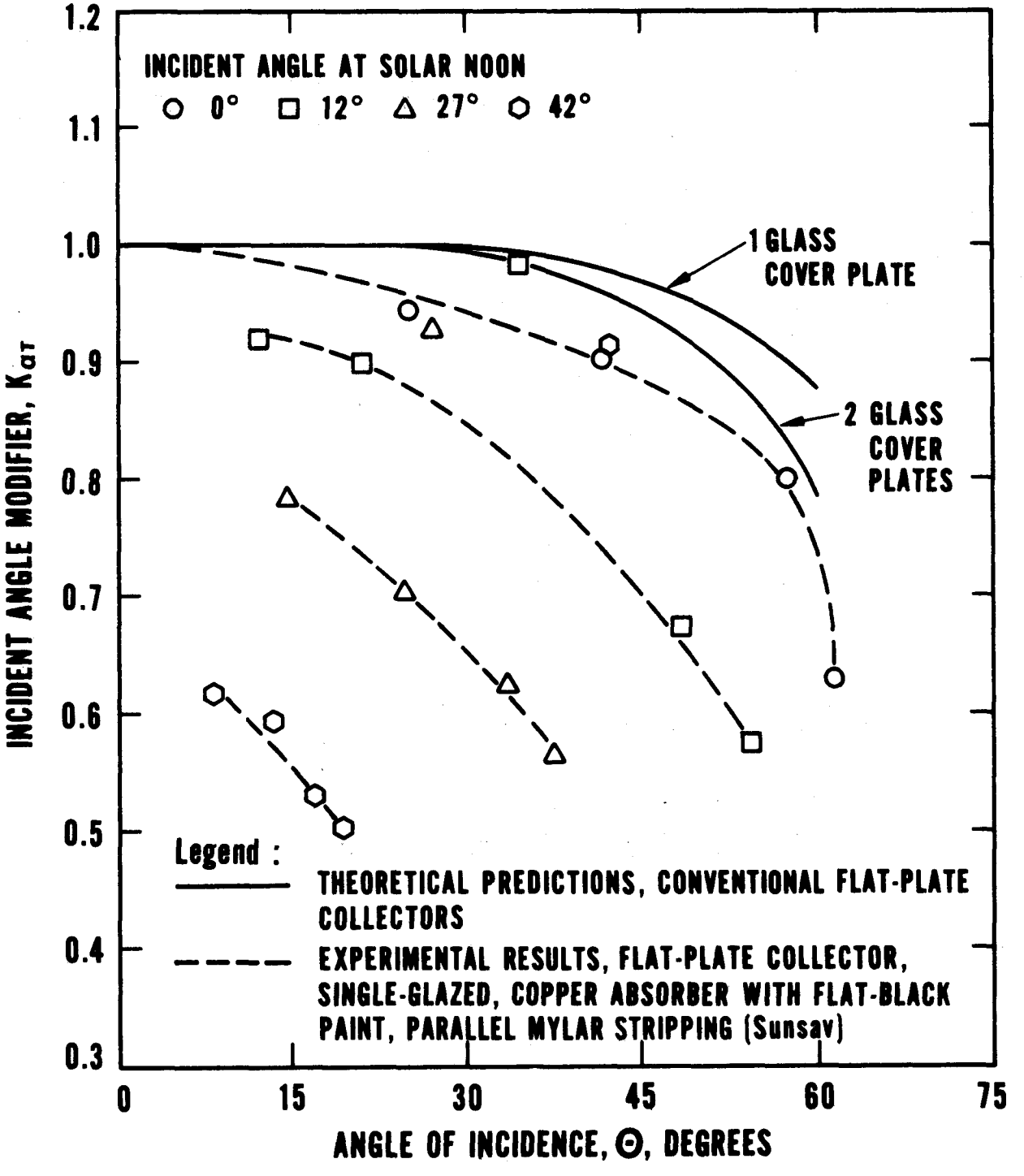

Figure 47 Experimental Results for a Incident Angle Modifier Test for a Water-Heating Flat-Plate Solar Collector with Parallel Mylar Stripping [22].

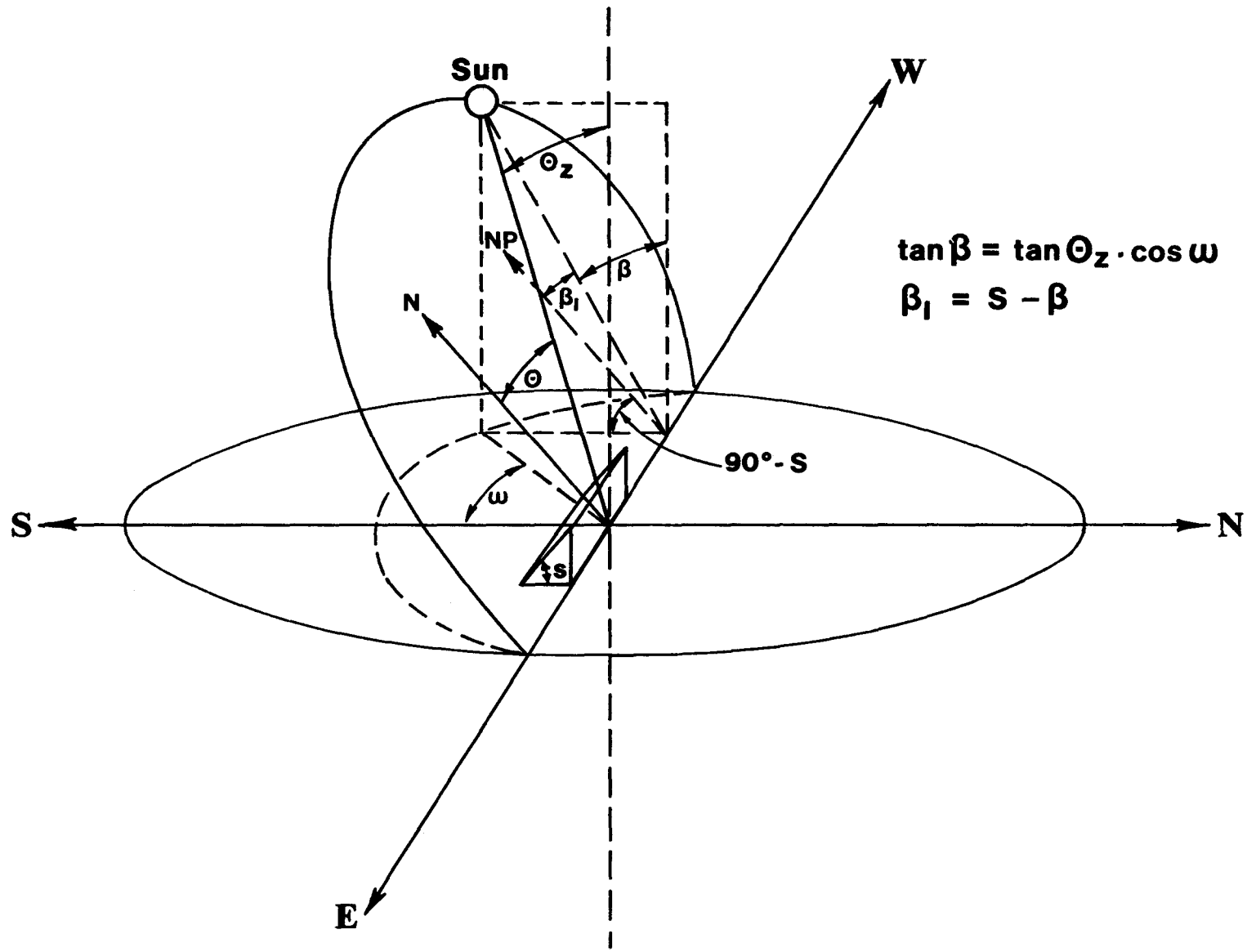

Figure 48 Sun Angle Diagram for Incident Angle Modifier Tests.

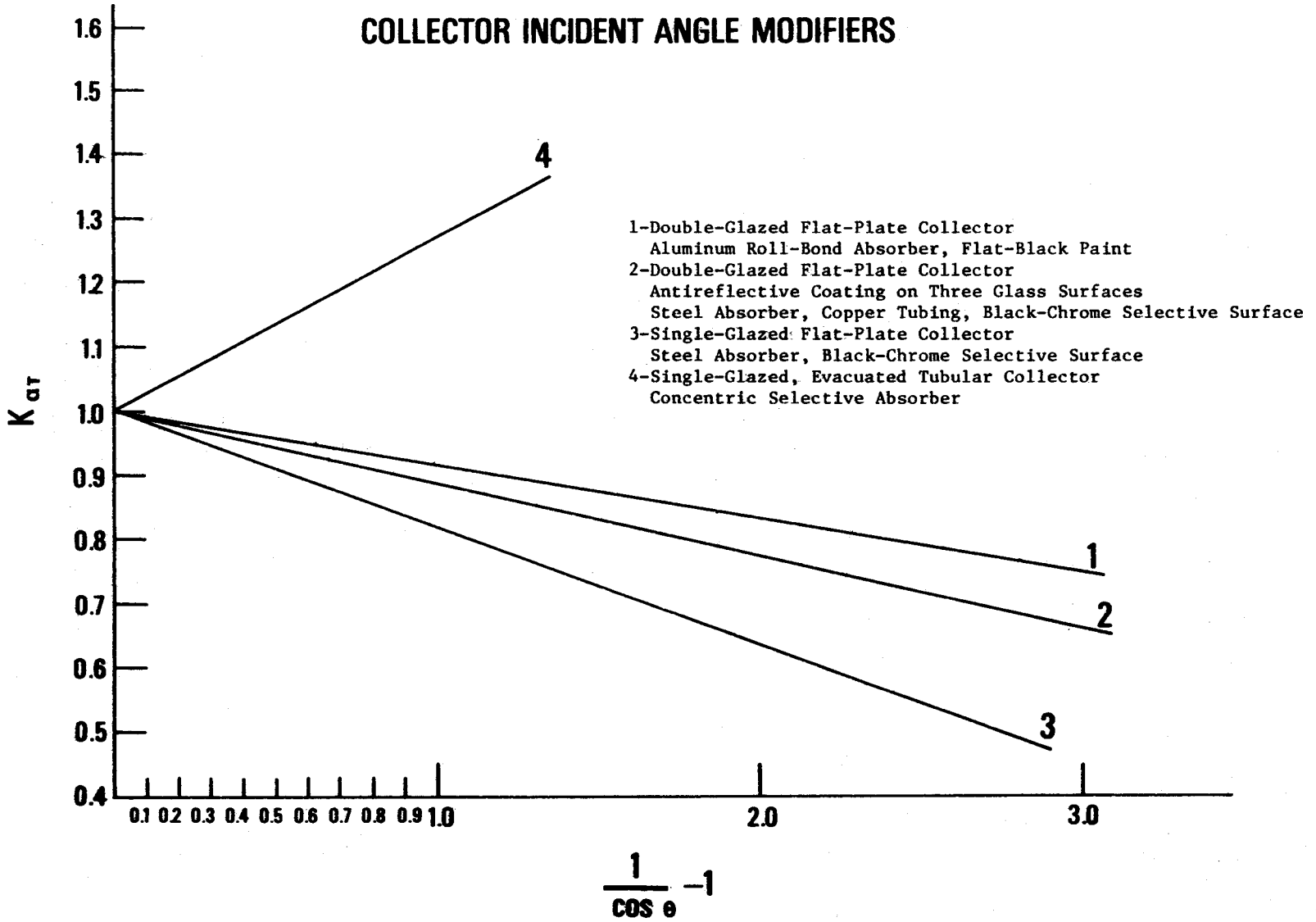

Figure 49 Incident Angle Modifiers for Selected Water-Heating Solar Collectors.

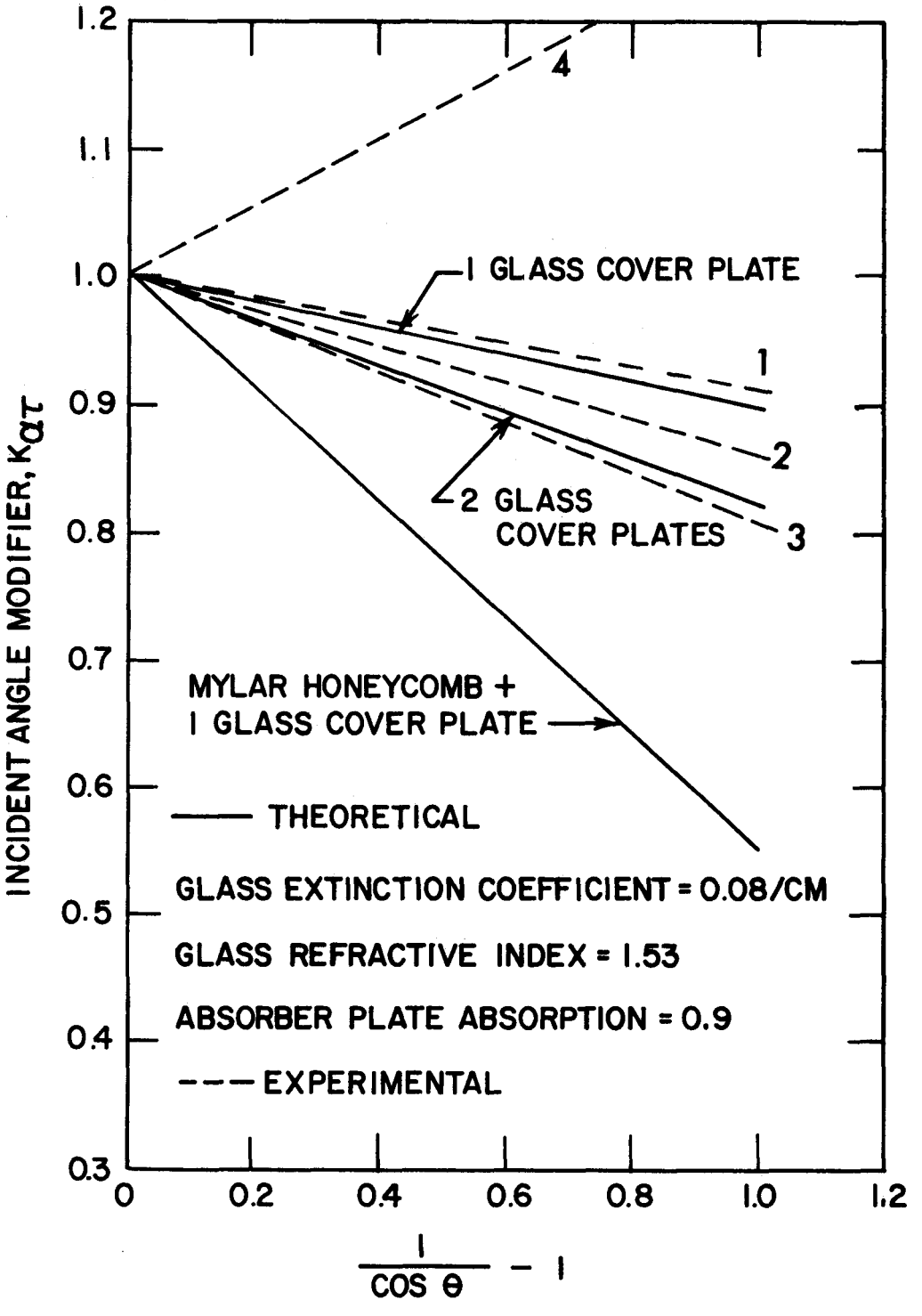

Figure 50 Incident Angle Modifiers for Selected Water-Heating Solar Collectors in Comparison with Theoretical Predictions.

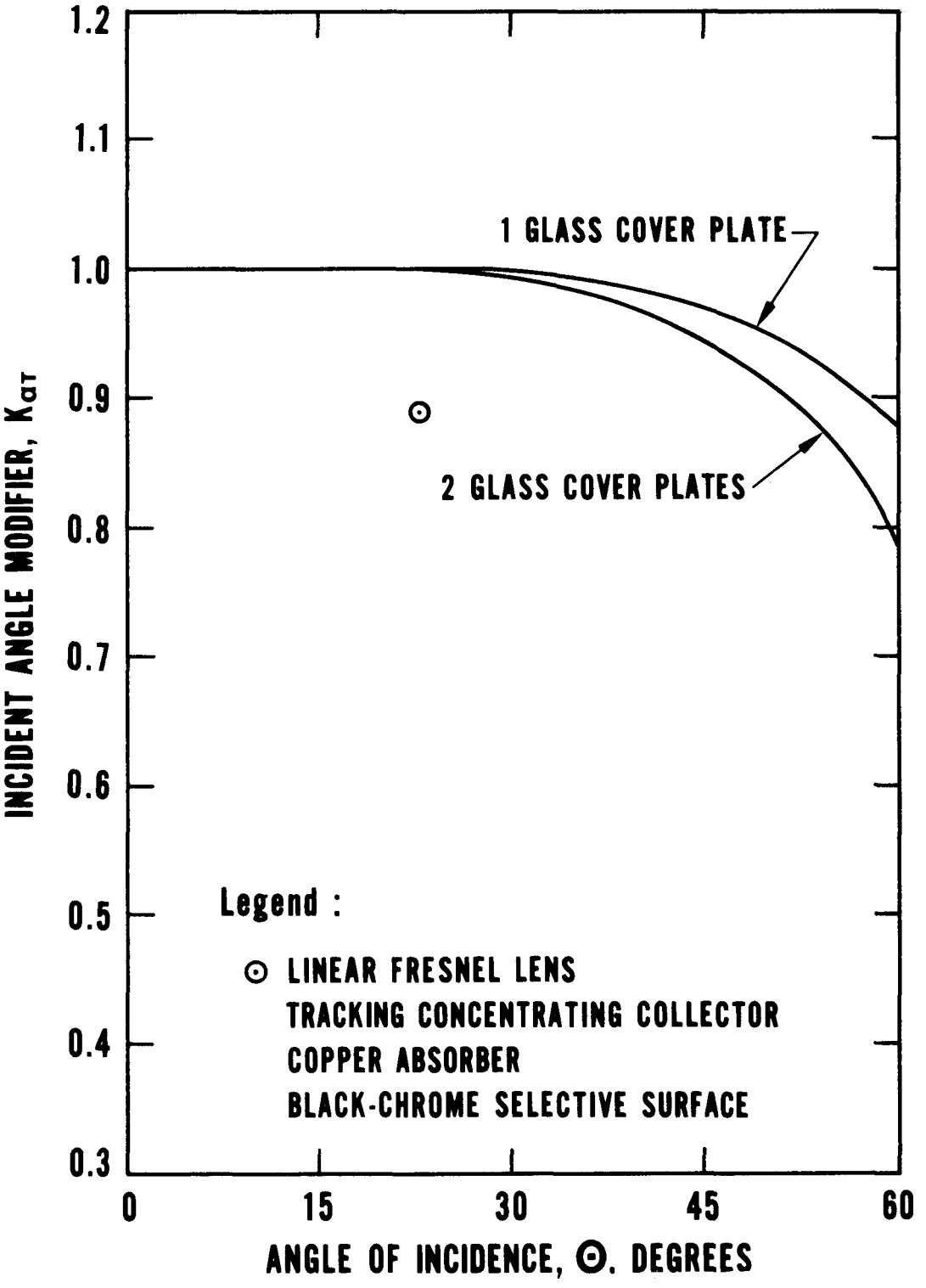

Figure 51 Incident Angle Modifier for Water-Heating Solar Collector No. 5 at One Angle of Incidence.

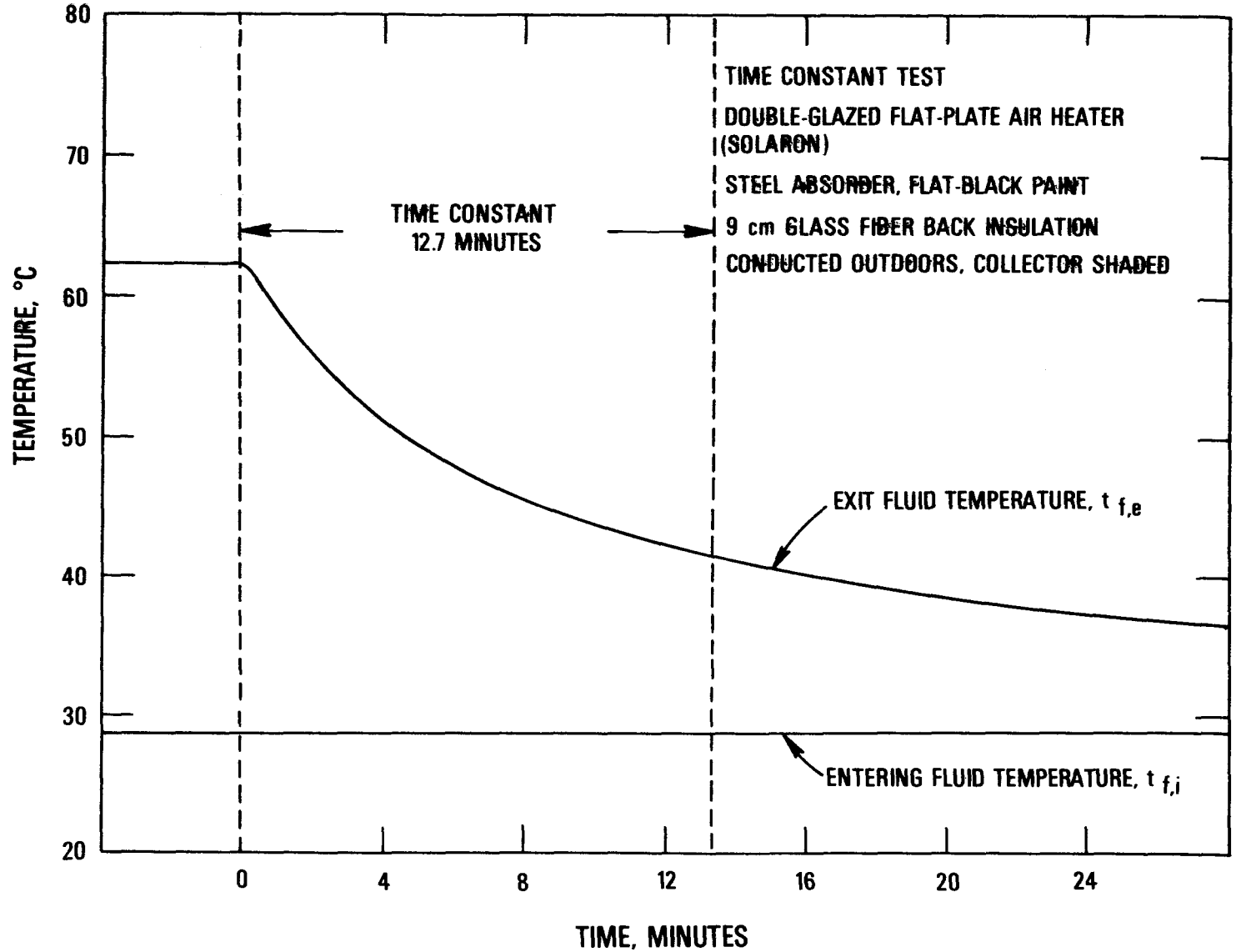

Figure 52 Experimental Results for the Time Constant Test for the Air-Heating Solar Collector.

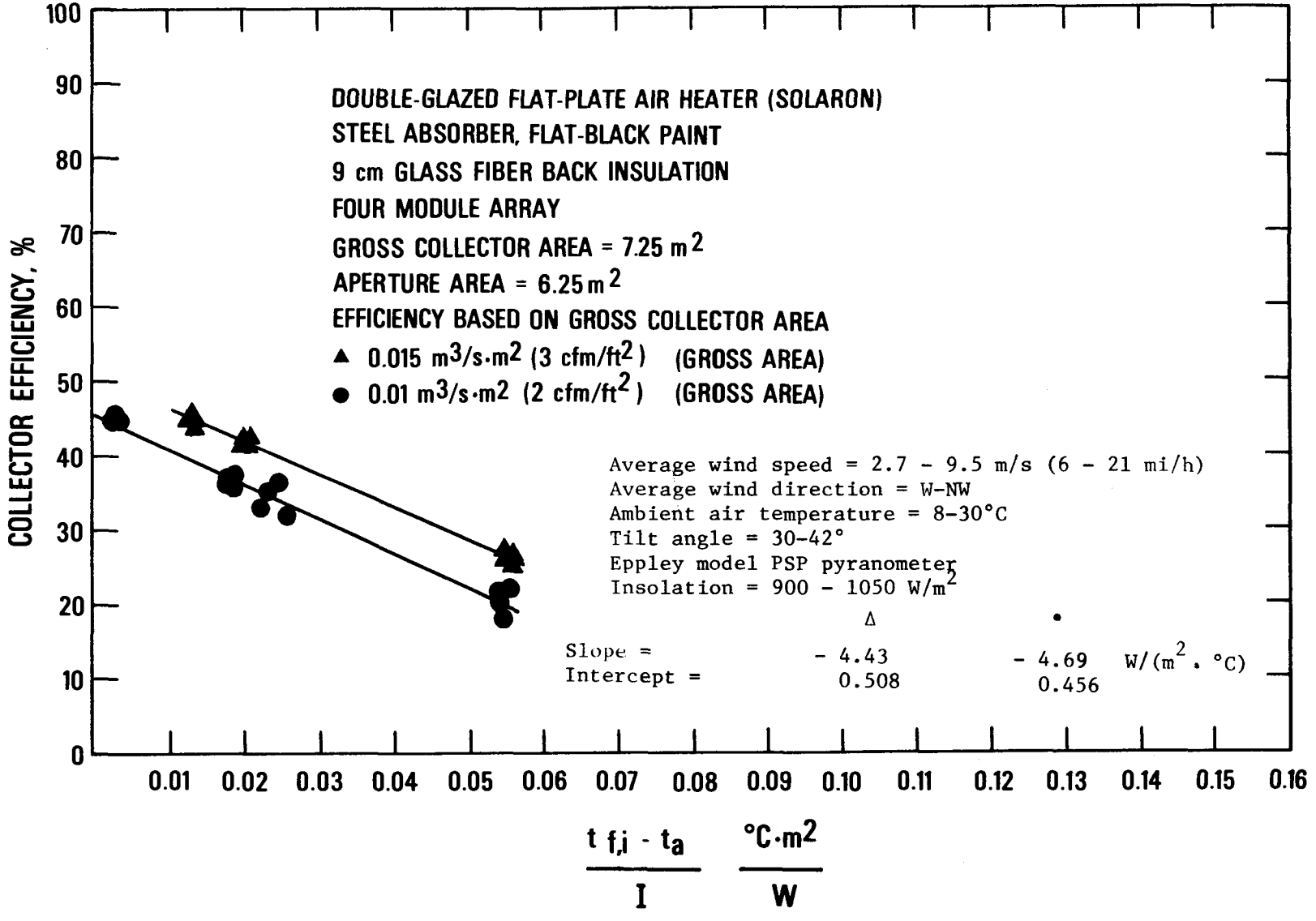

Figure 53 Experimental Results for the Near-Normal-Incidence Efficiency Test for the Air-Heating Solar Collector.

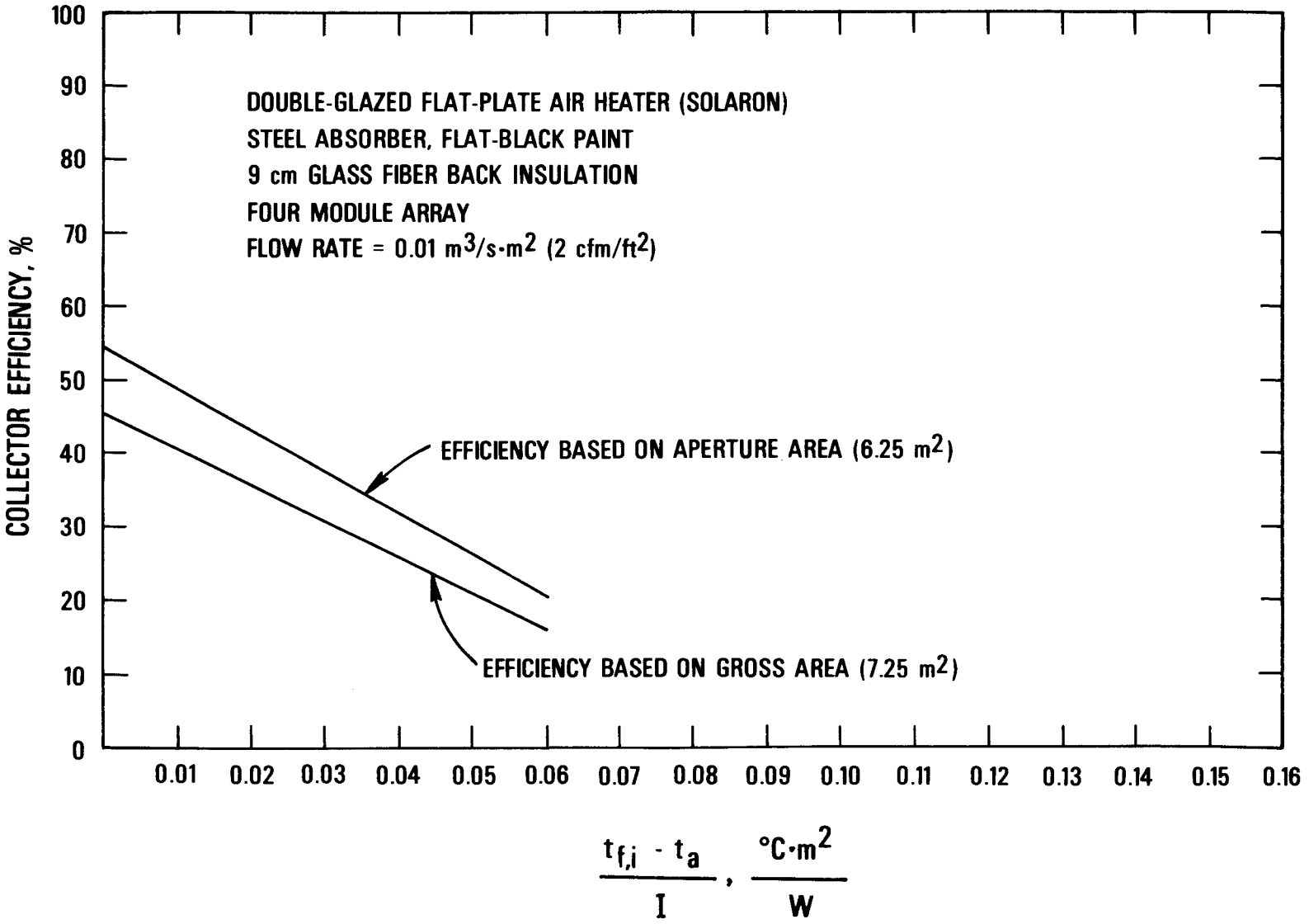

Figure 54 Near-Normal-Incidence Efficiency for the Air-Heating Solar Collector Based on Two Different Areas.

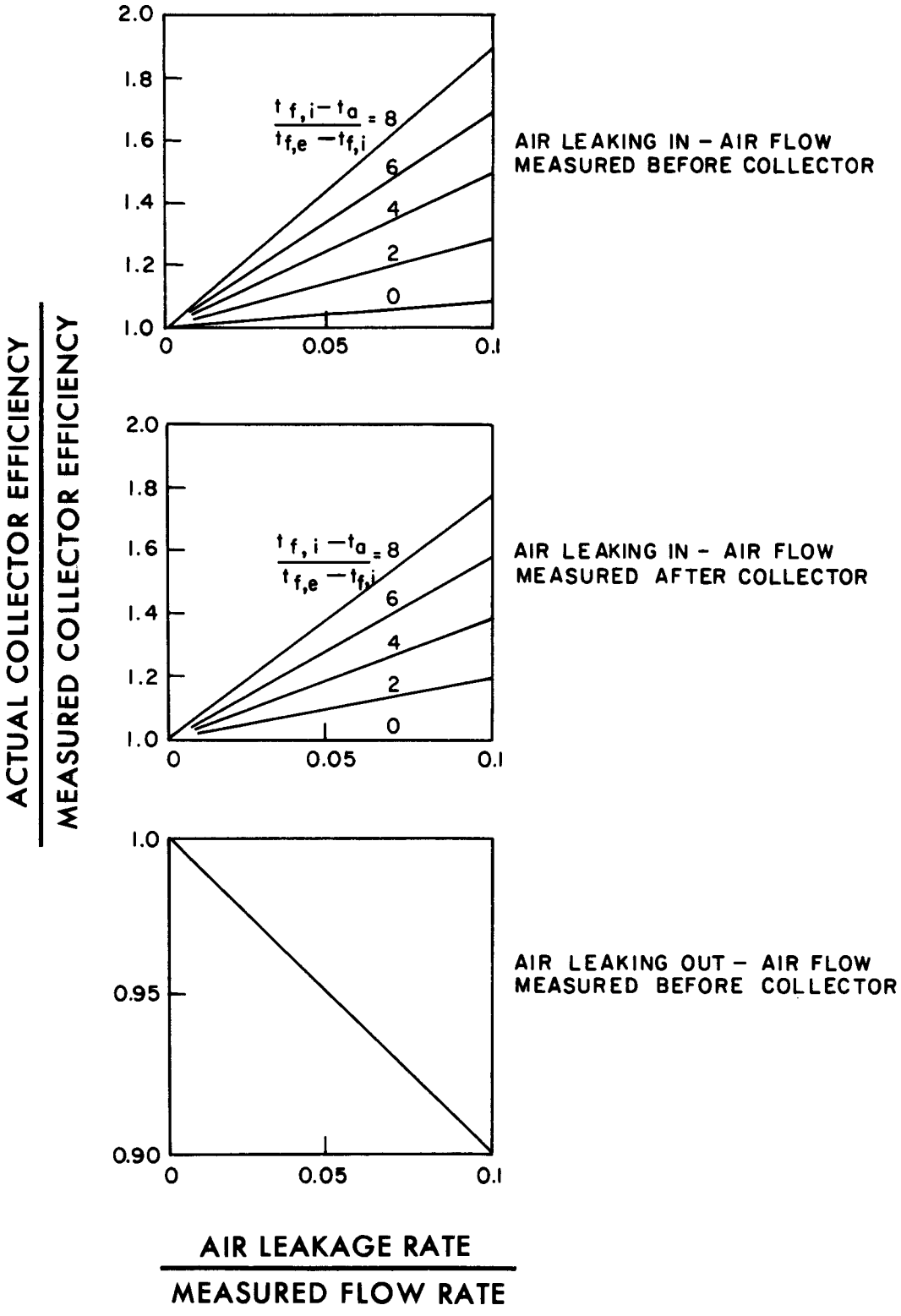

Figure 55 Relationship Between Actual Efficiency and Measured Efficiency as a Function of Air Leakage Rate for Air-Heating Solar Collectors [23].

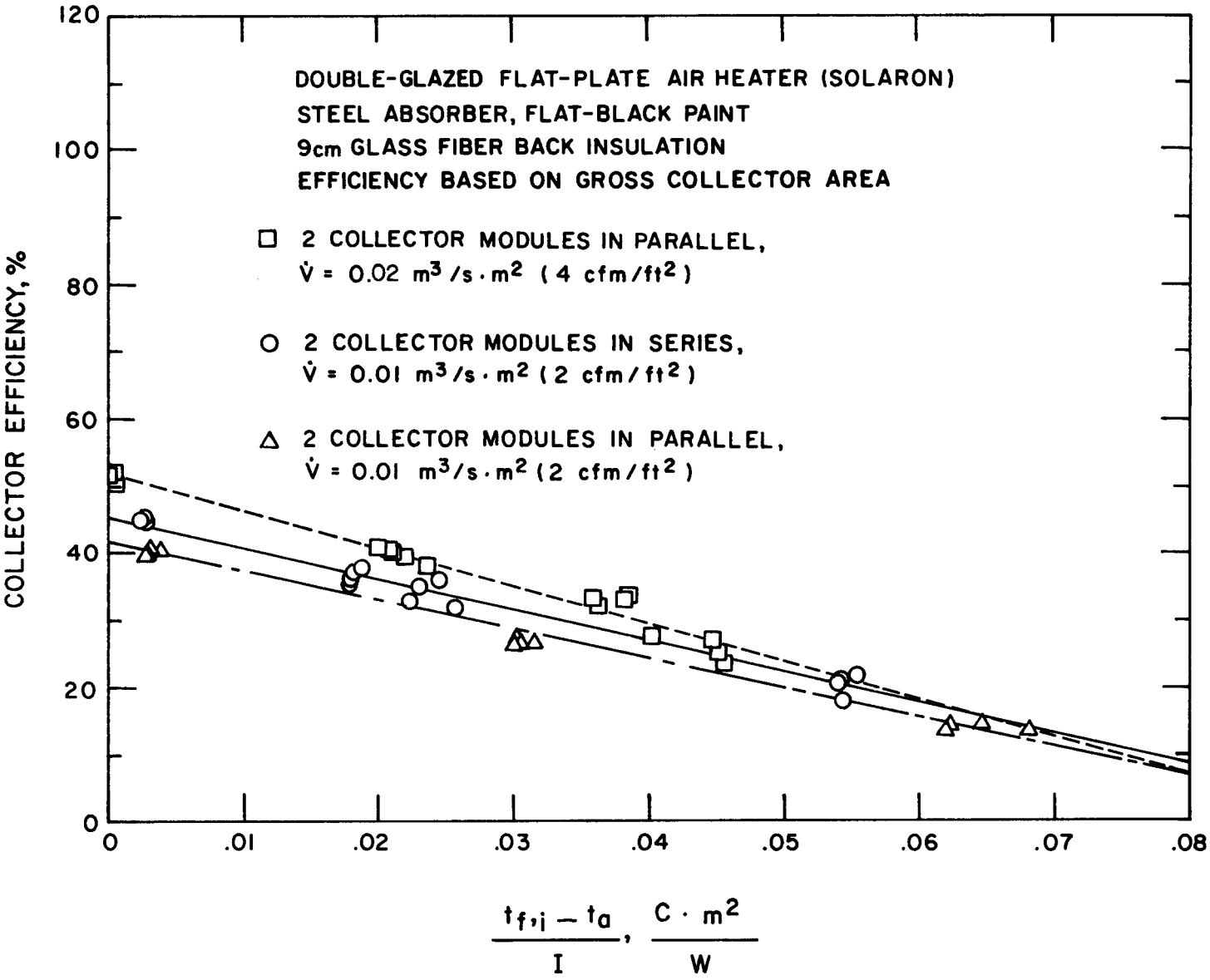

Figure 56 Near-Normal-Incidence Efficiency for the Air-Heating Solar Collector in Two Different Configurations.

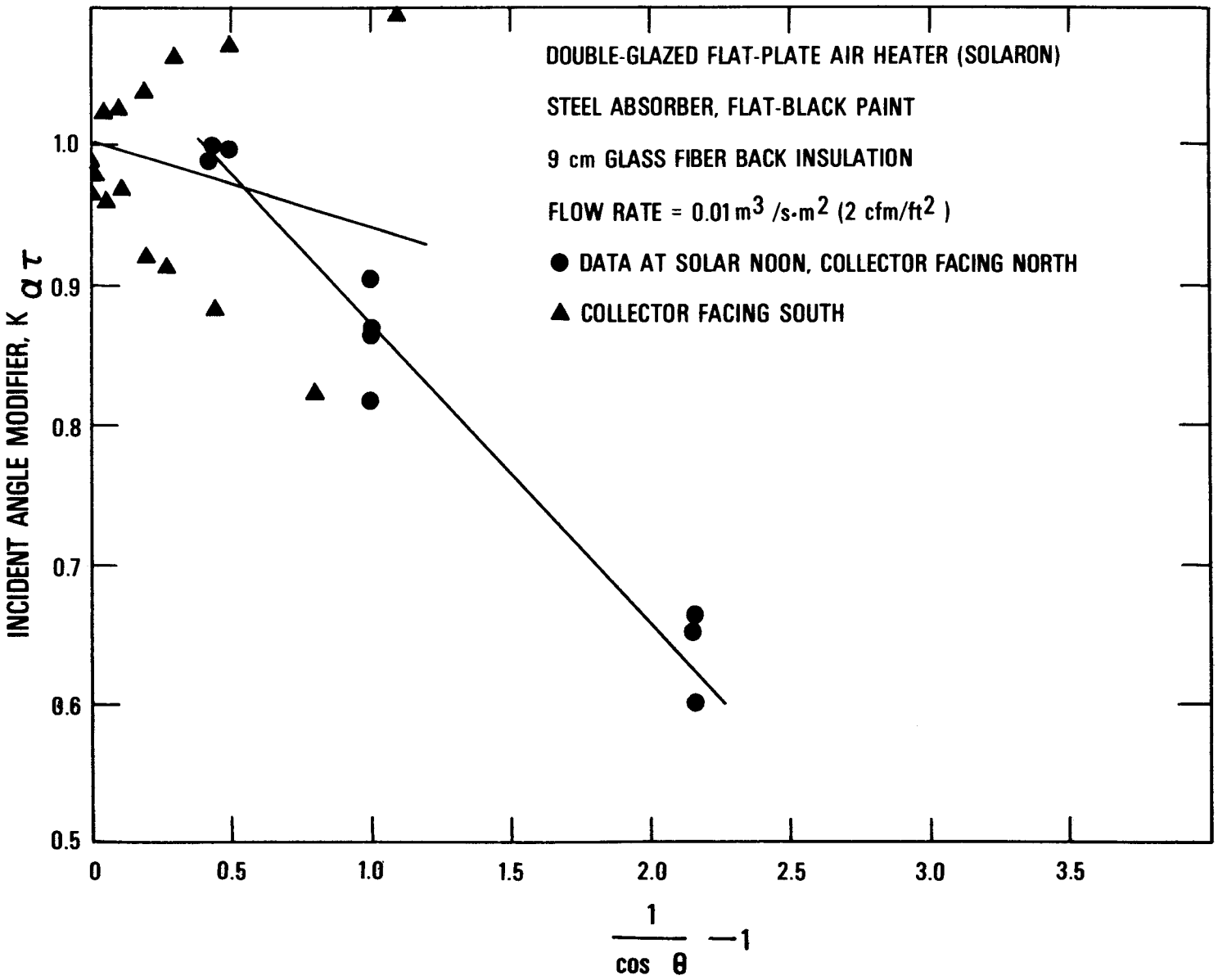

Figure 57 Experimental Results for the Incident Angle Modifier Test for the Air-Heating Solar Collector.

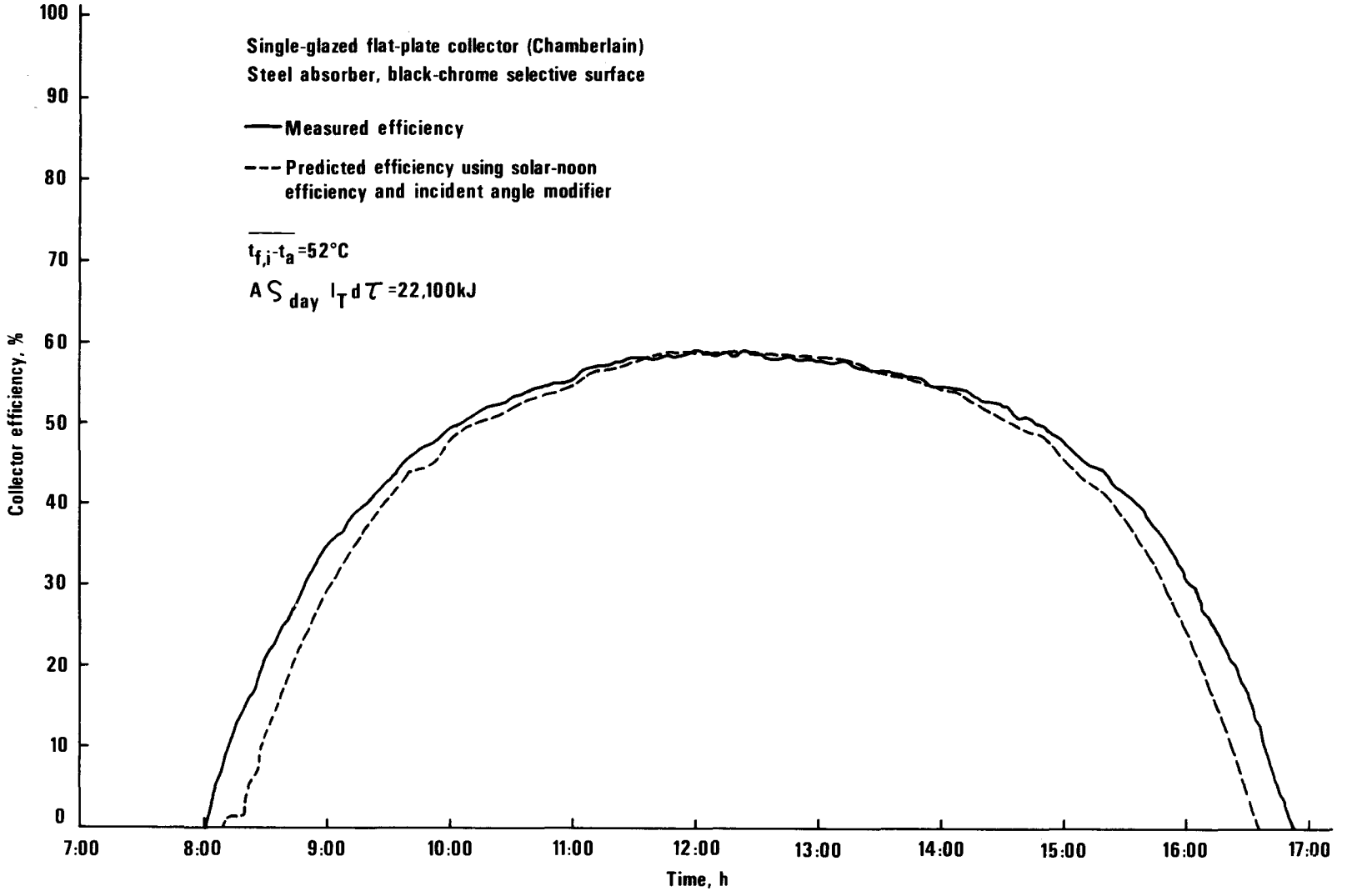

Figure 58 Comparison of Actual and Predicted Instantaneous Efficiency Throughout a Day for Water-Heating Solar Collector No. 3.

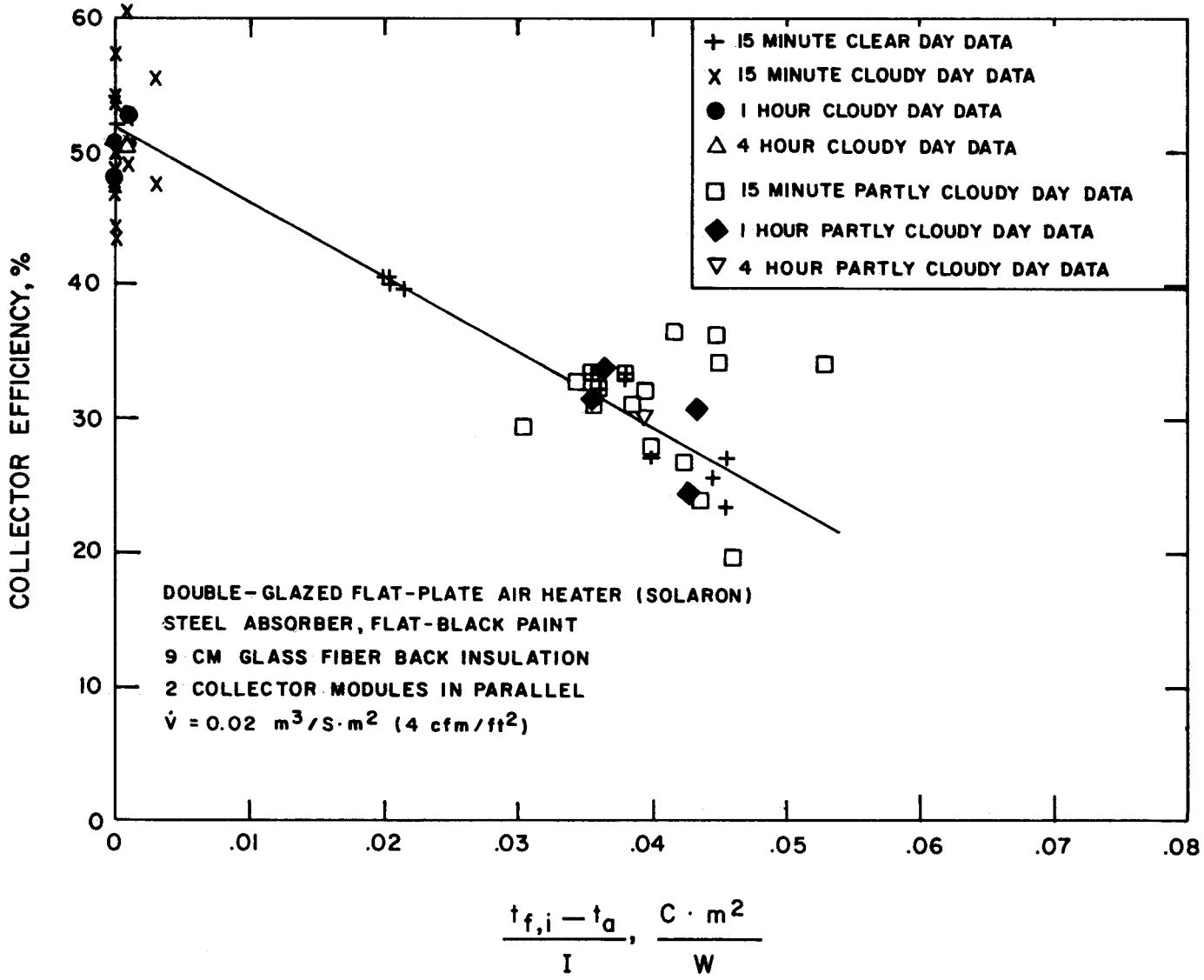

Figure 59 Experimentally Determined Efficiency for the Air-Heating Solar Collector Under Various Weather Conditions and Averaged over Various Time Periods.

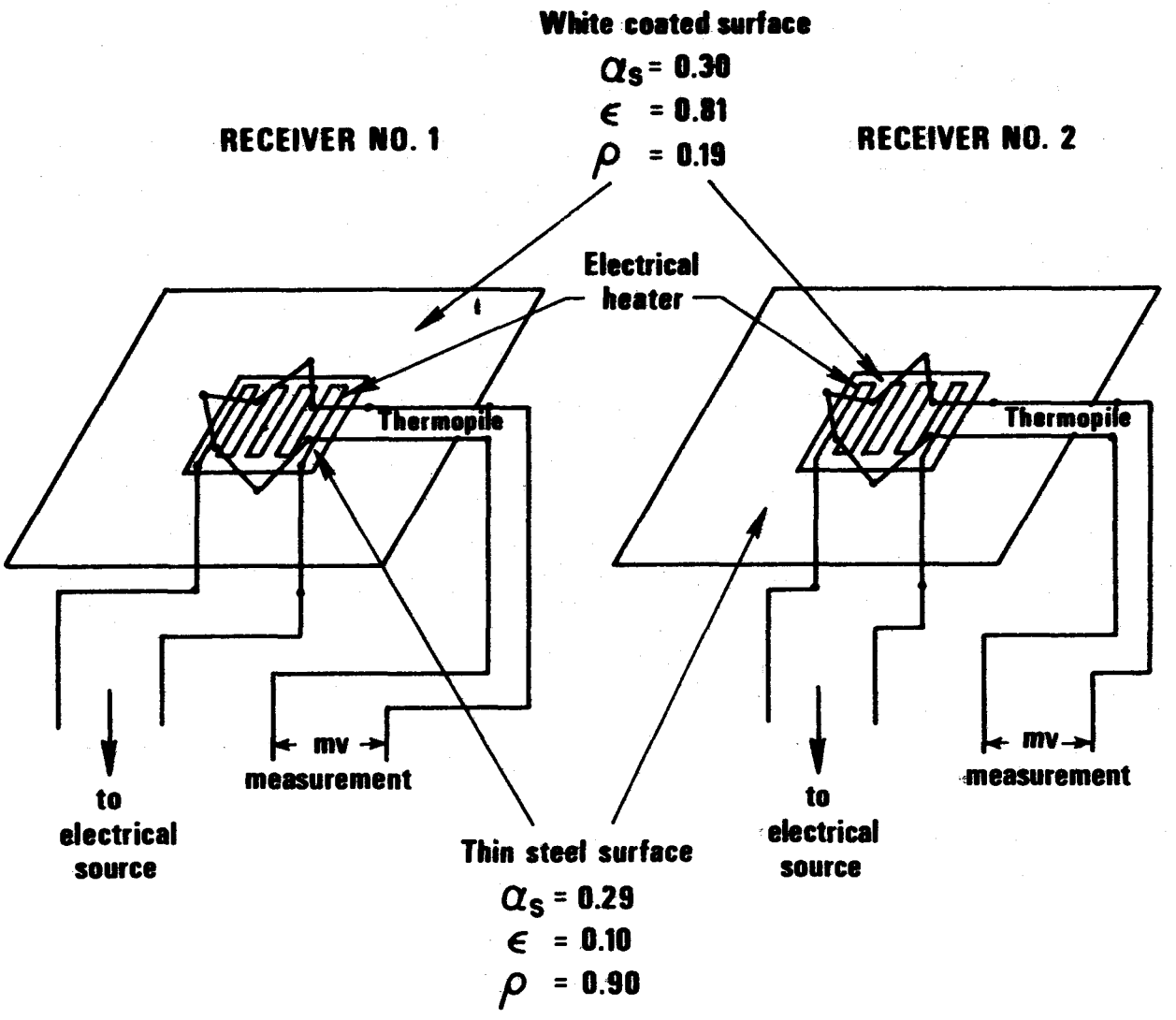

Figure 60 Schematic Diagram of a Radiometer for Determining Sky Temperatures.

NBS-114A (REV. 7-73)

U.S. DEPT. OF COMM. BIBLIOGRAPHIC DATA SHEET	1. PUBLICATION OR REPORT NO. NBS BSS 117	2. Gov't Accession No.	3. Recipient's Accession No.

4. TITLE AND SUBTITLE

EXPERIMENTAL VERIFICATION OF A STANDARD TEST PROCEDURE FOR SOLAR COLLECTORS

5. Publication Date January 1979

6. Performing Organization Code

7. AUTHOR(S) James E. Hill, John P. Jenkins, and Dennis E. Jones

8. Performing Organ. Report No.

9. PERFORMING ORGANIZATION NAME AND ADDRESS

NATIONAL BUREAU OF STANDARDS
DEPARTMENT OF COMMERCE
WASHINGTON, D.C. 20234

10. Project/Task/Work Unit No. 742 4417

11. Contract/Grant No.

12. Sponsoring Organization Name and Complete Address (Street, City, State, ZIP)
Department of Energy
Research and Development Branch for Solar Heating and Cooling
Office of the Assistant Secretary for Conservation and
Solar Applications, Washington, D.C. 20545

13. Type of Report & Period Covered

14. Sponsoring Agency Code

15. SUPPLEMENTARY NOTES

Library of Congress Catalog Card Number 78-600138

16. ABSTRACT *(A 200-word or less factual summary of most significant information. If document includes a significant bibliography or literature survey, mention it here.)*

A proposed procedure for testing and rating solar collectors based on thermal performance was published by the National Bureau of Standards (NBS) in 1974. Subsequently, the American Society of Heating, Refrigerating, and Air Conditioning (ASHRAE) developed a modified version of the NBS procedure which was adopted in early 1977 as ASHRAE Standard 93-77. A test facility for water-heating and air-heating collectors has been built at NBS and was used to support the development of Standard 93-77. The purpose of this report is to describe the recently adopted test procedure, the NBS test facility, and the tests that were conducted to support the development of the procedure.

17. KEY WORDS *(six to twelve entries; alphabetical order; capitalize only the first letter of the first key word unless a proper name; separated by semicolons)* Measurement; solar collector; solar energy; solar radiation; standards; standard test; testing.

18. AVAILABILITY

☒ Unlimited

☐ For Official Distribution. Do Not Release to NTIS

☒ Order From Sup. of Doc., U.S. Government Printing Office Washington, D.C. 20402, SD Stock No. SN003-003

☐ Order From National Technical Information Service (NTIS) Springfield, Virginia 22151

19. SECURITY CLASS (THIS REPORT)	21. NO. OF PAGES
UNCLASSIFIED	127
20. SECURITY CLASS (THIS PAGE)	**22. Price**
UNCLASSIFIED	$3.00

USCOMM-DC 66035-P78

☆ U.S. GOVERNMENT PRINTING OFFICE: 1978 O—281-067 (339)